BBA Advances 7 (2025) 100141

Contents lists available at ScienceDirect

BBA Advances

journal homepage: www.sciencedirect.com/journal/bba-advances

The second wave of formose research

Akihito Hashidzume

Department of Macromolecular Science, Graduate School of Science, Osaka University, 1-1 Machikaneyama-cho, Toyonaka, Osaka 560-0043, Japan

ARTICLE INFO

Keywords:
Formose reaction
Prebiotic monosaccharide synthesis
Mechanistic studies
Origin of life
Applications

ABSTRACT

This review article highlights key developments in the second wave of formose research (from approximately 2000), summarizing approximately 100 relevant studies. Section 1 introduces the basics of formose reaction and its historical context. Section 2 provides a brief overview of the pioneering works from the first wave of formose research (from 1970 to 1990). Section 3 then overviews the second wave of formose research, in which formose reactions under various conditions, mechanistic studies of the formose reaction, formose reactions and the origin of life, and applications of formose reactions are described. Finally, Section 4 offers summary and outlook.

1. Introduction

The molecular formula of formaldehyde is CH_2O, and it can be thus considered as the smallest carbohydrate consisting of a carbon atom and a water molecule. The general molecular formula of monosaccharides, *i.e.*, sugar, is $(CH_2O)_n$. For example, the molecular formula of pentoses including ribose is $C_5H_{10}O_5$, and that of hexoses containing glucose, galactose, and fructose is $C_6H_{12}O_6$. In other words, if formaldehyde molecules are successfully connected, monosaccharides can be obtained. In 1861, Butlerow [1], a famous Russian organic chemist, discovered that a sugar-like product was obtained by heating an aqueous solution of formaldehyde under basic conditions (Scheme 1). Later, Loew [2] named the product "formose", meaning sugar produced from formaldehyde, and the reaction came to be called "formose reaction".

Plants synthesize monosaccharides from carbon dioxide and water through the Calvin–Benson cycle of photosynthesis. Before the Calvin–Benson cycle was discovered, it had been believed that formose reaction took place in plants. Currently, the origin of life is proposed to be explained by the ribonucleic acid (RNA) world hypothesis, which states that life began with RNA, as RNA exhibits enzymatic activities [3,4]. RNA consists of ribonucleosides, which contain ribose as an important component. Ribose must be formed in order for RNA to be produced under prebiotic conditions. It is considered that formose reaction is one of possible prebiotic pathways for the formation of ribose (see Section 3.3.3).

In relation to photosynthesis and the origin of life, the mechanism and products of formose reaction have been studied in the early 20th century [5–7]. As a result, it was revealed that formose reaction is a complicated reaction that includes acyloin condensation, aldol reaction, retro-aldol reaction, carbonyl shift, and Cannizzaro reaction, and that formose is a complicated mixture containing >30 types of monosaccharides and sugar alcohols. Formose reaction is divided into three periods, *i.e.*, the induction period, the sugar formation period, and the sugar degradation period. During the induction period, two formaldehyde molecules form glycolaldehyde through acyloin condensation. Since glycolaldehyde acts as a cocatalyst, aldol reaction takes place favorably to form various monosaccharides when the amount of product glycolaldehyde exceeds a certain level. When most of the formaldehyde is consumed, the reaction mixture turns yellow. This point is called the yellowing point. After the yellowing point, the monosaccharides produced are degraded mainly through retro-aldol reaction and Cannizzaro reaction to form a complicated brown mixture containing monosaccharides and sugar alcohols, along with the formation of larger monosaccharides.

Abbreviations: BAL, benzaldehyde lyase which catalyzes conversion of (*R*)-benzoin to benzaldehyde; BSTFA, *N,O*-bis(trimethylsilyl)trifluoroacetamide; CWO, catalytic wet oxidation; Des0, an enzymes for formose reaction; DFT, density functional theory; ESI-MS, electrospray ionization-mass spectrometry; FLS, formolase, *i.e.*, an enzyme that catalyzes coupling of formaldehyde molecules; FT-ICR MS, Fourier transform-ion cyclotron resonance mass spectrometry; FTIR, Fourier transform infrared; GALS, an enzyme that catalyzes the conversion of formaldehyde to glycolaldehyde; GC, gas chromatography; GC-MS, gas chromatography-mass spectrometry; 4-HMF, 4-hydroxymethylfurfural; HPLC, high performance liquid chromatography; IMS-MS, ion mobility separation mass spectrometry; IR, infrared; ISM, interstellar medium; LC-MS, liquid chromatography-mass spectrometry; MO, molecular orbital; MS, mass spectrometry; MW, microwave; NMR, nuclear magnetic resonance; OD, optical density; RNA, ribonucleic acid; ThDP, thiamine diphosphate; UPLC-MS/MS, ultra-high pressure liquid chromatography-tandem mass spectroscopy; UV, ultraviolet; ZIF, zeolitic imidazolate framework.

E-mail address: hashidzume@chem.sci.osaka-u.ac.jp.

https://doi.org/10.1016/j.bbadva.2025.100141
Received 24 October 2024; Received in revised form 9 January 2025; Accepted 13 January 2025
Available online 17 January 2025

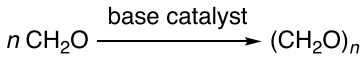

Scheme 1. Formose reaction.

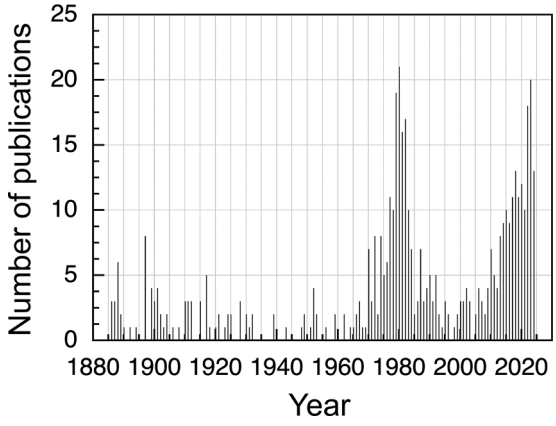

Fig. 1. Number of publications on formose from 1880 to 2024.

As of October 2024, a search for formose using SciFinder Scholar returns approximately 500 publications. Fig. 1 shows the trend in the number of publications. Except for certain periods, the average number of papers published per year is about one. As can be seen in Fig. 1, the first wave of formose research arrived from 1970 to 1990, and we are currently in the midst of the second wave since 2000. This review article mainly deals with the second wave of formose research. Section 2 briefly summarizes the pioneering works in the first wave of formose research. Section 3 then reviews the second wave of formose research, in which formose reaction under various conditions (Section 3.1), mechanistic studies of the formose reaction (Section 3.2), the origin of life and formose reaction (Section 3.3), and applications of formose reaction (Section 3.4) are described. Section 4 provides summary and outlook. Interested readers can refer to other reviews on formose reaction [5,6,8–10].

2. Pioneering works in the first wave of formose research

In the first wave, Shigemasa et al. [7] and Inoue et al. [11,12] led formose research, especially, to realize controlled formose reaction. For details of their research, please refer to their publications [7,11,12]. Shigemasa et al. [7] identified the induction period, the sugar formation period, and the sugar degradation period by measuring the redox potential of mixtures of formose reaction. Then, they successfully isolated a branched seven carbon sugar alcohol and a branched heptose by optimizing the reaction conditions in the sugar formation period. Inoue et al. [11] achieved the selective synthesis of 1,3-dihydroxyacetone, *i.e.*, a triose, by using a thiazolium salt as a catalyst. Inoue et al. [12] also synthesized DL-dendroketose, *i.e.*, a hexose, by coupling two 1,3-dihydroxyacetone molecules.

3. The second wave of formose research

3.1. Formose reactions under various conditions

3.1.1. Formose reactions in the gas phase

Eckhardt et al. [13–15] performed experimental and simulation studies of monosaccharide synthesis in the gas phase. They showed that formaldehyde reacted with its isomer, hydroxymethylene, to form glycolaldehyde through a nearly barrier-free reaction [13]. Hydroxymethylene acted as a building block for iterative monosaccharide formation to yield larger monosaccharides, *e.g.*, glyceraldehyde (Fig. 2a). The thermodynamically favored ketose, *i.e.*, 1,3-dihydroxyacetone, was not formed, and the formation of larger branched monosaccharides was unlikely in the iterative monosaccharide formation. Eckhardt et al. [14] reported the spontaneous formation of 1,3-dioxolan-4-ol, *i.e.*, a mixed hemiacetal, by addition of glycolaldehyde to formaldehyde in the gas phase. The hemiacetal was identified by matching matrix infrared (IR) spectra with coupled cluster calculations. 1,3-Dioxolan-4-ol is considered as a storage form of formaldehyde and glycolaldehyde and is fairly stable in the gas phase (Fig. 2b). Eckhardt et al. [15] also described the identification of glycolaldehyde enol (1,2-ethenediol, HOHC═CHOH) in methanol-containing ice at temperatures as low as 5 K (Fig. 2c). A reaction pathway to 1,2-ethenediol was revealed by isotopic labeling and isomer-selective photoionization combined with reflectron time-of-flight mass spectrometry (TOF-MS). 1,2-Ethenediol is kinetically stable, applicable for prebiotic formation of monosaccharides, and detectable in deep space. These studies suggests that the gas phase reaction may form selectively linear monosaccharides, which are difficult to form in conventional formose reaction, via reaction intermediates, which are different from those in solution.

3.1.2. Formose reactions in solutions

Simonov et al. [16] carried out formose reaction at 38 or 41 °C in a flow or batch reactor using an aqueous solution containing formaldehyde (0.14 M), a monosaccharide (a cocatalyst, *i.e.*, glycolaldehyde, glyceraldehyde, 1,3-dihydroxyacetone, D-erythrose, DL-arabinose, D-ribose, D-lyxose, D-L-xylose, D-glucose, L-sorbose, D-fructose, D-mannose, or D-galactose), and $Ca(OH)_2$ (0.027 M). The products were derivatized with 2,4-dinitrophenylhydrazine and characterized by high performance liquid chromatography (HPLC). The HPLC data indicated the formation of tetroses, pentoses, and hexoses. Tabata et al. [17] focused on the weak Brønsted basicity of oxometalate anions, *e.g.*, WO_4^{2-} and MO_4^{2-}, and utilized these anions as catalysts for formose reaction. For example, formose reaction was carried out using an aqueous formaldehyde solution (0.3 M) containing methanol (10 %) at 80 °C for *ca.* 4 h under weakly basic conditions (pH 7.8) in the presence of Na_2WO_4 (a catalyst) and glycolaldehyde (a cocatalyst). The products derivatized with 2,4-dinitrophenylhydrazine were characterized by HPLC. The HPLC data indicated that a mixture of pentoses and hexoses, *e.g.*, 1,3,4-trihydroxy-3-(hydroxymethyl)butan-2-one, 1,3,4,5-tetrahydroxypentan-2-one, and 1,2,4,5,6-pentahydroxyhexan-3-one, was obtained (Fig. 3a). Notably, Cannizzaro reaction was retarded in these reactions (Fig. 3b). Ono et al. [18] studied formose reaction using mixtures of formaldehyde (100 mM) and glycolaldehyde (10 mM) in a phosphate buffer (0.2 M, pH = 5.7 – 7.6) or water (pH 4.5) at 55, 75, and 95 °C under varying conditions. The products were derivatized into aldonitrile acetates and characterized by gas chromatography-mass spectrometry (GC-MS). At higher pH or temperature, monosaccharides, *e.g.*, pentoses, were obtained in higher yields. In the presence of $CaCl_2$, the yield of monosaccharides, *e.g.*, erythrose, threose, and glyceraldehyde, was higher. Notably, ribose was formed more efficiently at higher pH and glycolaldehyde concentration.

Hydrothermal conditions are used for crystal growth and reactions because of the improved solubility of solutes. Formose reaction has been conducted under hydrothermal conditions. Kopetzki and Antonietti [19] performed formose reaction using an aqueous formaldehyde solution (0.5 M) and various base catalysts ($Ca(CH_3COO)_2$, $NaHCO_3$, K_2HPO_4, and a mixture of $NaHCO_3$ and Na_2CO_3) in a flow-type reactor under hydrothermal conditions at 200 °C and 100 bar. The products were derivatized by the alditol acetate method and characterized by GC-MS. The reaction was completed within a few minutes without selective formation of specific monosaccharides independent of the cationic species. In contrast to formose reaction performed at low temperatures, smaller monosaccharides were formed as major products whereas hexoses were formed in lower yields (Fig. 4a). Omran et al. [20,21] also studied formose reaction under hydrothermal conditions. Omran et al. [20] carried out formose reaction using an aqueous formaldehyde

(a)

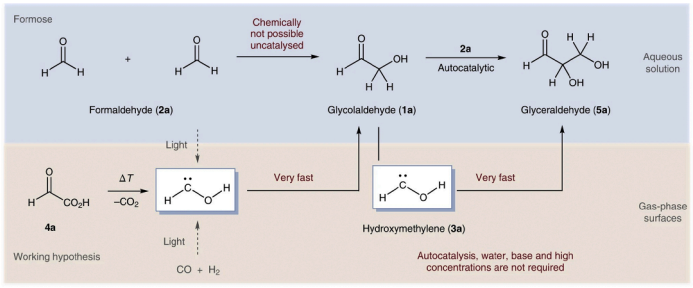

(b)

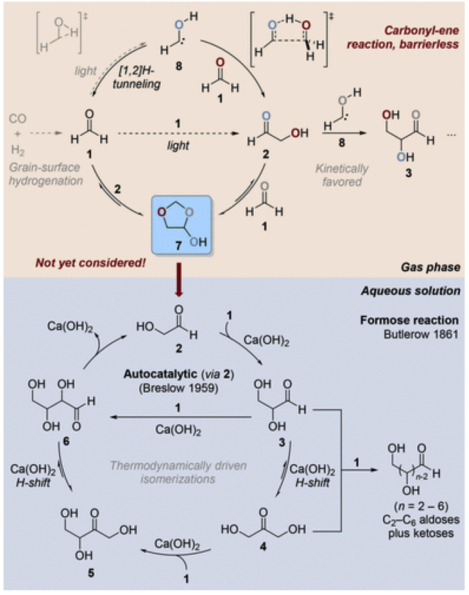

(c)

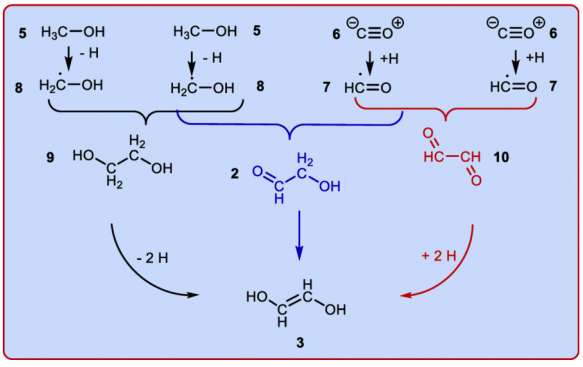

Fig. 2. (a) Simplified depiction of the traditional autocatalytic (with glycolaldehyde (**1a**)) formose reaction (top half) in aqueous media in the presence of base at ambient temperatures, and the proposed new reaction path via hydroxymethylene (**3a**) (bottom half) in the gas phase or on surfaces. Reproduced with permission from ref. [13]. Copyright 2018 Springer Nature. (b) Formation and equilibrium between gaseous **1, 2**, and **7** (top); Autocatalytic mechanism for the aqueous rormose reaction (bottom). Reproduced with permission from ref. [14]. Copyright 2018 American Chemical Society. (c) Derived reaction pathways in methanol–carbon monoxide ices leading to the formation of 1,2-ethenediol, in which *E*/Z isomers are omitted for clarity. Reproduced with permission from ref. [15]. Copyright 2021 American Chemical Society.

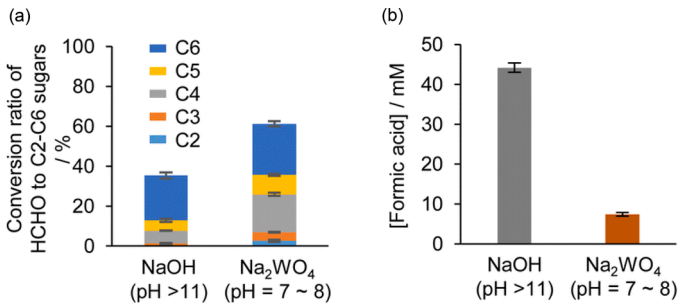

Fig. 3. (a) Conversion ratio of formaldehyde to C2 – C6 monosaccharides formed in the formose reaction at 80 °C with NaOH (60 mM, 17 min) and Na_2WO_4 (60 mM, 230 min) as a catalyst system. (b) Concentration of formic acid formed via the formose reaction at 80 °C using NaOH (60 mM, 17 min) or Na_2WO_4 (60 mM, 230 min) as a catalyst. Reproduced with permission from ref. [17]. Copyright 2023 The Royal Society of Chemistry.

solution (1 M), containing methanol (0.12 %), adjusted to pH 12 with NaOH at 120 °C and 200 kPa for 1 h. The products were trimethylsilylated and characterized by GC-MS. The GC-MS data exhibited signals ascribable to monosaccharides, *e.g.*, glucose, mannose, and xylose (Fig. 4b), although the yield of monosaccharides was 0.003 %. (Omran et al. [21] carried out formose reaction under the same hydrothermal conditions in the presence of a $CaCO_3$-based chemical garden, *i.e.*, a thin cylindrical solid consisting of silica and $CaCO_3$, and obtained similar results (see Section 3.1.3).)

Colloid systems have been utilized as media for formose reaction. Masaoka et al. [22] studied formose reaction in water pools of reverse micelles formed from Aerosol-OT (AOT), Triton X-100 (TX), and hexadecyltrimethylammonium bromide (CTAB), which contained formaldehyde (100 mM) and $Ca(OH)_2$ (20 mM), at 60 °C. The time–conversion plots exhibited no induction period, indicating that the formation of glycolaldehyde was accelerated in the interfacial water layer of reverse micelles (Fig. 5a). The ^{13}C nuclear magnetic resonance (NMR) spectrum for the product obtained in the AOT reverse micelles from formaldehyde-^{13}C as the starting material showed that the main product was ethylene glycol, which might be formed preferentially from glycolaldehyde and formaldehyde through Cannizzaro reaction. Gardner et al. [23] carried out formose reaction in vesicles formed from 1, 2-di-*O*-phytanoyl-*sn*-glycero-3-*O*-phosphocholine. The vesicles encapsulated formaldehyde (> 1.0 M) and $CaCl_2$. The reaction was initiated by adjusting the external pH to 12.5 and allowing OH^- to penetrate into the vesicles, and allowed to run at 37 °C for 4 h. The products were trimethylsilylated and characterized by GC-MS. The GC-MS data showed that pentoses (65 %), hexoses (15 %), tetroses, and heptoses were formed, indicating that pentoses were preferentially formed over the conventional formose reaction. Borate esters of the monosaccharides formed were able to stimulate a bioluminescence response as signal molecules in the natural quorum sensing mechanism of marine bacterium *Vibrio harveyi* (V. *harveyi*) (Fig. 5b). This observation can be viewed as communication from the artificial cells to V. *harveyi*. To investigate the importance of compartmentalization in the origin of life, Lu et al. [24] examined formose reaction in droplets (50 – 100 μm in size, compartments) fabricated using microchannels with a fluorinated oil as the continuous phase, fluorosurfactant (008-FluoroSurfactant, RAN Biotechnologies) and an amphiphilic triblock copolymer (perfluorinated polyether-*b*-poly(ethylene glycol)-*b*-perfluorinated polyether, PFPE-PEG-PFPE) as the dispersion medium (Fig. 5c). A combination of $CaCl_2$ and 1,1,3,3-tetramethylguanidine, and glycolaldehyde were used as a catalyst system and a cocatalyst, respectively. The aqueous phases were injected at 180 mbar and the oil phases were injected at 130 and 200 mbar. The reaction was carried out at 40 °C for 4 h. As the reaction proceeded, the volume of droplets more than doubled. The droplets were also split by shear, and the growth rate was affected by the transfer of components between the droplets. The product was converted to 2-hydroxymethylphenylboronate and characterized by mass spectrometry (MS), indicative of the formation of monosaccharides with carbon numbers up to 16.

Since boric acid and boronic acid form esters with diols, the effect of boric acid or boronic acid species on formose reaction was investigated [25–27]. Kim et al. [25] conducted a formose-type reaction for a mixture of glycolaldehyde (100 mM) and formaldehyde-^{13}C (50 mM) in a borate buffer (pH 10.4), which prepared by dissolving Na_2CO_3 (4.68 g, 44 mmol) and H_3BO_3 (0.688 g, 11 mmol) in water (40 mL), at 65 °C for 1 h. ^{13}C NMR data indicated that the product contained 5-^{13}C-ribose, 5-^{13}C-arabinose, and 1-^{13}C-xylulose as major products presumably because of stabilization by the formation of borate esters (Fig. 6). Imai et al. [26] studied formose reaction at 60 °C for an aqueous solution of formaldehyde (200 mM) in the presence of varying concentrations of sodium phenylboronate (SPB) or a copolymer of sodium 4-vinylphenylboronate and sodium 4-styrenesulfonate (pVPB/NaSS) using $Ca(OH)_2$ (20 mM) as a catalyst with a cocatalyst (glycolaldehyde or fructose (6.9 mM)) (Fig. 7a). After treatment of ion exchange resins, the products were characterized by HPLC, NMR, and MS. Monosaccharides with smaller carbon numbers (3 and 4) were favorably formed in the presence of SPB, whereas sugar alcohols with larger carbon numbers (6, 7, and 8) were preferably obtained in the presence of pVPB/NaSS. Michitaka et al. [27] carried out formose reaction for an aqueous solution of formaldehyde (1.0 M) in the presence of varying concentrations of phenylboronic acid (PBA) or a copolymer of *N,N*-dimethylacrylamide and 4-vinylphenylboronic acid (pDMA/VBA) at 60 °C using $Ca(OH)_2$ (120 mM) as a catalyst (Fig. 7a). The reaction mixtures were analyzed by Fourier transform infrared (FTIR) spectroscopy, and the products were characterized by liquid chromatography-mass spectroscopy (LC-MS) and ^{13}C NMR after treatment with ion exchange resins. PBA or pDMA/VBA formed boronic acid esters with the product to deaccelerate the reaction, resulting in favorable formation of branched monosaccharides and sugar alcohols with carbon numbers of 6 and 7 (Fig. 7b). Ishihara et al. [28] designed boronic acid species that bind preferably to target monosaccharides by machine learning using density functional theory (DFT) calculations. A comprehensive pool of 615,876 possible combinations, including 42 monosaccharide-derived boronic acid esters and 3003 commercially available monoboronic acid molecules, exhibited that bortezomib, *i.e.*, a molecular targeted therapeutics, was a promising candidate for selective capture of glucose, fructose, ribose, and arabinose.

The thiazolium moiety of thiamine diphosphate (ThDP), used as a coenzyme, activates aldehydes [29]. In the presence of ThDP, enzymes that catalyze condensation of formaldehyde molecules were used for formose reaction to produce selectively glycolaldehyde or 1,3-dihydroxyacetone [30–32]. Poust et al. [30] introduced four mutations into the active domain of benzaldehyde lyase (BAL), which catalyzes conversion of (*R*)-benzoin to benzaldehyde, to obtain an enzyme for formose reaction (Des0) as well as three mutants of Des0, into which three of the four mutations were introduced. Formose reaction was carried out for a solution of formaldehyde (10 mM or 0.2 mM) in a phosphate buffer (100 mM, pH 8), containing $MgSO_4$ (1 mM) and ThDP (0.5 mM), in the presence of one of the enzymes obtained (12.5 μM). The product was derivatized with *O*-(2,3,4,5,6-pentafluorobenzyl)hydroxylamine and then extracted into the organic layer. The product extracted was silylated with *N,O*-bis(trimethylsilyl)trifluoroacetamide (BSTFA) and characterized by GC-MS. At 10 mM formaldehyde, Des0 yielded glycolaldehyde and 1,3-dihydroxyacetone more efficiently than did the wild type of BAL. At 0.2 mM formaldehyde, on the other hand, Des0 produced glycolaldehyde more favorably than did the wild type (Fig. 8a). Lu et al. [31] developed an enzyme that catalyzes the conversion of formaldehyde to glycolaldehyde (GALS). The reaction was carried out at 37 °C for 2 h using an aqueous formaldehyde solution (2 g L^{-1}, 67 mM), which contained a potassium phosphate buffer (50 mM, pH 7.5), $MgSO_4$ (5 mM), ThDP (1 mM), and GALS (2 g L^{-1}), to produce

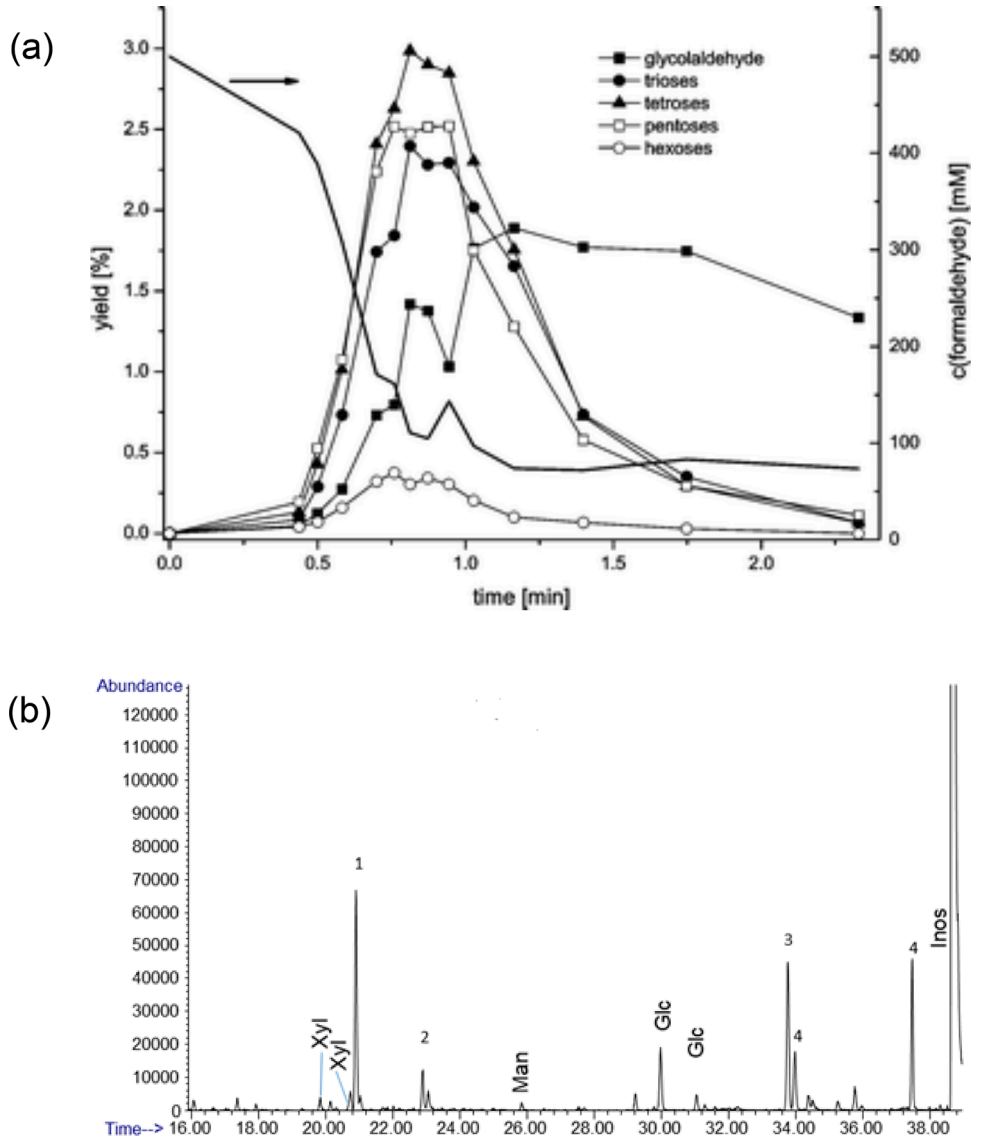

Fig. 4. (a) Kinetics of formaldehyde consumption and product formation of a 0.5 M formaldehyde solution in 0.1 M K_2HPO_4 at 200 °C and 100 bar. Reproduced with permission from ref. [19]. Copyright 2011 The Royal Society of Chemistry. (b) Gas chromatogram for an uncatalyzed formose reaction: an aqueous formaldehyde solution (1 M) of pH 12.5 containing methanol (0.5 M) was heated at 80 °C for 1 h. Glc, Man, and Xyl, represent glucose, mannose, and xylose, respectively. Peaks labeled 1 and 2 are organic acids coeluting with xylose, likely including saccharic acids. Peak 3 is sorbitol and peak 4 is myo-inositol, these were formed from the inositol standard, not the formose reaction. Reproduced from ref. [20] under the terms and conditions of the Creative Commons Attribution (CC BY) license (http://creativecommons.org/licenses/by/4.0/).

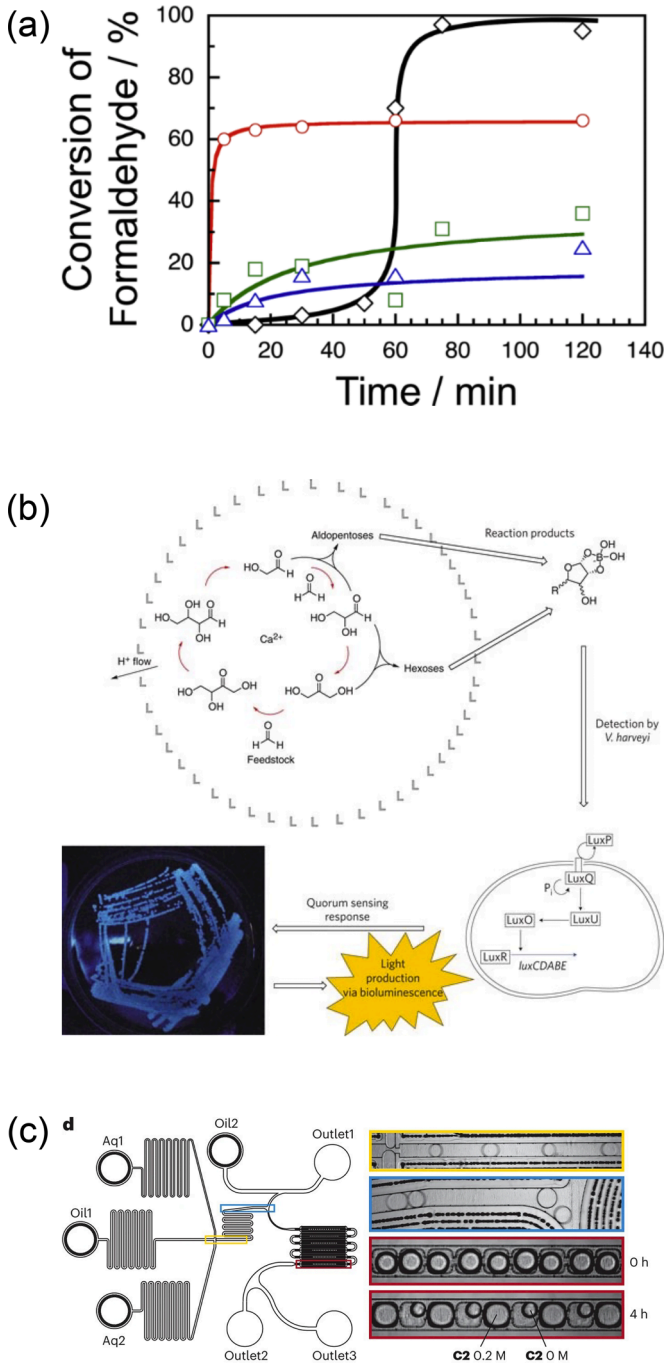

Fig. 5. (a) Time–conversion plots for formose reaction in an aqueous solution (black) and in water pools of AOT (red), TX (green), and CTAB reverse micelles (blue) at 60 °C. Reproduced from ref. [22] under the terms and conditions of the Creative Commons Attribution (CC BY) license (http://creativecommons.org/licenses/by/4.0/). (b) The chemical cell concept. The components of the autocatalytic formose reaction are encapsulated within a lipid (L) vesicle. The increased pH outside the vesicle initiates the production of carbohydrates. Carbohydrate–borate complexes are formed (top right), and these diffuse through the medium to interact with the bacterium V. *harveyi*. Reproduced with permission from ref. [23]. Copyright 2009 Springer Nature. (c) Microfluidic device used for 1D droplet arrays (left). Images of droplet formation (yellow rectangle), hydrodynamic switch (blue rectangle) and alternating 0.2 M glycolaldehyde (**C2**) droplets and no-**C2** droplets after 0 h and 4 h (red rectangles) (right). Reproduced with permission from ref. [24]. Copyright 2024 Springer Nature.

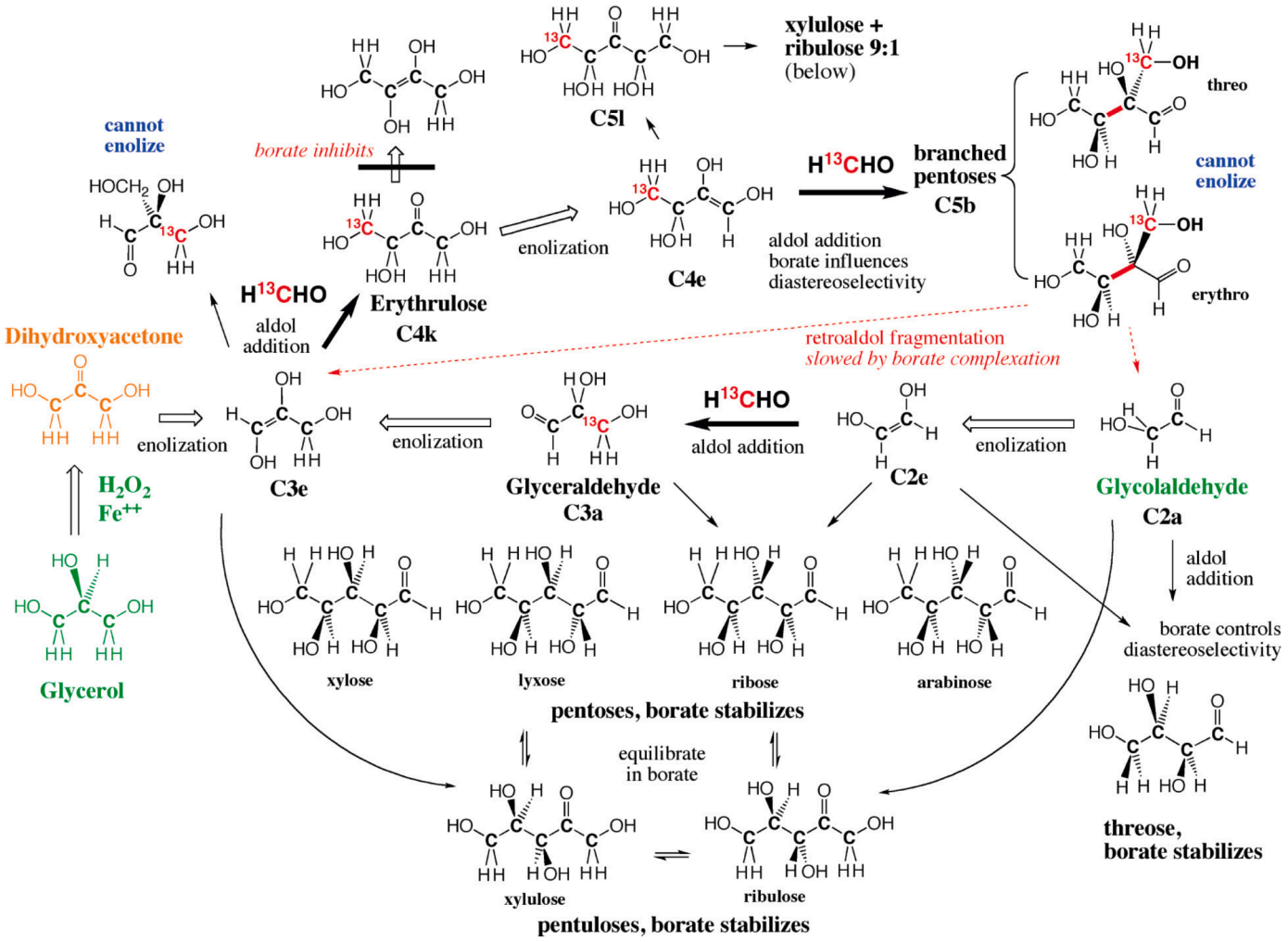

Fig. 6. Proposed borate-constrained abiotic metabolic cycle of formose reaction to form pentoses and pentuloses. Reproduced with permission from ref. [25]. Copyright 2011 American Chemical Society.

glycolaldehyde in a yield as high as *ca.* 80 % (Fig. 8b). Li et al. [32] constructed four mutants based on the enzyme (Des0) prepared by Poust et al. [30]. Formose reaction was performed using a mixture of a purified enzyme (0.027 mM), formaldehyde (100 mM), ThDP (0.5 mM), K_2HPO_4/KH_2PO_4 (50 mM), and $MgSO_4$ (5 mM) at pH 7.4 and 30 °C for 3 h. A colorimetric quantitative method that detects glycolaldehyde and 1, 3-dihydroxyacetone indicated that two of the mutants produced selectively glycolaldehyde whereas the other two mutants formed dominantly 1,3-dihydroxyacetone (Fig 8c). Massad and Banta [33] computationally engineered a 575 amino acid formolase (FLS) enzyme that catalyzes coupling of formaldehyde molecules to produce a mixture of glycolaldehyde and 1,3-dihydroxyacetone, and synthesized FLS together with two mutants (FLS M3 and FLS A3) using the *E. coli* expression system. Formose reaction was kinetically studied at 25 °C using solutions containing formaldehyde (0 – 260 mM), a sodium phosphate buffer (100 mM, pH 8), $MgSO_4$ (2 mM), and ThDP (0.1 mM) in the presence of one of the enzymes (FLS (0.2 – 1.8 μM), FLS M3 (0.2 – 1.8 μM), or FLS A3 (2 – 4.5 μM)). The glycolaldehyde and 1,3-dihydroxyacetone produced were detected using a coupling assay with glycerol dehydrogenase (50 mg L^{-1}) and reduced β-nicotinamide adenine dinucleotide (NADH) (0.8 mM). Massad and Banta [33] evaluated rate constants using an empirical kinetic model and ranked FLS and GALS mutants based also on the data by Lu et al. [31] (Fig. 8d). Yang et al. [34] showed that a stepwise cascade reaction combining FLS and D-fructose-6-phosphate aldolase (FSA) produced L-erythrulose and L-sorbose from formaldehyde (Fig. 8e).

3.1.3. *Formose reactions catalyzed by solid catalysts*

Tajima et al. [35–38] used thiazolium salts immobilized on solid supports as solid catalysts for formose reaction. The thiazolium catalyst was supported on a cation exchange resin, and a mixture of paraformaldehyde (6.7 mmol), 2-(dimethylamino)ethanol (5 mmol), 1, 4-dioxane (18 mL), and the catalyst resin (in the H form and wet state, 10 mL) was heated using a water bath thermostated at 60 °C for 2 h under an argon atmosphere with stirring [36]. The product was trimethylsilylated and characterized by gas chromatography (GC). The GC data indicated that a mixture containing 1,3-dihydroxyacetone and erythrulose was obtained. The catalytic activity of the resin decreased upon washing with organic solvents, but was restored upon washing with water (Fig. 9a). Tajima et al. [37] studied quantitatively the effects of counter anions and solvents on the catalytic activity of thiazolium in formose reaction using a highly active immobilized catalyst in which thiazolium salts were supported on crosslinked polystyrene. Formose reaction was carried out using mixtures of paraformaldehyde (0.5 M), 2-(dimethylamino)ethanol (0.5 M), catalyst resins (0.1 g) containing various counter anions (at 80 °C), and various solvents (at 60 °C) under an argon atmosphere. The concentrations of formaldehyde were determined at varying times. Using time–conversion plots, the pseudo-first-order reaction rate constants (k_{app}) were evaluated. A higher k_{app} was obtained for a counter anion with larger pK_a and for a solvent with larger solvent parameter (Dimroth–Reichardt ET parameters) (Fig. 9b). Tajima et al. [38] also carried out formose reaction for a solution of paraformaldehyde (6.7 mmol) and 2-(dimethylamino)

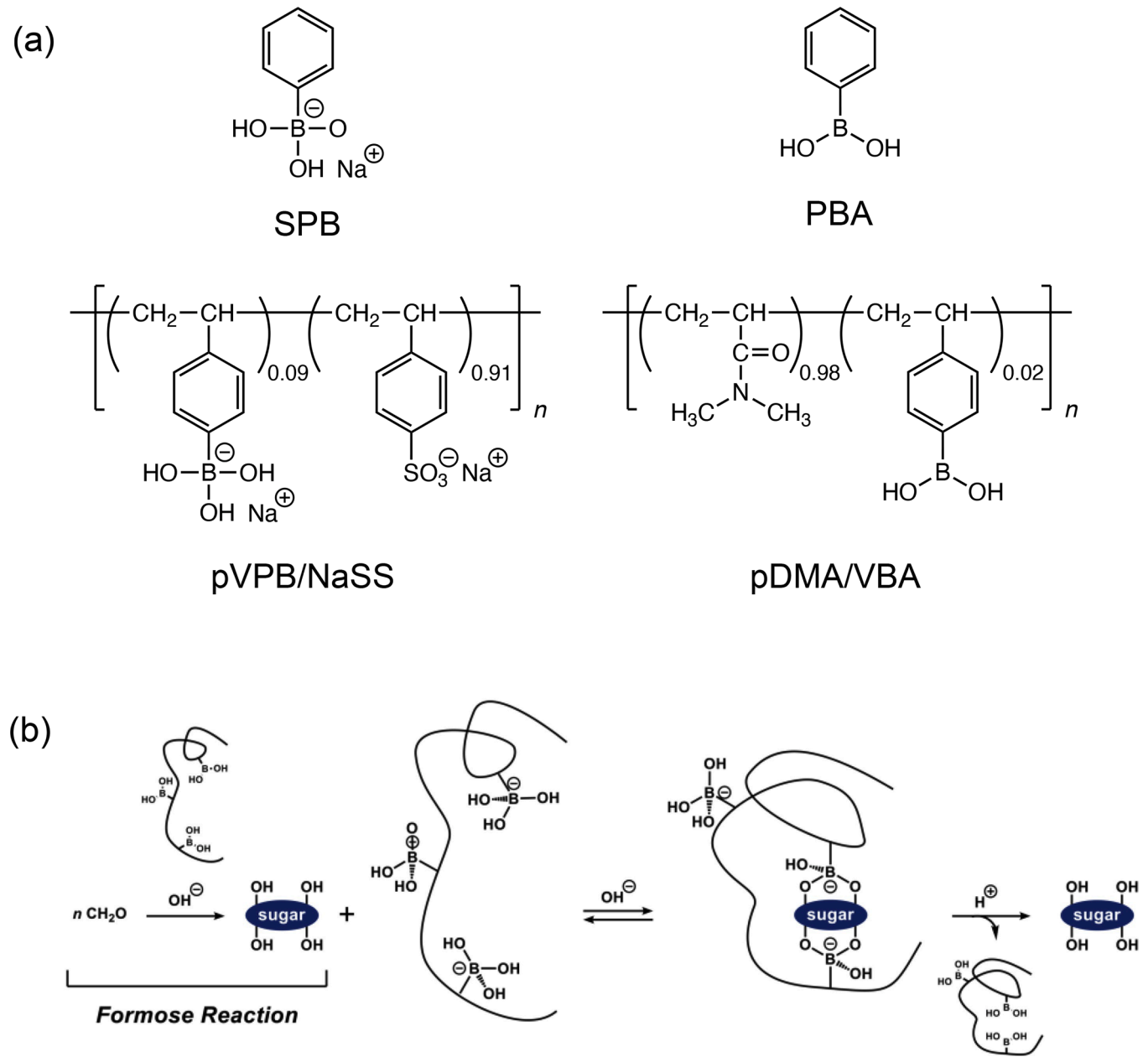

Fig. 7. (a) Structures of the boronic acid compounds used (*i.e.*, SPB, PBA, and pVPB/NaSS, pDMA/VBA). (b) Conceptual illustration of formose reaction in the presence of a boronic acid polymer, in which the polymer stabilizes the product via ester formation, leading to an enhanced selectivity. Reproduced from ref. [27] under the terms and conditions of the Creative Commons Attribution (CC BY) license (http://creativecommons.org/licenses/by/4.0/).

ethanol (5 mmol) in a solvent (*i.e.*, 1,4-dioxane, 1,4-dioxane/water (1/1), ethanol, or *N,N*-dimethylformamide) (18 mL) at 60 °C under an argon atmosphere using zeolite (Wako, F-9, pore size 0.9 nm) loaded with thiazolium catalysts (thiamine (Th), 3-ethylbenzothiazolium (BTh), or 3-ethyl-5-(2-hydroxyethyl)-4-methylthiazolium (ETh)). The products were trimethylsilylated and characterized by GC-MS. The GC-MS data exhibited that 1,3-dihydroxyacetone, erythrulose, and 4-hydroxymethyl-2-pentulose were obtained, indicating that zeolites loaded with Th or ETh catalyzed formose reaction in organic solvents. Furthermore, Tajima et al. [39] investigated the mechanism of formose reaction catalyzed by thiazolium salts using the MOPAC-PM3 semi-empirical molecular orbital (MO) method. They indicated that an ion pair of the zwitterionic intermediate and an ammonium ion was first formed and then the intermediate 2-hydroxymethyl-3-ethyl-5-(2-hydroxyethyl)-4-methylthiazolium was formed (Fig. 9c). Recently, Wang et al. [40] immobilized thiamine (vitamin B1) onto an insoluble aromatic polymer network obtained by Sonogashira coupling of 1,3,5-tribromo-2-(4-bromobutoxy)benzene and 1,4-diethynylbenzene (Poly-OC4Br-VcB1). They also treated Poly-OC4Br-VcB1 with a (trimethylsilyl)methyllithium solution to obtain Poly-OC4Br-VcB1-TMSiL. A mixture of Poly-OC4Br-VcB1 (60 mg), powdered paraformaldehyde (180 mg), triethylamine (84 μL), and *N,N*-dimethylformamide (1 mL) was heated at 90 °C for 2 h with stirring. ^{1}H NMR showed that the product was 1,3-dihydroxyacetone. When Poly-OC4Br-VcB1-TMSiL was used, 1,3-dihydroxyacetone was produced even in the absence of triethylamine. Notably, formaldehyde was repeatedly converted to 1,3-dihydroxyacetone by a continuous flow reaction using a Soxhlet extractor containing Poly-OC4Br-VcB1-TMSiL (a solid catalyst) and 1,4-dioxane (a solvent) (Fig. 10).

Simonov et al. [41] carried out formose reaction using a phosphate (pH 7.3) or borate buffer (pH 7.7) containing formaldehyde (0.1 M), 1,3-dihydroxyacetone (5 mM), and a catalyst at 40 or 60 °C. A solid

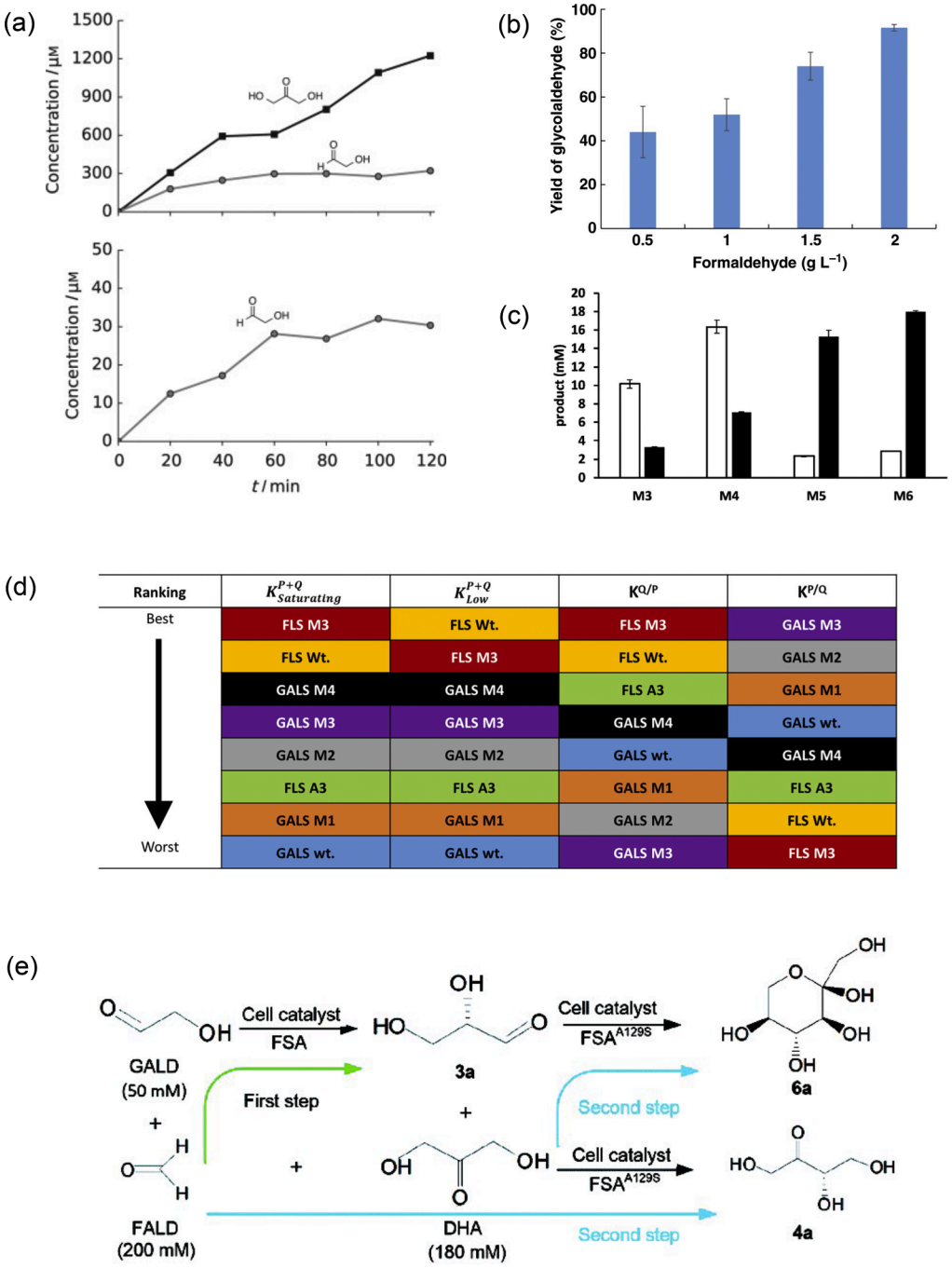

Ranking	$K_{Saturating}^{P+Q}$	K_{Low}^{P+Q}	$K^{Q/P}$	$K^{P/Q}$
Best	FLS M3	FLS Wt.	FLS M3	GALS M3
	FLS Wt.	FLS M3	FLS Wt.	GALS M2
	GALS M4	GALS M4	FLS A3	GALS M1
	GALS M3	GALS M3	GALS M4	GALS wt.
	GALS M2	GALS M2	GALS wt.	GALS M4
	FLS A3	FLS A3	GALS M1	FLS A3
	GALS M1	GALS M1	GALS M2	FLS Wt.
Worst	GALS wt.	GALS wt.	GALS M3	FLS M3

Fig. 8. (a) Product profiles of the formolase Des0 at 10 mM (upper) and 0.2 mM (lower) formaldehyde concentrations. Reproduced with permission from ref. [30]. Copyright 2015 Wiley-VCH. (b) The synthesis of glycolaldehyde from formaldehyde by GALS. Reactions were executed under different formaldehyde concentrations with 2 mg mL^{-1} purified GALS at 37 °C for 2 h. Reproduced from ref. [31] under the terms and conditions of the Creative Commons Attribution (CC BY) license (http://creativecommons.org/licenses/by/4.0/). (c) The amount of glycolaldehyde (white bar) and 1,3-dihydroxyacetone (black bar) produced by the parent M3 and variants M4, M5, and M6. The reaction was carried out using enzyme (0.027 mM) and formaldehyde (100 mM) at 30 °C for 3 h. Reproduced with permission from ref. [32]. Copyright 2019 The Royal Society of Chemistry. (d) Ranking of FLS variants based on overall activity at saturating substrate concentrations, dilute substrate concentrations, preference for 1,3-dihydroxyacetone (Q) production, and preference for glycolaldehyde (P) production. Reproduced with permission from ref. [33]. Copyright 2022 Wiley-VCH. (e) Stepwise whole-cell transformation to synthesize **4a** and **6a**. In the first step, FALD, GALD, and the resting cells expressing FSA were mixed. Once GALD was completely consumed, DHA and the resting cells expressing FSA^{A129S} were added in the second step. Reproduced with permission from ref. [34]. Copyright 2017 The Royal Society of Chemistry.

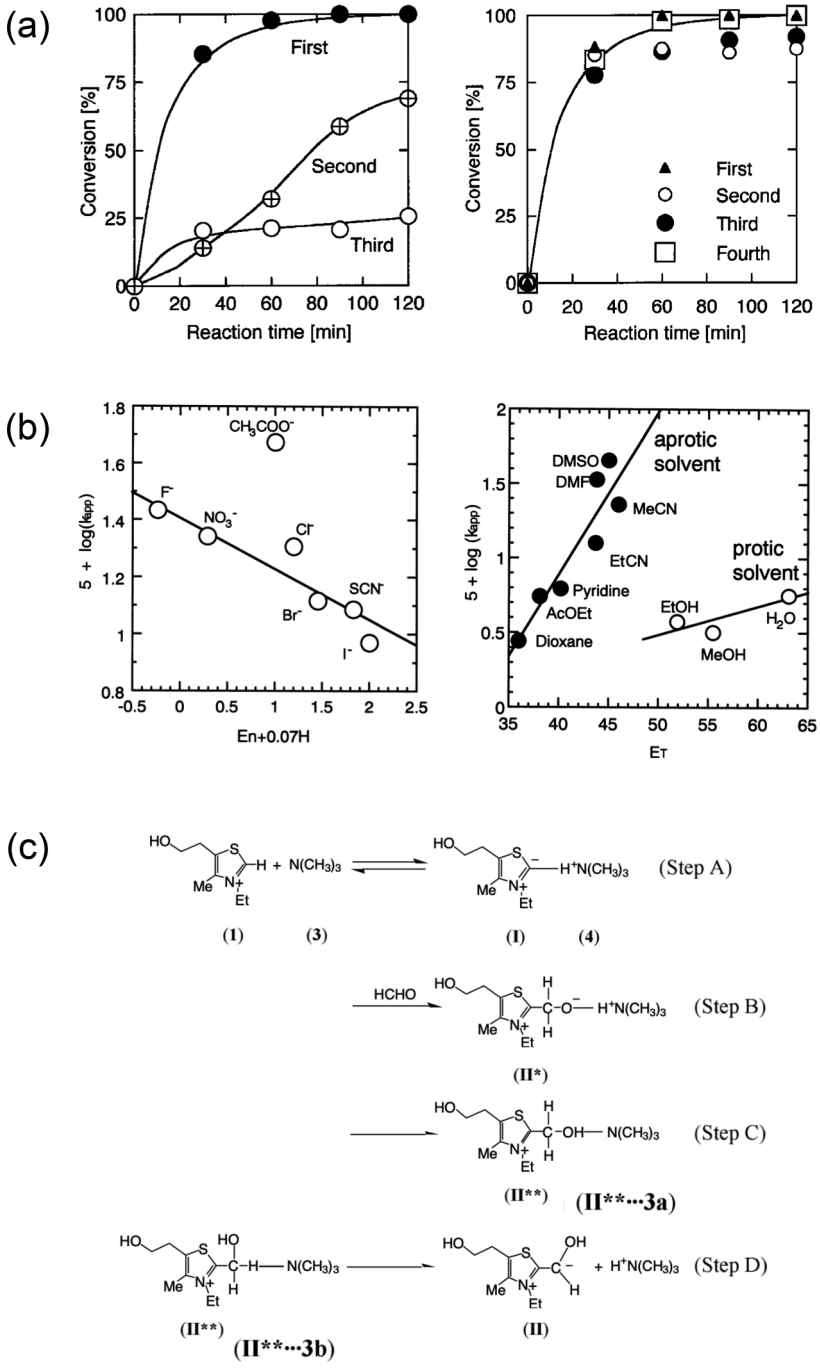

Fig. 9. (a) Time–conversion plots in formose reaction with 1,4-dioxane (left) and water-washed (right) catalyst resin. Paraformaldehyde, 6.7 mmol: DAE, 5 mmol: 1,4-dioxane, 1.8×10^{-5} m^3: IR-120B (in H^+ form, wet state), 1.0×10^{-5} m^3: thiamine hydrochloride, 3 mmol: argon atmosphere, 60 °C. Reproduced with permission from ref. [36]. Copyright 2000 The Chemical Engineering of Japan. (b) Relationship between k_{app} and parameter *En* or *H* (left) and the plot of $\log(k_{app})$ against E_T parameter (right). Reproduced with permission from ref. [37]. Copyright 2001 The Chemical Engineering of Japan. (c) Proposed mechanism of formose reaction catalyzed by a thiazolium salt with an ammonium ion. Reproduced with permission from ref. [39]. Copyright 2003 Society of Computer Chemistry, Japan.

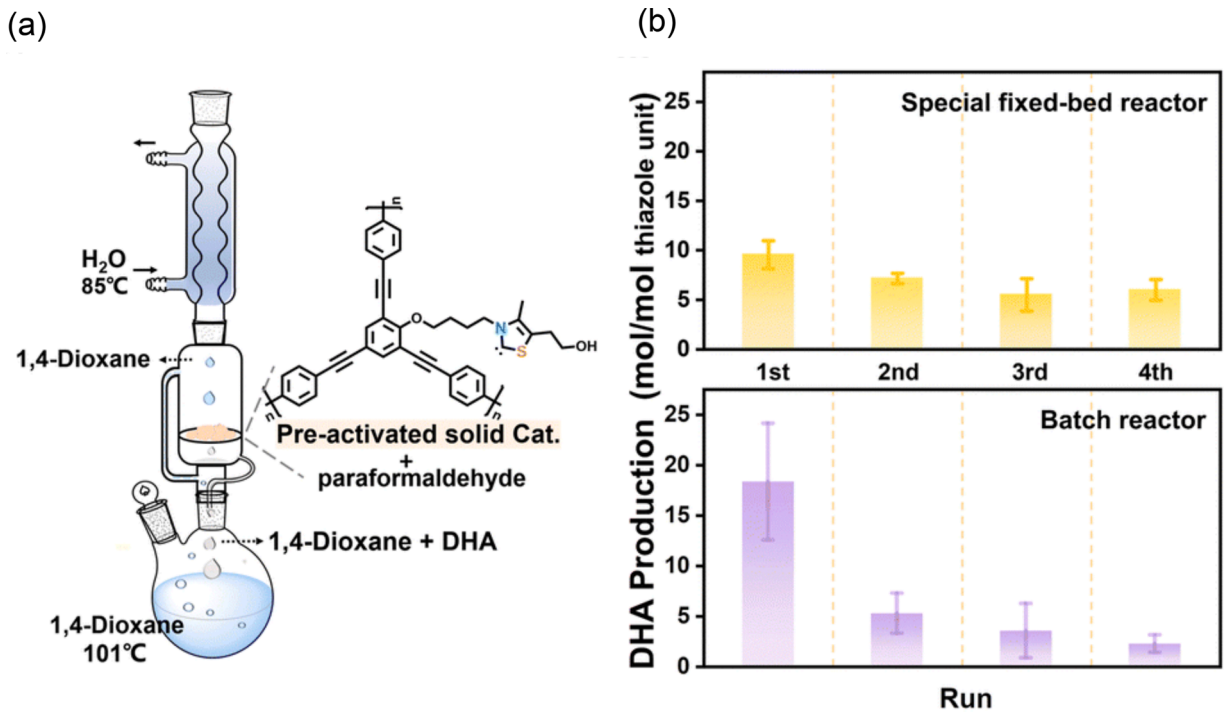

Fig. 10. (a) The reactor based on the Soxhlet extractor for the continuous solvent-flow formaldehyde condensation reaction. (b) Reusability of pre-activated poly-OC_4Br-VcB1-TMSiLi under continuous-flow or batch conditions. Reproduced with permission from ref. [40]. Copyright 2023 The Royal Society of Chemisty.

compound (hydroxylapatite, $Ca_3(PO_4)_2$, or $CaCO_3$), a natural mineral (apatite or vivianite), or soluble phosphates was used as a catalyst. The products were derivatized with 2,4-dinitrophenylhydrazine and characterized by HPLC. The HPLC data indicated that erythrulose and 3-pentulose were formed as main products, and branched pentulose and hexulose were also produced as minor components (Fig. 11a). In addition, Simonov et al. [42] reported that erythrose, threose, ribose, arabinose, and fructose were produced by a reaction between glycolaldehyde and glyceraldehyde using apatite (10 g L^{-1}), Na_2HPO_4/KH_2PO_4 (0.02 M), or $Na_2B_4O_7$ (0.02 M) as a catalyst at 40 °C (Fig. 11b).

Hashidzume et al. [43] prepared porous alumina samples by the sol-gel method using aluminum tri-*sec*-butoxide in the presence of D-glucose, D-ribose, or sucrose, followed by calcination. The crystallinity and porosity of the obtained alumina samples were dependent on the amount of added sugar and the calcination temperature; The crystallinity increased whereas the porosity decreased as the amount of added sugar was decreased or the calcination temperature was increased. The alumina samples with lower crystallinity exhibited higher sugar adsorption capacity and higher catalytic activity for formose reaction of an aqueous formaldehyde solution (36 % (*ca.* 13 M), 1.25 mL) at 90 °C using an alumina sample (1.0 g) and fructose (13 mM) as catalyst and cocatalyst, respectively (Fig. 12). These observations indicate that defects in the porous alumina samples act as strong basic sites.

Schreibersite is a rare iron-nickel phosphide mineral $(Fe,Ni)_3P$ that may react with organic compounds to form nucleotides and phospholipids [44]. Pallmann et al. [45] used synthetic schreibersite (1 g) as a catalyst for formose-type reaction of monosaccharides. They carried out reactions using aqueous solutions (1 mL) containing monosaccharides (0.250 M) at 80 °C for 1 or 7 day(s). The products were trimethylsilylated with BSTFA and characterized by GC-MS. In the presence of synthetic schreibersite, tetroses and hexoses were formed from glycolaldehyde, and hexoses were obtained from a combination of glyceraldehyde and 1,3-dihydroxyacetone. In addition, larger monosaccharides were produced using combinations of formaldehyde and glycolaldehyde, glycolaldehyde and glyceraldehyde, and glycolaldehyde and 1,3-dihydroxyacetone. These results were indicative of the catalytic activity of synthetic schreibersite for formose reaction (Fig. 13a). Colón-Santos et al. [46] repeated the formose reaction cycle in the presence of minerals and characterized the products. An aqueous formaldehyde solution (37 % (*ca.* 13.6 M), 0.5 mL), glycolaldehyde (0.0126 g), and $Ca(OH)_2$ (0.0705 g) were dissolved in a mixed solvent of water and formamide (2.25 mL/2.25 mL). The solution was heated at 50 °C for 48 h in the presence of goethite (α-FeO(OH), montmorillonite ($(Na,Ca)_{0.33}(Al,Mg)_2(SiO_{10})$), hydroxyapatite ($Ca_5(OH)(PO_4)_3$), chalcopyrite ($CuFeS_2$), ulexite ($NaCaB_5O_6(OH)_6\bullet 5H_2O$), zoisite ($Ca_2Al_3(SiO_2)_3(OH)$), or quartz ($SiO_2$) with stirring at 1200 rpm (Fig. 13b). The products were treated with an ion exchange resin and then characterized by ultra-high pressure liquid chromatography-tandem mass spectroscopy (UPLC-MS/MS). The UPLC-MS/MS characterization data indicated that the products included ribose, uracil, and hexamethylenetetramine, and the total number of products detected decreased with increasing the number of cycles. Omran et al. [47] heated an aqueous solution containing formaldehyde (1 M), methanol (0.5 M), and NaOH (pH 12.5) at 90 °C in the presence of various solid catalysts (0.5 g). The solids used were minerals of olivine, serpentine, and Ca-Mg carbonates, and artificial Ca/Mg-chemical garden. The products were characterized by NMR in D_2O or by GC-MS after per-*O*-trimethylsilylation with Pierce's Tri-Sil reagent. The characterization data exhibited that the main products were formic acid, glycolic acid, lactic acid, acetic acid, and methanol, and only small amounts of monosaccharides were also produced. These results indicate that Cannizzaro reaction was predominant. Vinogradoff et al. [48] carried out formose reaction by heating an aqueous mixture of olivine (100 g L^{-1}) and formaldehyde (10 g L^{-1} (*ca.* 0.33 mM)) at 80 °C for 2, 7, or 45 days in the presence and absence of glycolaldehyde (1 g L^{-1} (*ca.* 0.017 mM)) (Fig. 13c). The products were trimethylsilylated with BSTFA and characterized by two-dimensional GC-MS using CPChirasil-Dex CB and DB Wax columns. All the products were complicated mixtures containing trioses, tetroses, pentoses, and hexoses, whereas the amount of sugar alcohols increased with increasing the reaction time, indicating that Cannizzaro reaction became predominant for a longer reaction time. Furthermore, the mechanism of glycolaldehyde formation on the olivine surface was investigated by

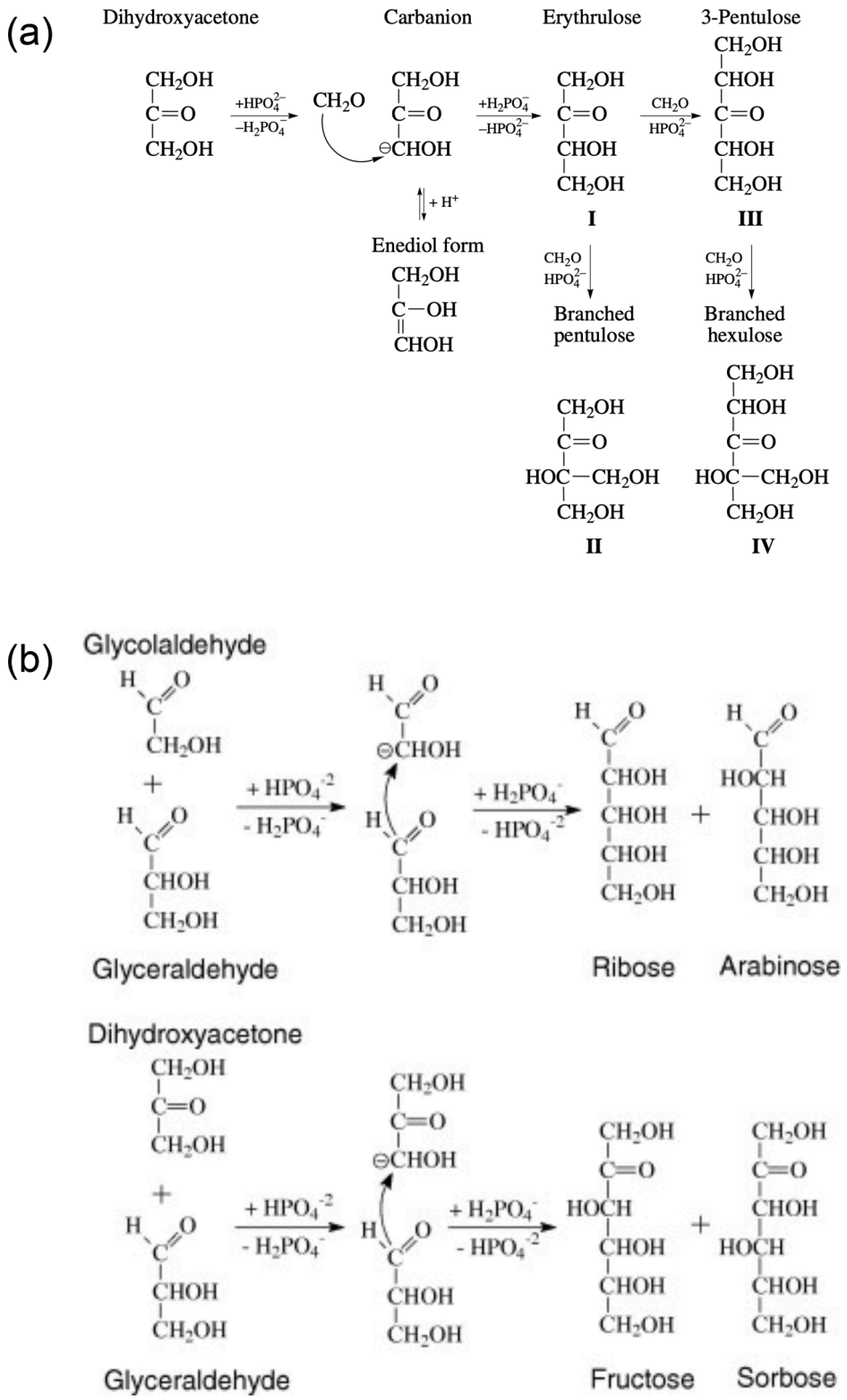

Fig. 11. (a) Condensation of formaldehyde and dihydroxyacetone in the presence of phosphates. Reproduced with permission from ref. [41]. Copyright 2007 Springer Nature. (b) Formation of ribose and fructose from glycolaldehyde and glyceraldehyde in the course of aldol reactions. Reproduced with permission from ref. [42]. Copyright 2007 Elsevier.

DFT calculations.

Vojood et al. [49–51] used fumed silica catalyst for formose reaction. In the presence of fumed silica or montmorillonite (0.17 g), formose reaction was conducted for an aqueous formaldehyde solution (*ca.* 3.8 % (*ca.* 1.3 M)) by adjusting the solution pH to 7.5 – 9.6 with 2 M NaOH at 60 ± 5 °C under a nitrogen atmosphere [49]. After quenching with 6 M hydrochloric acid and removing the solvent, the products were extracted with methanol and characterized by GC-MS. In the presence of fumed silica catalyst, as the pH increased from 7.6 to 9.3, the amount of ethylene glycol produced decreased, whereas the amount of

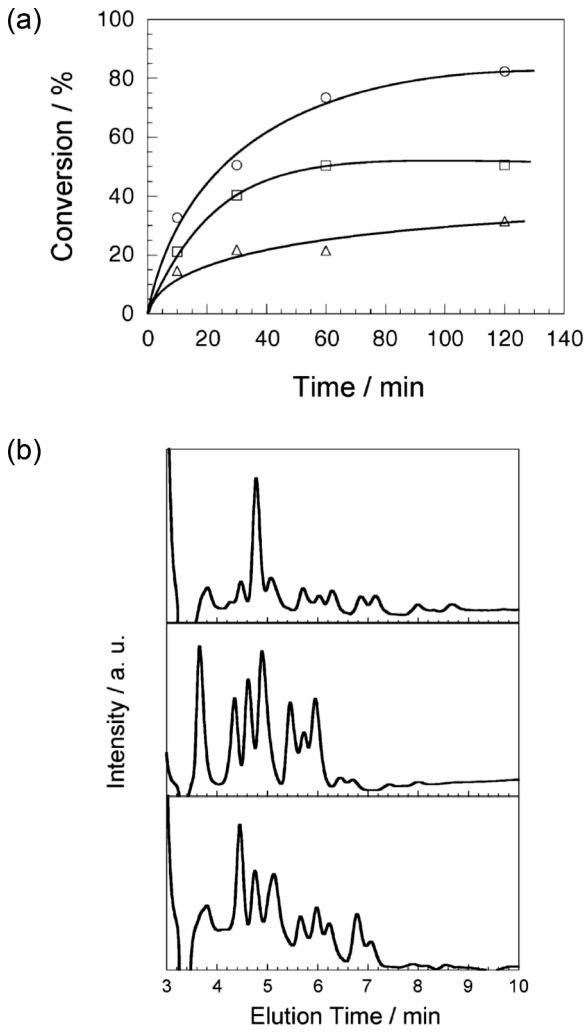

Fig. 12. (a) Time–conversion plots for formose reaction at 90 °C using commercially available activated alumina (triangle) and the porous alumina samples prepared in the absence and presence of glucose (PA-300 (square), and PA-G10–300 (circle), respectively). (b) HPLC diagrams for the formose products at 90 °C after 1 h using commercially available activated alumina (top), PA-300 (middle), and PA-G10–300 (bottom). Reproduced with permission from ref. [43]. Copyright 2010 The Society of Polymer Science, Japan.

glyceraldehyde produced increased (Fig. 14a). When montmorillonite was used, the activity was lower than that of fumed silica, but the same tendency was observed. In the presence of fumed silica (0.08 g), an aqueous formaldehyde solution (37 % (*ca.* 13.6 M), 11 mL) was dissolved in methanol (100 mL), and a reaction was carried out at 60 °C by adjusting the solution pH to 7.8 with 2 M NaOH [50] (Fig. 14b). The production of ethylene glycol (*ca.* 9 mM) was confirmed after 600 min by GC-MS in the same way. Ethylene glycol was obtained more efficiently (*ca.* 30 mM after 600 min) when montmorillonite was used in water. When the reaction was carried out in methanol in the presence of fumed silica at pH 10.6 and 60 °C for 90 min, ethylene glycol (*ca.* 5 mM) was also produced [51]. There was no significant difference in the reactions at pH 7.8 and pH 10.6.

Balloi et al. [52] used four types of zeolitic imidazolate frameworks (ZIF) as catalysts for formose reaction. Formose reaction was carried out using an aqueous mixture (*ca.* 1 mL) of formaldehyde (0.4 mmol), a ZIF (a catalyst, 20 mg), and glycolaldehyde (a cocatalyst, 0.5 mmol) at 60 °C for 30 min or 24 h. The products were derivatized with 2,4-dinitrophenylhydrazine and characterized by HPLC. The HPLC data indicated that the product consisted dominantly of trioses and tetroses after 30 min, whereas the product was a complicated mixture containing pentoses, hexoses, and sugar alcohols (*e.g.*, ribose, ribulose, arabinose, xylitol, fructose, tagatose, glucitol, and dulcitol) after 24 h. Waki et al. [53] utilized zeolitic materials, including Linde type A zeolite, faujasite type zeolite, and mordenite type zeolite, as heterogeneous catalysts for formose reaction. Formose reaction was carried out by simply adding Ca^{2+}-loaded Linde type A zeolite (Ca-LTA) (300 mg) to an aqueous solution (10 mL) containing formaldehyde (0.15 M) and glycolaldehyde (0.075 M, a cocatalyst) for 72 h at room temperature. The product was derivatized with 2,4-dinitrophenylhydrazine and characterized by HPLC. The HPLC data revealed that a mixture of trioses, tetroses, pentoses, and hexoses was obtained (Fig. 15a). Other zeolites were also active for formose reaction. A reaction mechanism was proposed in which the mild basicity of the oxygen atoms of the aluminosilicates on the zeolite surface and the acidity of the metal ions promoted the formation of C–C bonds (Fig. 15b).

3.1.4. *Formose reactions under mechanochemical conditions*

Mechanochemical reactions are conducted in the solid state under solvent-free conditions, and thus have attracted attention as an environmentally friendly synthetic method. Recently, formose reaction has been performed under mechanochemical conditions to model events upon meteorite impacts [54–56]. Trapp et al. [54] performed formose reaction by grinding glycolaldehyde (20.8 mmol) and $Ca(OH)_2$ (4.18 mmol), or a one-to-one glycolaldehyde/glyceraldehyde mixture (0.86 mmol/0.86 mmol) and $Ca(OH)_2$ (0.35 mmol), in a vibratory ball mill with a 7 mm stainless steel ball at a frequency of 30 Hz for 90 min. The products were dissolved in pyridine, trimethylsilylated with BSTFA, and characterized by GC-MS. The GC-MS data indicated that tetroses and hexoses were obtained from glycolaldehyde, whereas tetroses, pentoses, hexoses, and heptoses were obtained from the glycolaldehyde/glyceraldehyde mixture (Fig. 16a). In addition, when formaldehyde (4.16 mmol)-containing molecular sieves, glycolaldehyde (4.16 mmol), and $Ca(OH)_2$ (1.67 mmol) were milled at 400 rpm for 90 min, a mixture of trioses to heptoses was obtained (Fig. 16a). Trapp et al. [55] also studied mechanochemical formose reaction catalyzed by a rock (basalt) and representative minerals of hydroxides, carbonates, sulfates, silicates, mica, zeolites, clays, olivines, phosphates, phosphides, and borates (0.2 eq.), using glycolaldehyde (0.5 eq.) as a starting material. They carried out reactions at room temperature by milling mixtures at a frequency of 30 Hz for 90 min. As a result, basalt and all minerals, other than anhydrous ferrite (sulfate mineral) and colemanite (borate mineral), produced tetroses and hexoses (Fig. 16b). In addition, when formaldehyde (1.0 eq.)-containing minerals and glycolaldehyde (0.5 eq.) were milled at 400 rpm for 90 min, a mixture of trioses to heptoses was obtained (Fig. 16b).

Yang et al. [56] synthesized a novel covalent organic framework (COF) material (Zn-COF), which was based on tetrakis(4-ethynylphenyl) methane (5,5′,5′′,5′′′-((methanetetrayltetrakis(benzene-4,1-diyl))tetrakis(ethyne-2,1-diyl))tetrakis(3-(tertbutyl)-2-hydroxybenzaldehyde) and possessed a Zn–salen complex structure (Fig. 16c). Glycolaldehyde dimer (60 mg) and Zn-COF (100 mg) were placed in a stainless steel container with a stainless steel ball and the mixture was milled at 30 Hz and 37 °C for 2 h. The reaction under mechanochemical conditions showed a higher conversion than did the heterogeneous reaction in THF. The products were dissolved in pyridine and trimethylsilylated with BSTFA, and characterized by GC-MS. The GC-MS data exhibited that tetroses were preferentially produced (Fig. 16c). The coordination structures of two glycolaldehyde molecules to the Zn–salen complex, which yield different isomers, were compared based on DFT calculations.

3.1.5. *Formose reactions under light irradiation*

Some examples of photochemical formose reaction have been reported [42,57–62]. Pentunove et al. [57] irradiated an aqueous formaldehyde solution (0.5 M, 1 – 2 mL) in a quartz cell with ultraviolet (UV) light using an ArF excimer laser (wavelength 193 nm, pulse duration 15

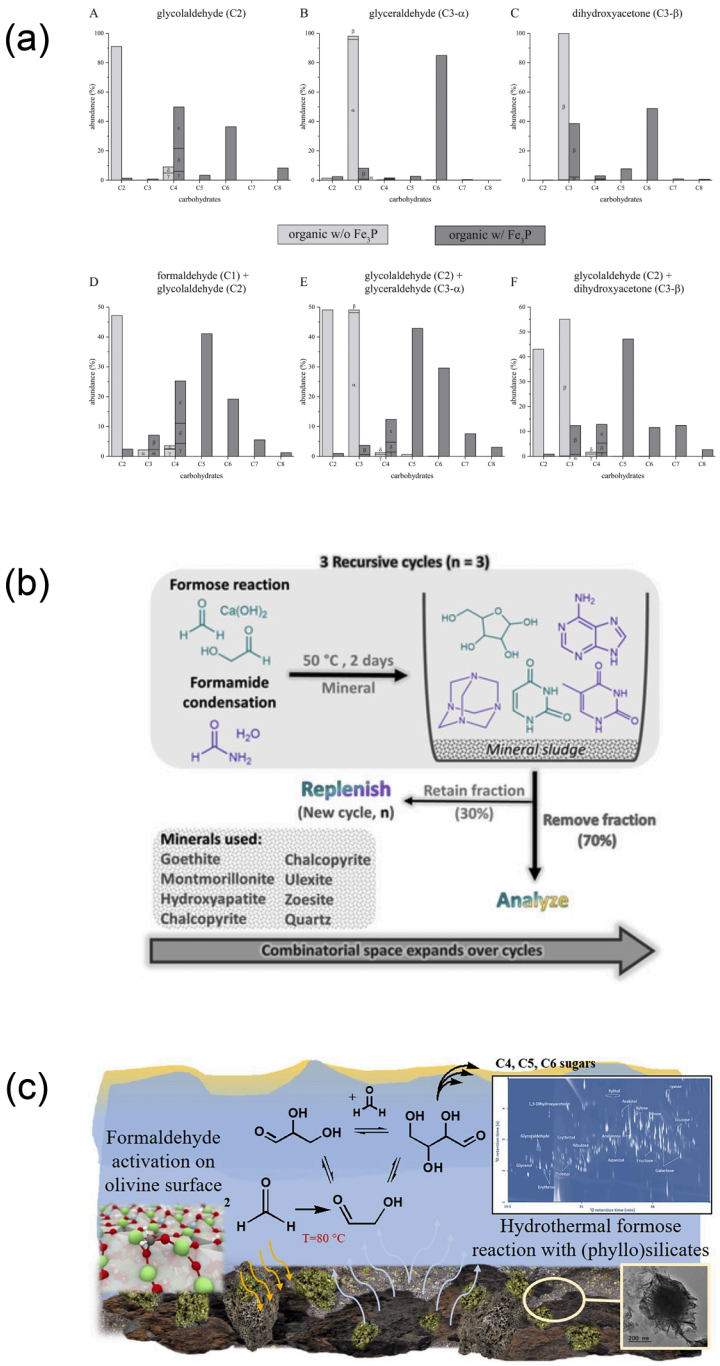

Fig. 13. (a) Product distribution of schreibersite catalyzed formose and formose type reaction in the presence of (A) glycolaldehyde, (B) glyceraldehyde, (C) 1,3-dihydroxyacetone, (D) formaldehyde and glycolaldehyde, (E) glycolaldehyde and glyceraldehyde, and (F) glycolaldehyde and dihydroxyacetone. Greek labeling denotes the following compounds: (α) glyceraldehyde, (β) dihydroxyacetone, (γ) erythrose, (δ) threose, (ε) erythrulose. Reproduced from ref. [45] under the terms and conditions of the Creative Commons Attribution (CC BY) license (http://creativecommons.org/licenses/by/3.0/). (b) Recursive cycles: A formose reaction (green) in formamide/water (purple) is carried out in the presence of a mineral. After each cycle of 48 h at 50 °C, a fraction of the total volume (70 %, from the top) is removed and the vial is replenished with fresh starting materials to start the next cycle. Reproduced from ref. [46] under the terms and conditions of the Creative Commons Attribution (CC BY) license (http://creativecommons.org/licenses/by/4.0/). (c) Olivine-catalyzed glycolaldehyde and sugar synthesis under aqueous conditions. Reproduced with permission from ref. [48]. Copyright 2024 Elsevier.

ns, 2 Hz pulse frequency with 75 mJ pulse energy; the beam area 24 mm^2). Carbon monooxide, methane, carbon dioxide, and hydrogen were detected in the gas phase by GC. The products in the solution were derivatized with 2,4-dinitrophenylhydrazine and characterized by HPLC. The HPLC data indicated that glycolaldehyde and glyceraldehyde were formed in 4.2 % and 0.18 % yield, respectively. Snytnikova et al. [58] irradiated an aqueous formaldehyde solution (11.8 M, pH 3.18) in a quartz cell with full light from a DRSh-500 high pressure mercury lamp for 4, 8, 18, 24, and 28 h. The products were derivatized with 2,4-dinitrophenylhydrazine and characterized by HPLC. The pH of the irradiated solution decreased with the irradiation time, indicating that Cannizzaro reaction proceeded preferentially to form formic acid as the main product. Notably, the HPLC data indicated that glycolaldehyde and small amounts of 3 – 6 carbon monosaccharides were also formed (<

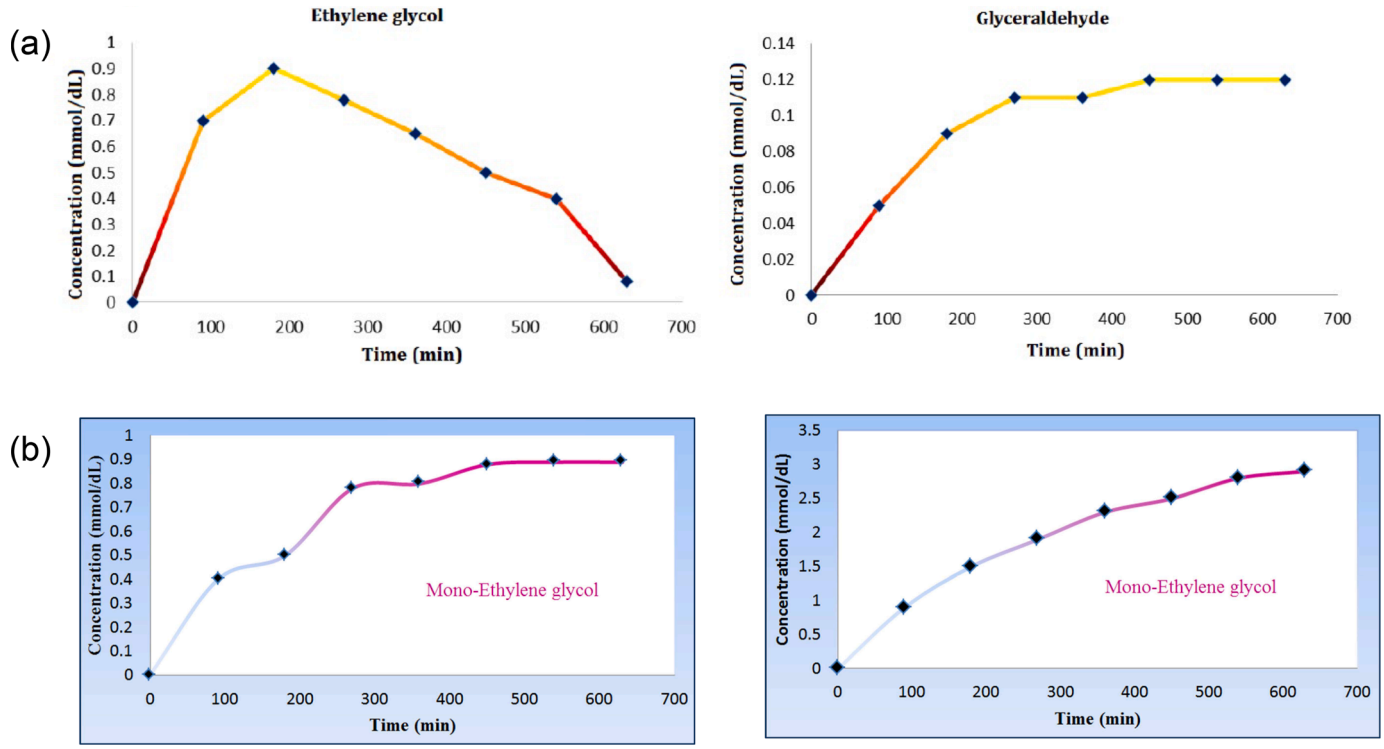

Fig. 14. (a) The time evolutions of concentrations of ethylene glycol (pH = 9.3, left) and glycolaldehyde (pH = 9, right) for formose reaction in the presence of a fumed silica catalyst under basic conditions. Reproduced from ref. [49] under the terms and conditions of the Creative Commons Attribution (CC BY) license (http://creativecommons.org/licenses/by/4.0/). (b) The time evolutions of concentration of ethylene glycol for formose reaction using methanol (left) or water (right) as a solvent in the presence of a fumed silica catalyst. Reproduced from ref. [50] under the terms and conditions of the Creative Commons Attribution (CC BY) license (http://creativecommons.org/licenses/by/4.0/).

1 % yield in total).

Simonov et al. [42] performed formose reaction by irradiating a solution of formaldehyde (1.12 M or 1.79 M) in a phosphate buffer (0.01 M Na_2HPO_4/KH_2PO_4) with a high-pressure mercury lamp (254, 297, 313, and 365 nm) and then heating at 60 or 70 °C for varying times. HPLC data for the samples derivatized with 2,4-dinitrophenylhydrazine confirmed that erythrulose and 3-pentulose were produced as main products (< 2 % yield in total) with production of erythrose and threose as minor components.

Stovbun et al. [59–62] irradiated an aqueous formaldehyde solution (95 %), which was prepared by decomposition of paraformaldehyde at 160 – 170 °C for 1.5 h, with UV light using a DRSh-100 lamp (without filters) at 70 °C for 8.5 h after the solution had completely solidified. Most of the formaldehyde was converted to paraformaldehyde, but a non-sublimable product (analyte 1) was obtained in 0.7 % yield. The product (analyte 1) was fractionated into water-soluble (analyte 2) and water-insoluble (analyte 3) components. Analytes 2 and 3 were trimethylsilylated and then characterized by GC-MS. The GC-MS data exhibited that analytes 2 and 3 contained monosaccharides and sugar alcohols. Analyte 1 transmitted light in a crossed Nicol state, suggesting that analyte 1 contained optically active components. The xerogels obtained from analytes 2 and 3 exhibited long fibrous morphologies with partial helical structures (Fig. 17).

Abe et al. [63] carried out formose reaction under gamma ray irradiation. They prepared and degassed two aqueous solutions containing formaldehyde (2.8 M), methanol (0.46 M), and ammonia (0 – 2.8 M) with and without glycolaldehyde (0.56 M). They conducted reaction for these solutions by heating at 50 °C for 72 h or by irradiating with gamma rays (^{60}Co source at Tokyo Institute of Technology, 1.5 kGy h^{-1}) at temperatures < 40 °C for 60 h. Under gamma ray irradiation, the pH decreased significantly, indicating that Cannizzaro reaction occurred. The aldoses contained in the reaction mixtures were derivatized by the aldononitrile acetate ester derivatization method and characterized by GC-MS. Glyceraldehyde, erythrose, and threose were observed as main products, and the production of pentoses and hexoses was also confirmed (Fig. 18). When glycolaldehyde was used as a cocatalyst, formose reaction proceeded significantly in the presence of ammonia (0.56 M or 2.8 M), both by heat and gamma ray irradiation. Even in the absence of glycolaldehyde, the formose reaction proceeded significantly when the ammonia concentration was 0.28 M or 0.56 M under gamma ray irradiation. Based on these data, the authors stated that gamma ray irradiation should play a significant role in the production of monosaccharides in meteorite parent bodies containing radioactive nuclides, *e.g.*, ^{26}Al.

3.1.6. *Formose reactions under microwave irradiation*

There have been some examples of reactions that occur with high efficiency and selectivity under microwave (MW) irradiation. Hashidzume et al. [64] investigated formose reaction under MW irradiation under various conditions. Using formaldehyde (1.0 mol kg^{-1}) and Ca$(OH)_2$ (55 mmol kg^{-1}) as a catalyst, formose reaction proceeded very quickly at a high set temperature (150 °C) for a short time (1 min) even in the absence of any cocatalyst, preferentially producing branched hexoses and heptoses. After treatment with ion exchange resin, the main products were isolated by thin layer chromatography (TLC) and characterized by MS and NMR (Fig. 19a and b). The characterization data revealed that the hexose and heptose were 2-hydroxymethyl-1,2,4,5-tetrahydroxy-3-pentanone (**C6***) and 2,4-bis(hydroxymethyl)-1,2,4,5-tetrahydroxy-3-pentanone (**C7***), respectively. DFT calculation data for the energies of all isomers of trioses, tetroses, and pentoses indicate that **C6*** and **C7*** are likely produced preferentially by repeated aldol reactions with formaldehyde via 1,3-dihydroxyacetone, 1,3,4-trihydroxy-2-butanone, and 1,2,4,5-tetrahydroxy-3-pentanone (Fig. 19c). Homnan et al. [65] performed formose reaction using an aqueous

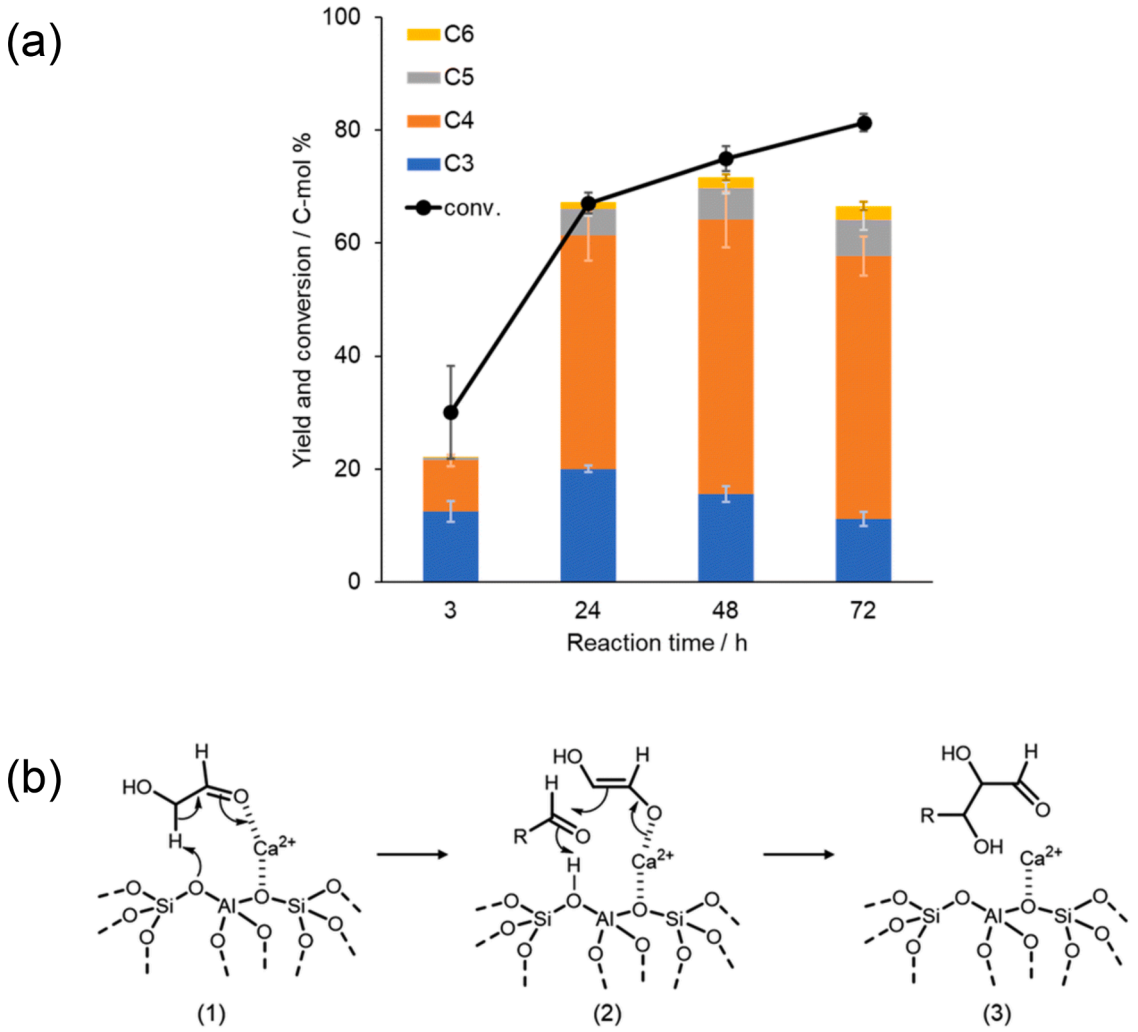

Fig. 15. (a) Time course of conversion and yields of C3 – C6 in formose reaction using Ca-LTA. (b) A proposed mechanism for C–C bond formation during formose reaction using Ca-LTA. Reproduced from ref. [53] under the terms and conditions of the Creative Commons Attribution (CC BY) license (http://creativecommons.org/licenses/by/3.0/).

solution containing formaldehyde (1 M) and $Ca(OH)_2$ (pH 12.5) by heating and under MW irradiation at 800 W. FTIR spectra showed that monosaccharides were obtained within 1 min under MW irradiation. However, the monosaccharides obtained were not fully characterized.

3.1.7. *Formose reactions utilizing electrochemical reactions*

Cestellos-Blanco et al. [66] used glycolaldehyde (15 μM), which was electrochemically generated from CO_2 in $KHCO_3$ (0.1 M) at −0.81 V (vs. reversible hydrogen electrode) using copper nanoparticles as a catalyst, as a cocatalyst for formose reaction of formaldehyde (70 mM) at pH 11 in the presence of NaOH (60 mM) at 75 °C for 75 min. The product was benzylated with benzyl chloride and characterized by electrospray ionization-MS (ESI-MS). The ESI-MS data indicated the production of monosaccharides with carbon numbers 3 to 8 (Fig. 20a). Soland et al. [67] used a palladium foil electrode to generate formaldehyde with a faradaic efficiency of about 90 % by applying a voltage of 0.9 V (vs. Ag/AgCl electrode) to a methanol/water (9/1, w/w) mixture containing 0.1 M $NaClO_4$. Without purifying the resulting formaldehyde, they added $Sr(OH)_2$ (40 mM) and glycolaldehyde (0.1 mM), adjusted the pH to 10 – 12 with 1 M NaOH, and carried out formose reaction at 80 °C. The yellowing point was observed within 20 min, and the product was obtained in *ca.* 25 % yield, which was evaluated by the phenol-sulfuric acid assay. HPLC data for the product, which was not derivatized, indicated that pentoses and hexoses were produced (Fig. 20b).

3.2. *Mechanistic studies on formose reaction*

3.2.1. *Experimental studies*

Delidovich et al. [68] carried out formose reaction using an aqueous formaldehyde solution (0.1 M) containing glycolaldehyde (5 mM) and glyceraldehyde (5 mM) at pH 10.4 (0.027 M MgO) or pH 7.3 (0.2 M Na_2HPO_4/KH_2PO_4). The reaction temperature was adjusted to 30 – 70 °C at pH 10.4 or 60 – 80 °C at pH 7.3. The products were derivatized with 2,4-dinitrophenylhydrazine and characterized by HPLC. The HPLC data confirmed the formation of monosaccharides up to heptoses. Based on the temperature dependence of the pseudo-first-order reaction rate constants (k_{app}), the apparent activation energies for the consumption of glycolaldehyde and glyceraldehyde were estimated to be 64 ± 3 and 69 ± 4 kJ mol^{-1} at pH 10.4 and 109 ± 8 and 90 ± 4 kJ mol^{-1} at pH 7.3, respectively.

Ricardo et al. [69] applied Fourier transform-ion cyclotron resonance MS (FT-ICR MS) with 2-hydroxymethylphenylboronate to the characterization of complicated mixtures of monosaccharides produced by formose reaction (Fig. 21a). Formose reaction was carried out for an aqueous solution containing formaldehyde (350 mM), $CaCl_2$ (50 mM), and NaOH (60 mM) at 68 or 40 °C. The products derivatized with 2-hydroxymethylphenylboronate were characterized by FT-ICR MS. The FT-ICR MS data exhibited that hexoses and heptoses were the main components before the yellowing point. When formose reaction was

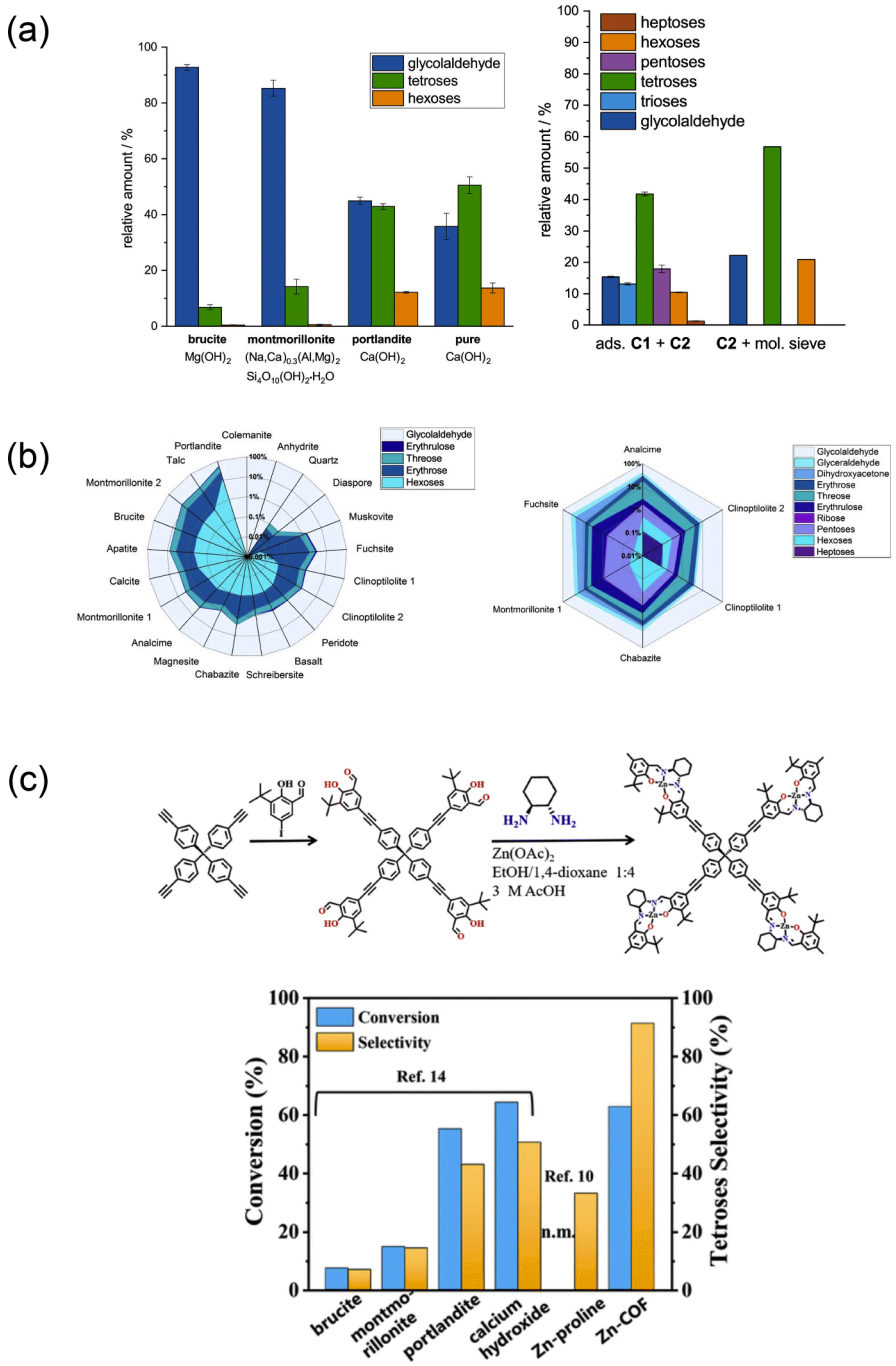

Fig. 16. (a) Comparison of different mineral catalysts with pure $Ca(OH)_2$ used in mechanochemical formose-type reaction starting from glycolaldehyde; Oscillatory ball mill, 30 Hz, 90 min, 20 mol% catalyst (left). Product distribution of the mechanochemical formose-type reaction in a planetary ball mill at 400 rpm after 90 min starting from glycolaldehyde, 20 mol% $Ca(OH)_2$, and molecular sieves with adsorbed formaldehyde or dry molecular sieves (right). Reproduced from ref. [54] under the terms and conditions of the Creative Commons Attribution (CC BY) license (http://creativecommons.org/licenses/by/4.0/). (b) Comparison of product distribution observed after ball milling of glycolaldehyde and the different minerals catalysts (20 mol% catalyst, head space gas: air, oscillatory ball mill, 90 min, 30 Hz) (left). Comparison of product distribution observed after ball milling of formaldehyde adsorbed onto minerals with 1:1 glycolaldehyde (head space gas: nitrogen, planetary ball mill, 90 min, 400 rpm) (right). Reproduced from ref. [55] under the terms and conditions of the Creative Commons Attribution (CC BY) license (http://creativecommons.org/licenses/by/4.0/). (c) The synthetic route of Zn-COF from tetrakis(4-ethynylphenyl)methane and benzaldehyde, 3-(1,1-dimethylethyl)-2-hydroxy-5-iodo (upper). Activity comparison between different catalysts (previous reports) and Zn-COF under mechanical reaction conditions for sugar production from glycolaldehyde (lower). Reproduced with permission from ref. [56]. Copyright 2023 The Royal Society of Chemisty.

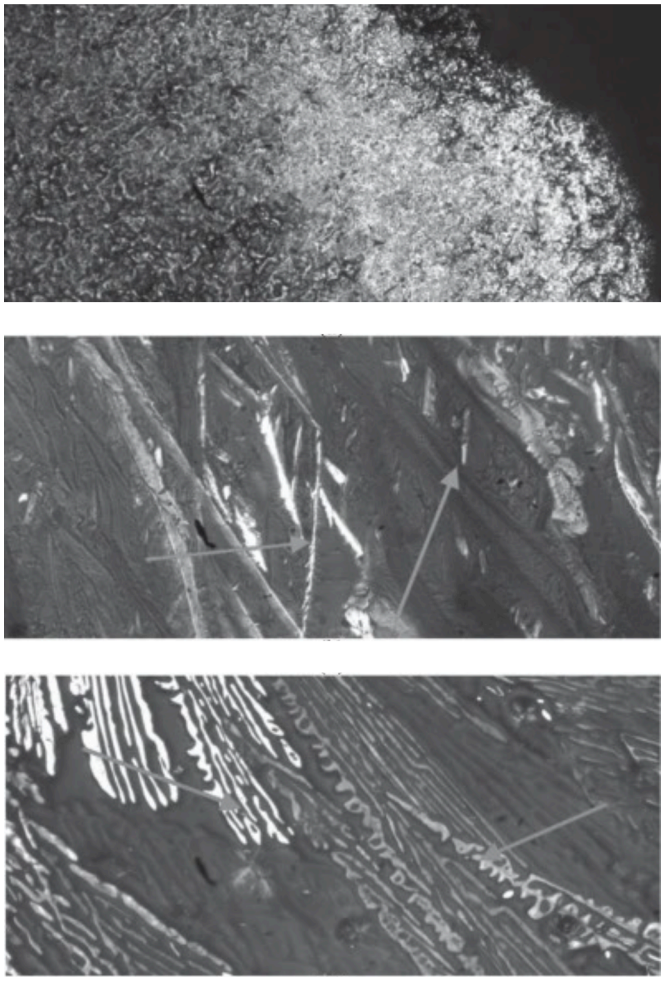

Fig. 17. Microscopic image (magnification, × 40) of xerogel of analyte-1 (top), xerogel of water-soluble analyte-2 (middle), and a dispersed sediment of water-insoluble analyte-3 (bottom) in a crossed Nicol state. Reproduced with permission from ref. [62]. Copyright 2019 Springer Nature.

carried out in D_2O at 65 °C, it took a longer time (39 min) that the mixture started to turn yellow. (In the case of formose reaction in H_2O, the onset of yellowing was observed after 18 min.) Notably, only *ca.* 10 % of the heptoses observed after 32 – 34 min incorporated a single deuterium atom. This observation indicates that most of the intermediate enols are not protonated, and that no formaldehyde molecule is released during retro-aldol reaction. Appayee and Breslow [70] re-examined the mechanism of formose reaction. They carried out the elementary reactions of formose reaction catalyzed by $Ca(OH)_2$, and the products derivatized with 2-nitrophenylhydrazine were characterized by HPLC and NMR. The reaction of 2-deuterated glyceraldehyde with formaldehyde in H_2O gave 74 % deuterated 1,3-dihydroxyacetone. This observation indicates that the carbonyl transfer does not involve enolate formation accompanied by proton abstraction, which Breslow [71] described previously, but rather involves hydride shift through Ca^{2+} coordination (Fig. 21b). Furthermore, Breslow et al. [72] investigated the deuterium isotope effect associated with hydrogen shift in the isomerization of glyceraldehyde to 1,3-dihydroxyacetone to reveal the contribution of hydrogen tunneling. Based on the Arrhenius plot of the rate constants obtained at 0, 40, and 80 °C, the ratio of pre-exponential factors (A_H/A_D) and the activation energy difference ($E_a(H) - E_a(D)$) were estimated to be 0.28 and 9.1 kJ mol^{-1}, respectively. These data are suggestive of a significant contribution of quantum mechanical tunneling in the isomerization mechanism (Fig. 21c).

Briš et al. [73] investigated the detailed mechanism of the initial stage of formose reaction by online detection of the reaction mixture by ion mobility separation MS (IMS-MS) (Fig. 22). Formaldehyde-^{13}C (70 mM) was added to an aqueous solution containing $CaCl_2$ (6.5 mM) and KOH (13 mM) and the solution was then heated at 40 °C. After 2 min, 1, 3-dihydroxyacetone (10 or 20 mM), glyceraldehyde (10 or 20 mM), glycolaldehyde (10 or 20 mM), erythrose (20 mM), or erythrulose (20 mM) was added as a cocatalyst and the reaction was allowed to run for another 13 min (for 15 min in total). A large data set obtained by the IMS-MS online detection of the reaction mixtures was analyzed by non-negative matrix factorization to obtain the time-dependent data on ion signals corresponding to monosaccharide/calcium complexes. The kinetic profiles of these complexes were analyzed by the multivariate method to provide an overview of the interconnected kinetic processes in solution. Notably, fast retro-aldol reactions were observed for calcium complexes with ketoses, and the diversity of reaction mixtures was greater when ketones rather than aldehydes of the same size were utilized as cocatalyst. Ion mobility separation of the individual monosaccharide complexes revealed cyclization of pentoses and branching of hexoses and heptoses.

Huck et al. [74–76] focused on the importance of environmental fluctuations in prebiotic reactions. Thus, Huck et al. [74] studied non-equilibrium formose reaction in the flow state using a conical continuous stirred tank reactor (CSTR) equipped with five input channels and one output channel under various conditions (the formaldehyde concentration, $CaCl_2$ concentration, NaOH concentration, temperature, and cocatalyst). The time evolutions of components in the products were monitored by HPLC (for the samples derivatized with 2, 4-dinitrophenylhydrazine) and GC-MS (for the samples trimethylsilylated). In particular, the concentration of cocatalyst (glycolaldehyde, 1, 3-dihydroxyacetone, erythrulose, or ribose) was sinusoidally varied. The product data were subjected to hierarchical clustering using a correlation-based pairwise dissimilarity metric, and the relationships between the average composition and kinetic properties produced under various conditions were visualized as tree diagrams (Fig. 23a). The results indicated that the product composition was controlled by altering the feedstock and catalyst conditions. Detailed pathways of formose reaction were also presented. Huck et al. [75] investigated the product distribution of formose reaction under similar flow conditions at varying the magnitudes and rates of temporal fluctuation of the concentrations of Ca^{2+} and OH^- (Fig. 23b). It was shown that the product composition of formose reaction under the dynamic conditions was different from that under conventional stationary conditions. The temporal concentration patterns were analyzed by hierarchical clustering and correction analysis, indicating that each compound does not respond independently to the applied dynamics but a collection of compounds respond together due to the structure of the underlying reaction network. It is thus likely that the key gate reaction branching off from the autocatalytic cycle proposed by Breslow [71] is an important reaction characteristic of formose reaction. More recently, Huck et al. [76] developed a system that uses the formose reaction system to produce monosaccharides and others and converts their amounts into numbers for information processing. This system converts the output of formose reaction into numbers, enabling information processing according to goals such as input classification, mimicking chemical dynamics, and predicting the behavior of complicated systems (Fig. 23c). Furthermore, machine learning was used to optimize the weight parameters to provide accurate output. Based on these procedures, the authors indicate that the chemical reaction network can act as a chemical reservoir computer that processes information.

3.2.2. Simulations

Jalbout et al. [77,78] investigated the mechanism of protic formose reaction under gas phase conditions using first-principles calculations. Jalbout et al. [77] performed first-principles calculations for the formation of glycolaldehyde mediated by a hydronium cation in the gas phase. The calculation data indicated that hydronium cations mediated

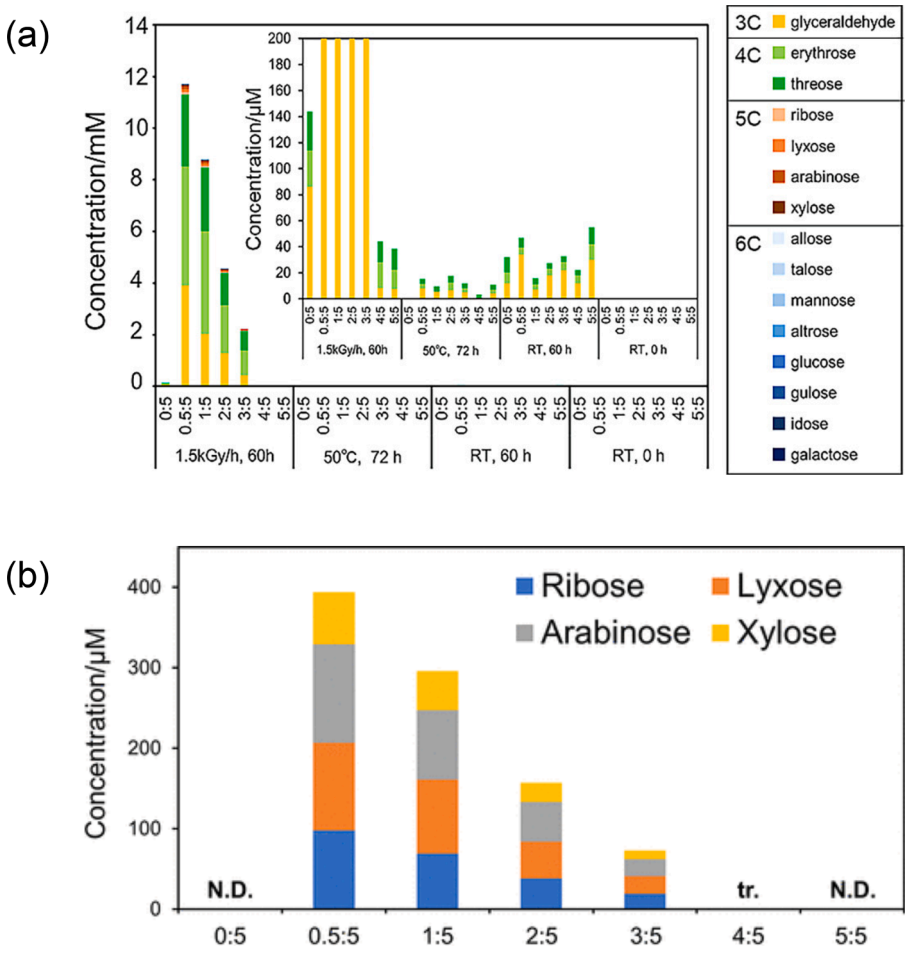

Fig. 18. (a) Aldose production from FAW samples by gamma ray irradiation at 1.5 kGy h^{-1} for 60 h, heating at 50 °C for 72 h, and controls; the samples were kept at room temperature (RT) for 60 h and analyzed immediately (0 h). Horizontal axis is the ratio of ammonia: formaldehyde (NH_3:HCHO). (b) Pentose production in FAW gamma-irradiated (1.5 kGy h^{-1}, 60 h) samples (horizontal axis: NH_3:HCHO). Pentose production in control samples is below the quantification limit. Reproduced from ref. [63] under the terms and conditions of the Creative Commons Attribution (CC BY) license (http://creativecommons.org/licenses/by/4.0/).

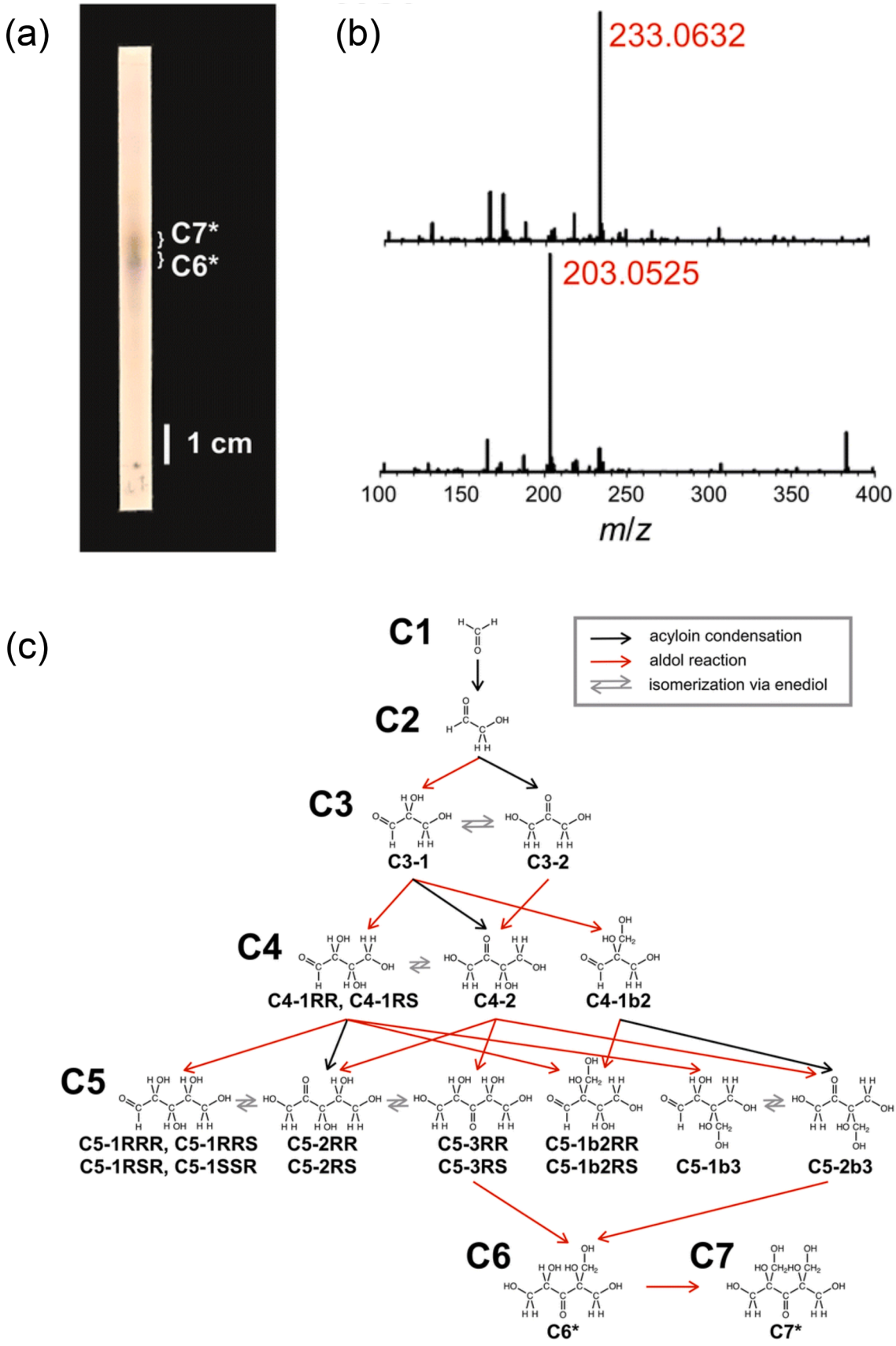

Fig. 19. (a) A photograph of a TLC plate for separation of the major products (heptose **C7*** and hexose **C6***) of formose reaction under MW irradiation using formaldehyde (1.0 mol kg^{-1}) and $Ca(OH)_2$ (55 mmol kg^{-1}) at a set temperature of 150 °C for 1 min. (b) MS for **C7*** (upper) and **C6*** (lower). (c) Plausible reaction pathways for the preferential formation of **C6*** and **C7*** in the formose reaction under MW irradiation. Reproduced with permission from ref. [64]. Copyright 2023 The Royal Society of Chemistry.

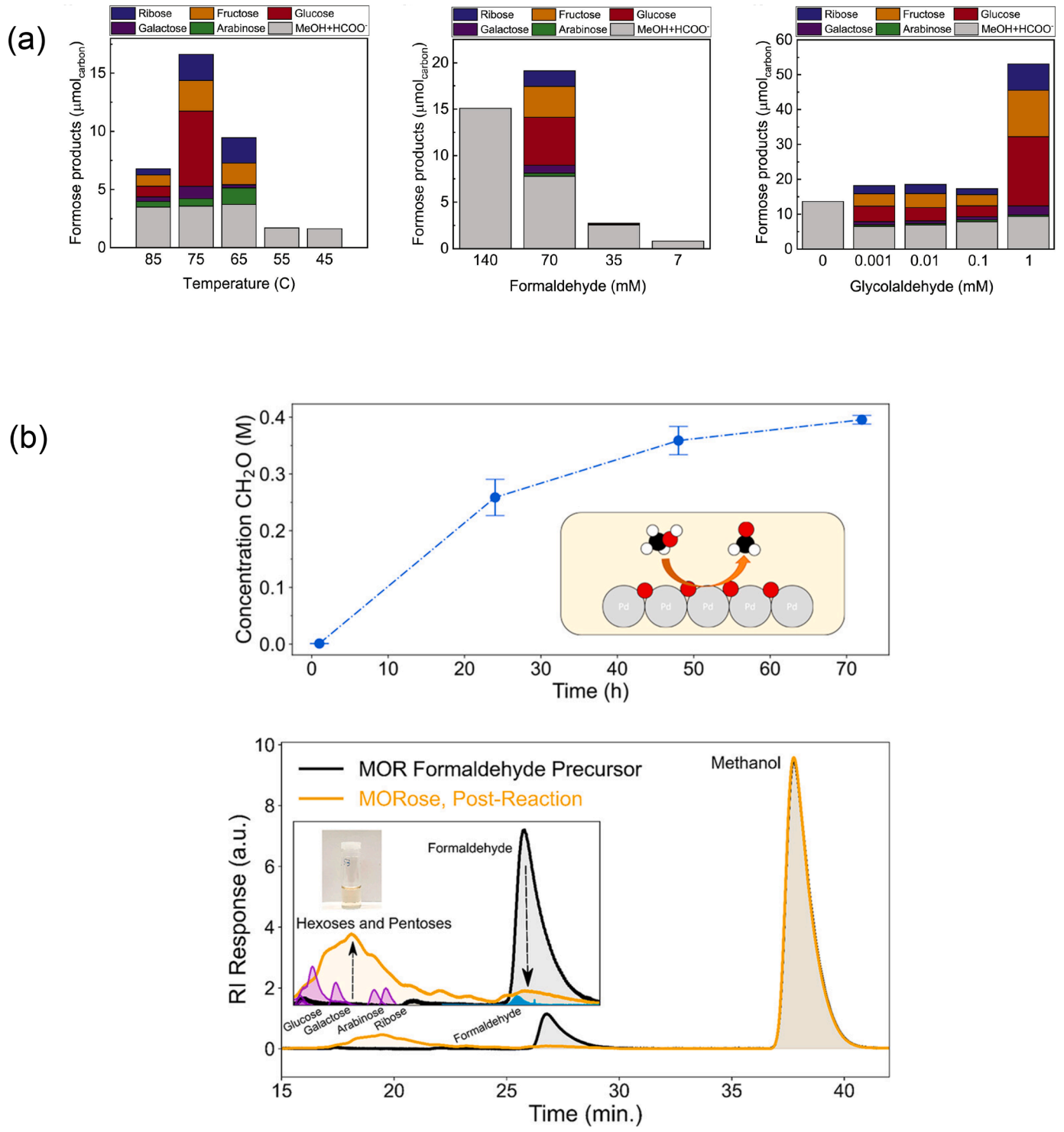

Fig. 20. (a) Formose product distributions obtained from glycolaldehyde (100 μM) and formaldehyde (70 mM) at different temperatures (left), from varying concentrations of formaldehyde and glycolaldehyde (100 μM) at 75 °C (middle), and from formaldehyde (70 mM) and varying concentrations of glycolaldehyde at 75 °C (right). Reproduced with permission from ref. [66]. Copyright 2022 Elsevier. (b) Total concentration of formaldehyde in a cell as a function of time at a 10 mA applied current in a galvanostatic time trial and a schematic illustraton of the partial oxidation reaction over the palladium surface (upper). HPLC chromatograms of a single reaction sampled before (black) and after (dark yellow) the formose reaction show the consumption of formaldehyde and the generation of multiple products (pentoses and hexoses) as discrete peaks (lower). Reproduced with permission from ref. [67]. Copyright 2023 American Chemical Society.

the dimerization of formaldehyde to form a covalent bond via a 1, 3-dioxocyclobutane intermediate, resulting in the formation of glycolaldehyde and water. Furthermore, based on first-principles calculations, Jalbout et al. [78] showed a mechanism, in which protonated glycolaldehyde and triose reacted with formaldehyde to form protonated triose and tetrose, respectively, via a 1,3-dioxocyclobutane intermediate, leading to growth (Fig. 24).

Proppe et al. [79] developed a protocol combining DFT calculations and kinetic simulations to the initial steps of formose reaction in order to accurately describe the complicated kinetic network by examining

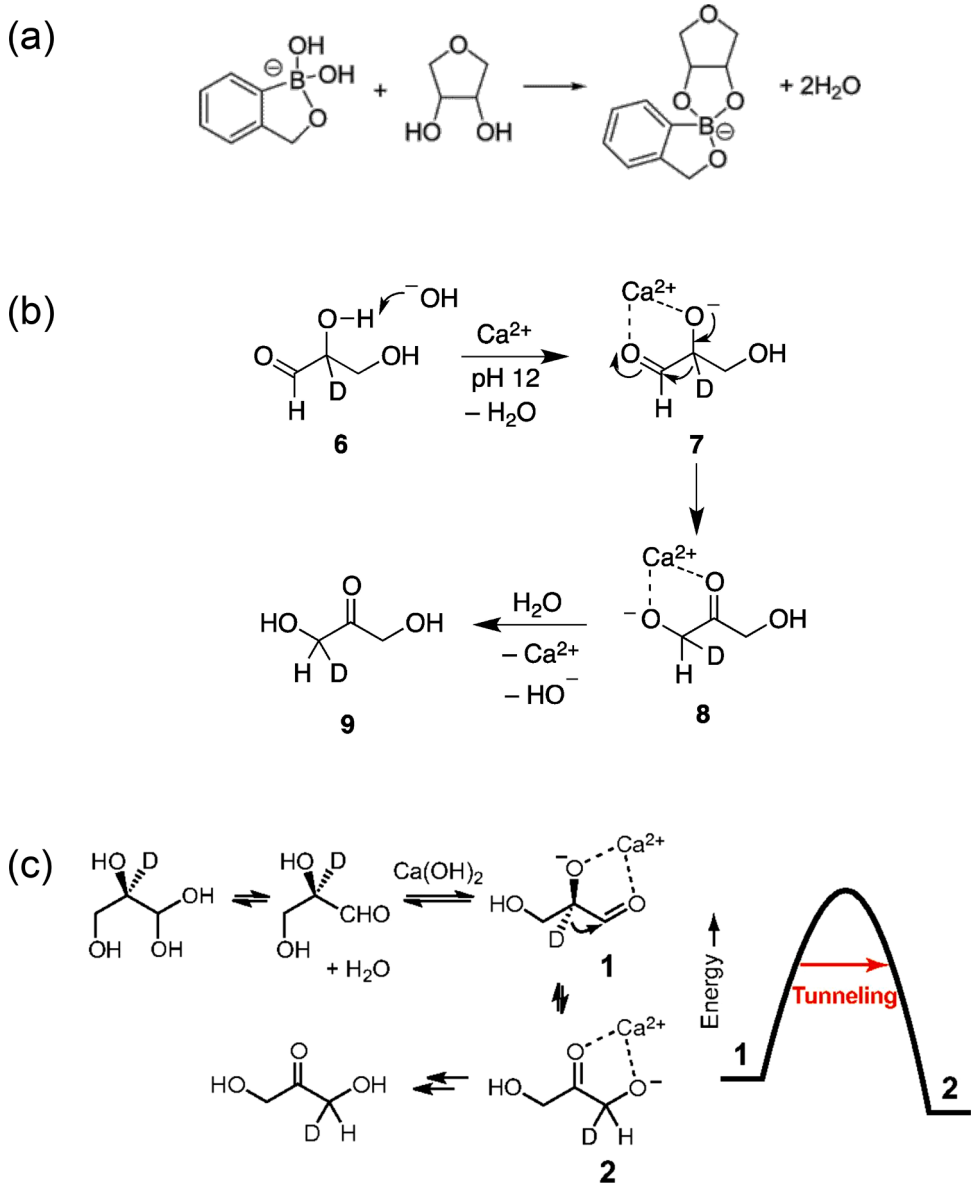

Fig. 21. (a) Reaction in water between 2-hydroxymethylboronate and a neutral *cis*-1,2-diol yielding an anionic complex detectable by FT-ICR MS. Reproduced with permission from ref. [69]. Copyright 2006 American Chemical Society. (b) Isomerization of 2-deuteroglyceraldehyde (**6**) to 1-deuterodihydroxyacetone (**9**) through a 1,2-hydride shift under formose reaction conditions. Reproduced with permission from ref. [70]. Copyright 2014 American Chemical Society. (c) Hydride shift mechanism for the isomerization of glyceraldehyde to dihydroxyacetone. Reproduced with permission from ref. [72]. Copyright 2015 The National Academy of Sciences.

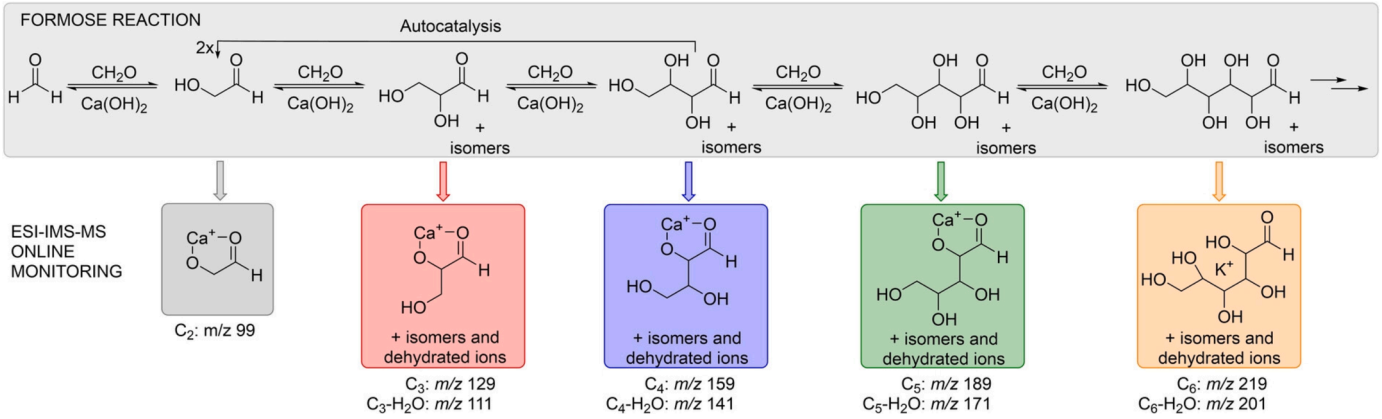

Fig. 22. Monosaccharides growing in the formose reaction and the ions monitored by IMS-MS. Reproduced from ref. [73] under the terms and conditions of the Creative Commons Attribution (CC BY) license (http://creativecommons.org/licenses/by/4.0/).

stationary points across multiple potential energy surfaces. The time evolutions of the component concentrations obtained for a reaction system containing C1 species (*i.e.*, formaldehyde and methanediol), C2 species (*i.e.*, glycolaldehyde, 1,2-ethenediol, and ethane-1,1,2-triol), and glyceraldehyde indicated that the C1 species (formaldehyde and methanediol) were consumed and the C2 species (glycolaldehyde, 1,2-ethenediol, and ethane-1,1,2-triol) were obtained (Fig. 25). During the reaction, the concentration of glyceraldehyde increased to reach a maximum, and then decreased.

Thripati and Ramabhadran [80] investigated the role of various cations (Na^+, K^+, Al^+, Mg^{2+}, and NH_4^+) and small molecules (H_2O, NH_3, H_2S, PH_3, HF, HCl, HCN, and HNC) found in the interstellar medium (ISM) in the first step of formose reaction, *i.e.*, the conversion of formaldehyde to glycolaldehyde in the gas phase, using electronic structure calculations (CCSD(T) and DFT methods). They proposed a novel mechanism in which metal–oxygen interactions and hydrogen bonds cooperatively promote the formation of glycolaldehyde from formaldehyde. The reactions containing Na^+, K^+, and NH_4^+ had large free energy barriers. However, the reaction involving Mg^{2+} exhibited no overall barrier because of the formation of stable precomplexes and the reaction featuring Al^+ ions had only a small barrier (Fig. 26a). Kong et al. [81] used DFT calculations to validate the proposed reaction mechanism for the sequential addition of hydroxycarbene to formaldehyde to form glycolaldehyde and 1,3-dihydroxyacetone (Fig. 26b). A favorable exothermic and de-ergonic pathway was found under ISM conditions (0 atm and 5 K), demonstrating the feasibility of the formation of 1,3-dihydroxyacetone.

Venturini and González [82] studied the initial steps of formose reaction using DFT calculations. The geometry of all stationary points found in the potential energy surface of formose reaction was optimized. Each stationary point was characterized as either a minimum or a first-order saddle point (transition state) by calculating the harmonic vibrational frequencies at 298.150 K and 1.0 atm. The connection between the reactants or products and the corresponding transition structures was established using the intrinsic reaction coordinate method. The dimerization of formaldehyde proceeds through aldol reaction of formaldehyde deprotonated by $Ca(OH)_2$ with formaldehyde molecules coordinated to the same $Ca(OH)_2$. Then, the *cis*-enediol tautomer of glycolaldehyde forms a complex with $Ca^{2+}(H_2O)_2$, and this complex reacts with formaldehyde coordinated to $Ca(OH)_2$ to form glyceraldehyde (Fig. 27).

Cantillo et al. [83] investigated the formation of pentoses from glycolaldehyde catalyzed by L-valine dipeptide (L-Val-L-Val) using first-principles calculations. The imine compound of L-Val-L-Val with glycolaldehyde forms a five-membered imidazolidinone ring (Fig. 28). Glyceraldehyde is then bound to the cyclic intermediate to form pentoses. Simulation results showed that the L-isomers of arabinose, lyxose, and xylose were stable, while the D-isomer of ribose was stable.

Rappoport et al. [84] presented a model of formose reaction at various stoichiometries, obtained by combining chemical heuristics with semi-empirical quantum chemistry (the PM7 method). Chemical heuristics provide a convenient way to traverse high-dimensional reaction potential energy surfaces, and the structures and energies of intermediates and products can be obtained in combination with quantum chemical structure optimization. The ninth generation network (T_9), which started with one glycolaldehyde molecule and two formaldehyde molecules to give tetroses, contained 146 species, including 6 monosaccharides, 78 acetals, and 9 enols (Fig. 29a). On the other hand, the ninth generation network (P_9), which started with one glycolaldehyde molecule and three formaldehyde molecules to give pentoses, contained 354 species, including 11 monosaccharides, 235 acetals, and 9 enols (Fig. 29a). These networks should be further improved because distorted three- and four-membered hemiacetals were contained. Simm and Reiher [85] proposed a new protocol to fully automate the complex exploration of chemical reactions. Starting materials and conditions are set, and a reaction network is built and expanded by repeatedly applying the protocol. Heuristic rules are used to efficiently narrow down possible reaction combinations and search for optimal reaction paths. Finally, the reaction network is visualized using an automatically generated graph structure (Fig. 29b). The protocol was applied to formose reaction to explore the complicated reaction network producing monosaccharides. Based on analysis of a large number of intermediates and minimum energy paths, a path for the formation of D-erythrose and the autocatalytic properties of forming glycolaldehyde was discovered.

Shahi and Cleaves [86] used *in silico* reaction modeling with the MØD software package to build a complicated reaction network for formose reaction in the presence and absence of iron ions, with an upper limit of 200 for the molecular weight of products, and to investigate the potential influence of iron ions. In the absence of iron ions, formose reaction was investigated using formaldehyde and water as reactants. In the presence of iron ions, on the other hand, the reaction was examined using Fe^{3+}, Fe^{2+}, and hydroxide ions as reactants as well as formaldehyde and water. The number of products increased as the generation of the reaction network increased. From the first to fifth generations of the reaction network, the network contained a larger number of products by 17 – 61 % in the presence of iron ions than that in their absence (Fig. 30). The connectivities of the network were also different, indicative of the significant effect of iron ions on formose reaction.

Stan et al. [87] investigated the autocatalytic formose reaction network using a computational nanoreactor. Simulations of six different starting configurations were performed. Starting with a 4:1 mixture of formaldehyde and glycolaldehyde containing 5 % argon under neutral conditions, the number of products in the network ranged from 22 to 81, with an average of 56 reactions identified (Fig. 31). Glyceraldehyde was

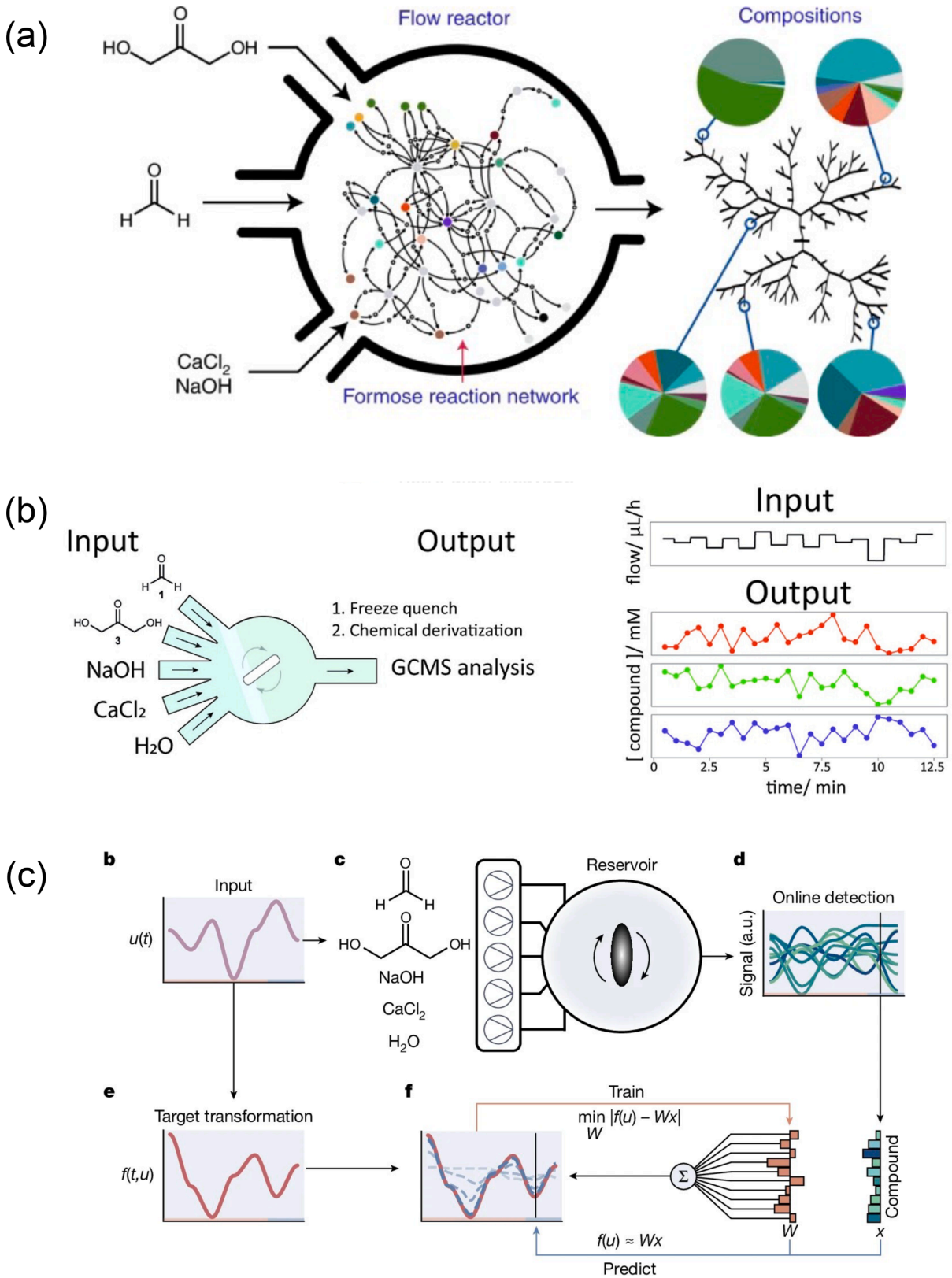

Fig. 23. (a) Non-equilibrium formose reaction in the flow state using a CSTR equipped with five input channels and one output channel under various conditions and a tree diagram of the relationships between the average composition and kinetic properties produced under various conditions. Reproduced with permission from ref. [74]. Copyright 2022 Springer Nature. (b) A schematic representation of a CSTR used to perform formose reaction under out-of-equilibrium conditions (left). Examples of an input for Ca^{2+}/hydroxide concentration profile and output carbohydrate concentration profiles (right). Reproduced from ref. [75] under the terms and conditions of the Creative Commons Attribution (CC BY) license (http://creativecommons.org/licenses/by/4.0/). (c) A schematic overview of the experimental set-up and reservoir training process. A set of input variables u used to obtain a target (dynamic) transformation $f(t,u)$. Reproduced from ref. [76] under the terms and conditions of the Creative Commons Attribution (CC BY) license (http://creativecommons.org/licenses/by/4.0/).

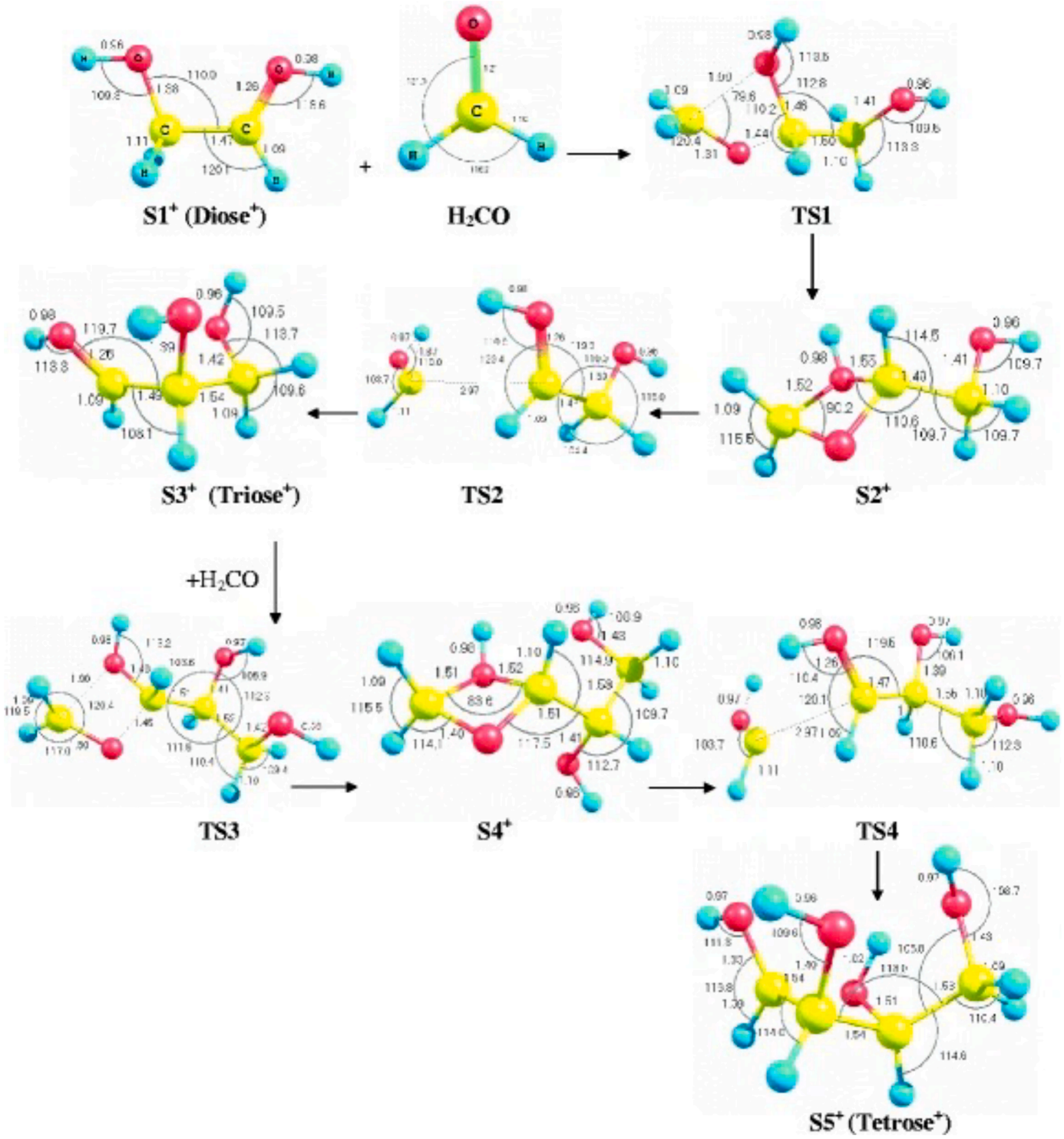

Fig. 24. Geometrical parameters for all species studied in this work in which bond lengths in angstroms (Å) and bond angles in degrees (°) are depicted. Reproduced with permission from ref. [78]. Copyright 2008 Springer Nature.

obtained by aldol reaction of formaldehyde with glycolaldehyde, followed by isomerization to 1,3-dihydroxyacetone. Aldotetroses and erythrulose were produced directly from the initial compound. The production of precursors of aldopentoses, *e.g.*, 2,3-hydroxypentanedial, was confirmed, but no aldohexoses were produced. Other than monosaccharides, water, carbon dioxide, carbon monoxide, hydrogen, methane, alcohols, carboxylic acids, and acetone were also formed.

Takehara et al. [88] developed a new Monte Carlo code to simulate photochemical reactions caused by intermittent UV irradiation on the surface of ice particles in a protoplanetary disk (Fig. 32). They used a model that tracks the reaction sequence of molecules without assuming a conventional chemical reaction network. Formaldehyde, carbon dioxide, methanol, hydrogen, and water were used as starting materials to compare the changes in the amount of tetroses and pentoses obtained by the simulation. Monosaccharides and related products, *e.g.*, pentoses and deoxypentoses were produced. These results were consistent with the experimental data previously reported. However, unlike the conventional stepwise formose reaction, the reaction under intermittent UV

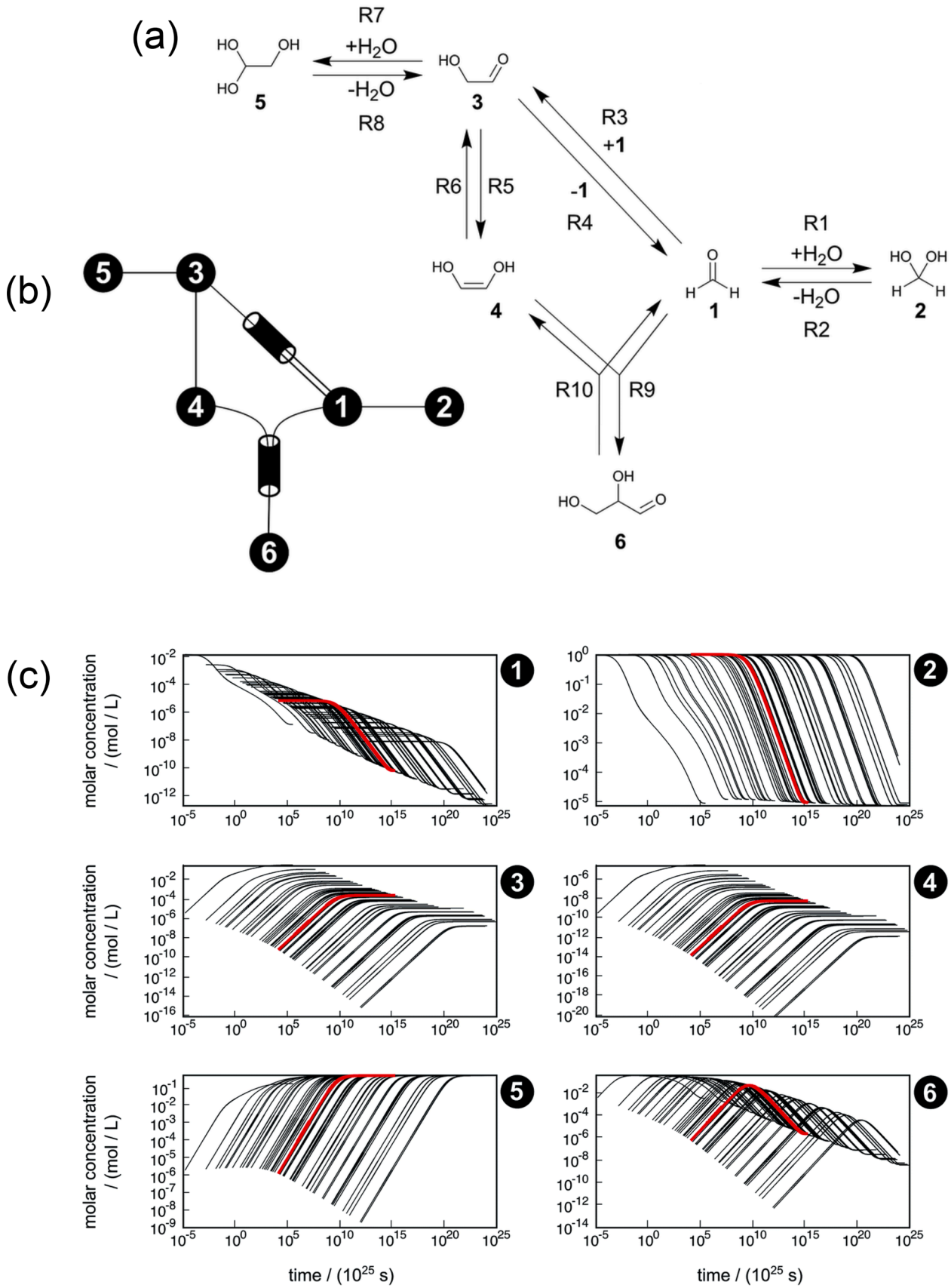

Fig. 25. (a) Possible mechanism of the first steps in the formose reaction. (b) An abstract graph representation of this reaction sub-network. (c) Concentration trajectories with respect to time for formaldehyde (**1**), methanediol (**2**), glycolaldehyde (**3**), 1,2-ethenediol (**4**), ethane-1,1,2-triol (**5**), and glyceraldehyde (**6**). Reproduced from ref. [79] under the terms and conditions of the Creative Commons Attribution (CC BY) license (http://creativecommons.org/licenses/by/3.0/).

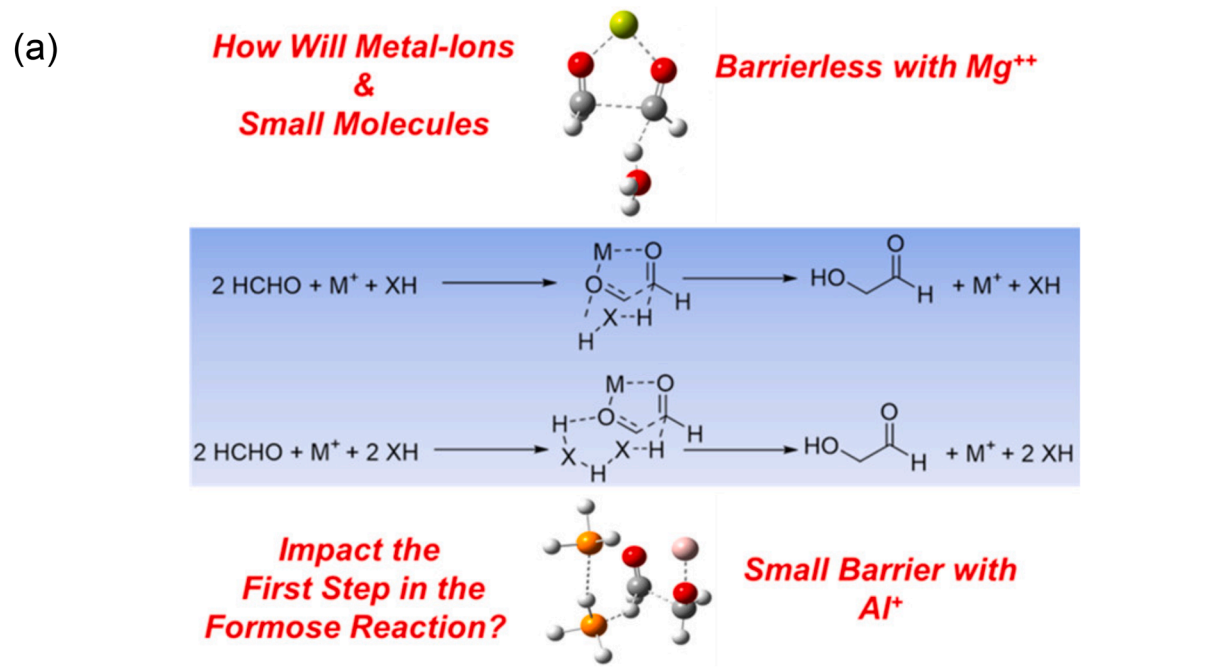

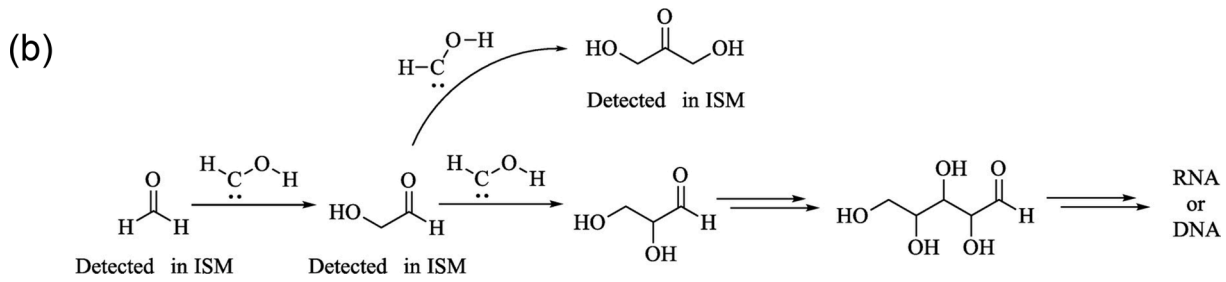

Fig. 26. (a) Formose reaction pathways for the gas phase conversion of formaldehyde to glycolaldehyde occurring under the ISM conditions. Reproduced with permission from ref. [80]. Copyright 2017 American Chemical Society. (b) The proposed reaction pathway of formose reaction towards larger monosaccharides mediated by hydroxycarbene under the ISM conditions. Reproduced with permission from ref. [81]. Copyright 2020 Canadian Science Publishing.

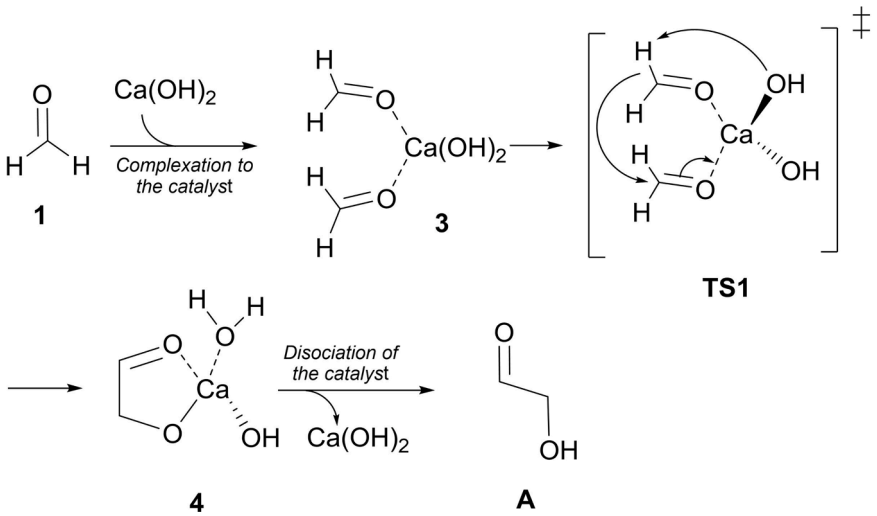

Fig. 27. A possible stepwise mechanism for the ionic dimerization of formaldehyde. Reproduced with permission from ref. [82]. Copyright 2024 Wiley-VCH.

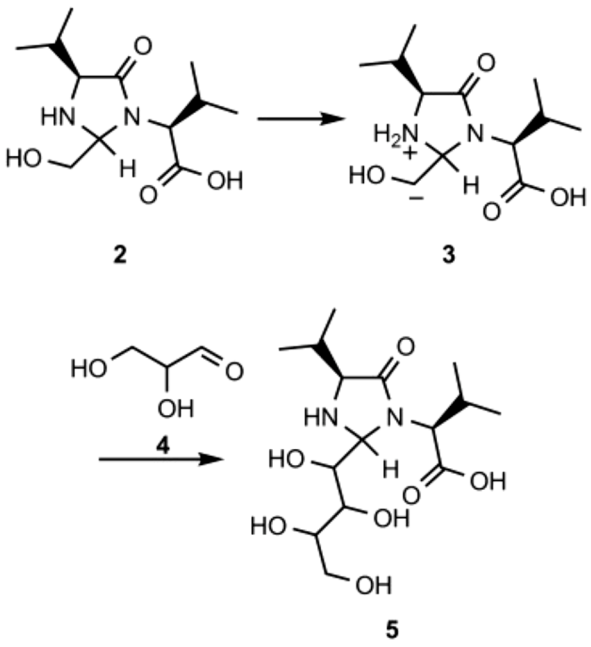

Fig. 28. Addition of a carbanion intermediate (**3**) to glyceraldehyde (**4**) to yield the divaline monosaccharide precursor (**5**). Reproduced with permission from ref. [83]. Copyright 2012 Wiley-VCH.

irradiation proceeded through less stable intermediates, and the amount of pentoses depended dominantly on the H/O ratio in the starting material mixture. It is presumed that the monosaccharides produced are stabilized by a cyclic structure.

Kua and Tripoli [89] performed DFT calculations of the energy changes and activation energies of the reactants and products for elementary reactions (*e.g.*, hydration, aldol reaction, Cannizzaro reaction, and retro-aldol reaction), involving formaldehyde, glycolaldehyde, glyceraldehyde, and tetroses, in the absence and presence of water, formic acid, ammonia, or hydrogen sulfide to construct an energy map for entire formose reaction (Fig. 33). Aldol reaction was thermodynamically favored. Cannizzaro reaction was thermodynamically driven by the formation of alcohol, but the kinetic barrier was relatively high. It was also shown that formic acid and ammonia acted as acid and base catalysts, respectively.

3.2.3. Mathematical models

Chemical reaction networks can be mathematically modeled as directed multi-hypergraphs by corresponding molecules and reactions to vertices and hyperedges, respectively. Benkö et al. [90] constructed a graph-theoretic toy model that provides a consistent framework, which allows ones to explore general properties of a wide range of chemical reaction networks in detail. They applied the model to formose reaction starting from formaldehyde and glycolaldehyde. The chemical reaction mechanism was implemented as graph rewrite rules acting on the structural formulas, and the reactivity and selectivity were modeled by a variant of frontier MO theory based on the extended Hückel scheme. Then, reaction networks were constructed for the isomers up to heptose (Fig. 34a). Andersen et al. [91] applied a generic approach for composing graph grammar rules to define chemically useful rule compositions to formose reaction. They illustrated the use of transformation rule compositions by deriving meta-rules from the graph grammar consisting of the four rules required for formose reaction (*i.e.*, forward and reverse keto–enol tautomerization, forward and reverse aldol reaction). By repeatedly applying these rule constructions to elementary transformations, an autocatalytic cycle in formose reaction was derived automatically; Two glycolaldehyde molecules were formed from two formaldehyde molecules and one glycolaldehyde molecule (Fig. 34b). Furthermore, Andersen et al. [92] extended the formose reaction network to include all derivable molecules with up to 9 carbon atoms to obtain a network consisting of 284 molecules and 978 reactions. Computational analysis of the chemical space of formose reaction indicated that there were many autocatalytic cycles associated particularly with monosaccharides of 5 to 8 carbon numbers, which branch off from compounds in the basic autocatalytic cycle and then back again to the basic cycle. Liu and Sumpter [93] set up a general mathematical model of a chemical reaction system that properly considers energetics, kinetics, and conservation laws. They applied the model to formose reaction. When formaldehyde was used as the starting material, glycolaldehyde and glyceraldehyde were formed exponentially, which is a characteristic of a self-replicating system (Fig. 34c). Notably, since the formation of glycolaldehyde was a low-barrier reaction, glycolaldehyde was produced whenever formaldehyde was added, leading to the formation of more glycolaldehyde in the entire system.

3.3. Formose reactions and the origin of life

3.3.1. Chemical evolution in the universe

Halfen et al. [94] conducted a comprehensive study of glycolaldehyde at 2 mm and 3 mm wavelengths using the 12 m telescope of Arizona Radio Astronomy Observatory toward the Sagittarius B2 molecular cloud core (Sgr B2(N)). Based on the rotational diagram analysis, the column density of glycolaldehyde was estimated to be 5.9×10^{13} cm^{-2}, with an abundance ratio to H_2 of 5.9×10^{-11}. From the observation of formaldehyde toward Sgr B2(N), formaldehyde and glycolaldehyde are thought to arise from the same gas with an abundance ratio of *ca.* 1:27. These observations imply that glycolaldehyde is formed through formose reaction in the gas phase.

3.3.2. Chemical evolution involving meteorites

Furukawa et al. [95] analyzed monosaccharides in three carbonaceous chondrites, *i.e.*, Murchison meteorite, NWA801, and NWA7020. The carbonaceous chondrites were crushed and extracted with 2 % hydrochloric acid and water, and the solvents were removed by distillation, followed by extraction with methanol to remove inorganic salts. The residues obtained after removal of methanol were treated with a cation exchange resin to obtain samples. The samples were dissolved in pyridine containing hydroxylammonium chloride, heated, and acetylated with acetic anhydride. The derivatized samples were characterized by GC-MS. The GC-MS data exhibited that the samples contained monosaccharides, *e.g.*, ribose, arabinose, xylose, and lyxose. The ^{13}C-enriched stable carbon isotope composition of the detected monosaccharides indicated that these monosaccharides were of extraterrestrial origin. In addition, formose reaction using formaldehyde (100 mM) and glycolaldehyde (10 mM) in an ammonia buffer (pH 9.6) at 90 °C for 360 min gave a product containing pentoses, and the composition of pentoses was similar to that in the meteorites. It is thus likely that the monosaccharides in the chondrites were formed by formose reaction.

3.3.3. Formation of ribose

Ribose, an important component of RNA, is unstable under basic conditions. Ricardo et al. [96] indicated that ribose was stabilized in the presence of boric acid by the formation of borate esters (Fig. 35). They also conducted formose-type reaction using a suspension mixture of glycolaldehyde (0.5 mM), glyceraldehyde (0.5 mM), and $Ca(OH)_2$ (0.5 M) at 45 °C for 20 min, and detected the formation of small amounts of pentoses by GC of the trimethylsilylated product. After incubation for 1 h, the pentoses decomposed. On the other hand, when the same incubation was performed in the presence of the borate minerals ulexite ($NaCaB_5O_9 \bullet 8H_2O$), kernite ($Na_2B_4O_7$), or colemanite ($Ca_2B_6O_{11} \bullet 5H_2O$), aldopentoses (*i.e.*, arabinose, lyxose, xylose, and ribose) were detected even after 2 months. These observations suggest that organic molecules in star- and planet-forming nebulae form pentoses in the presence of borate minerals.

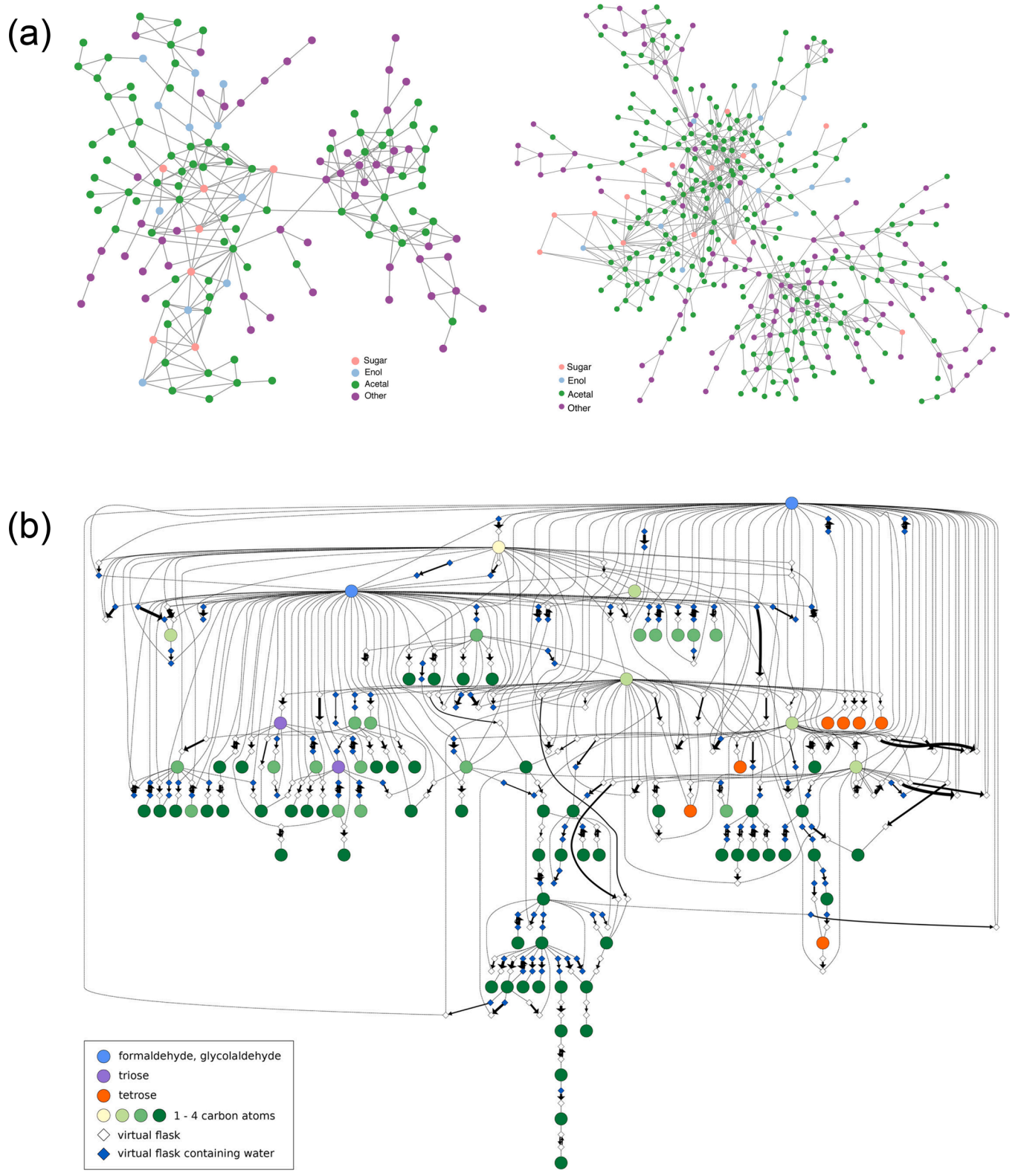

Fig. 29. (a) Representations of the T_9 (left) and P_9 (right) networks. Filled circles represent product flasks. Color coding and chemical formulas denote the largest constituent molecule of the respective flask (see legend). Black solid lines indicate major pathways of monosaccharide formation. Reproduced with permission from ref. [84]. Copyright 2014 American Chemical Society. (b) Reaction network generated from formaldehyde, glycolaldehyde, and water consisting of reactions with activation barriers below 85 kJ mol^{-1}. Reproduced with permission from ref. [85]. Copyright 2017 American Chemical Society.

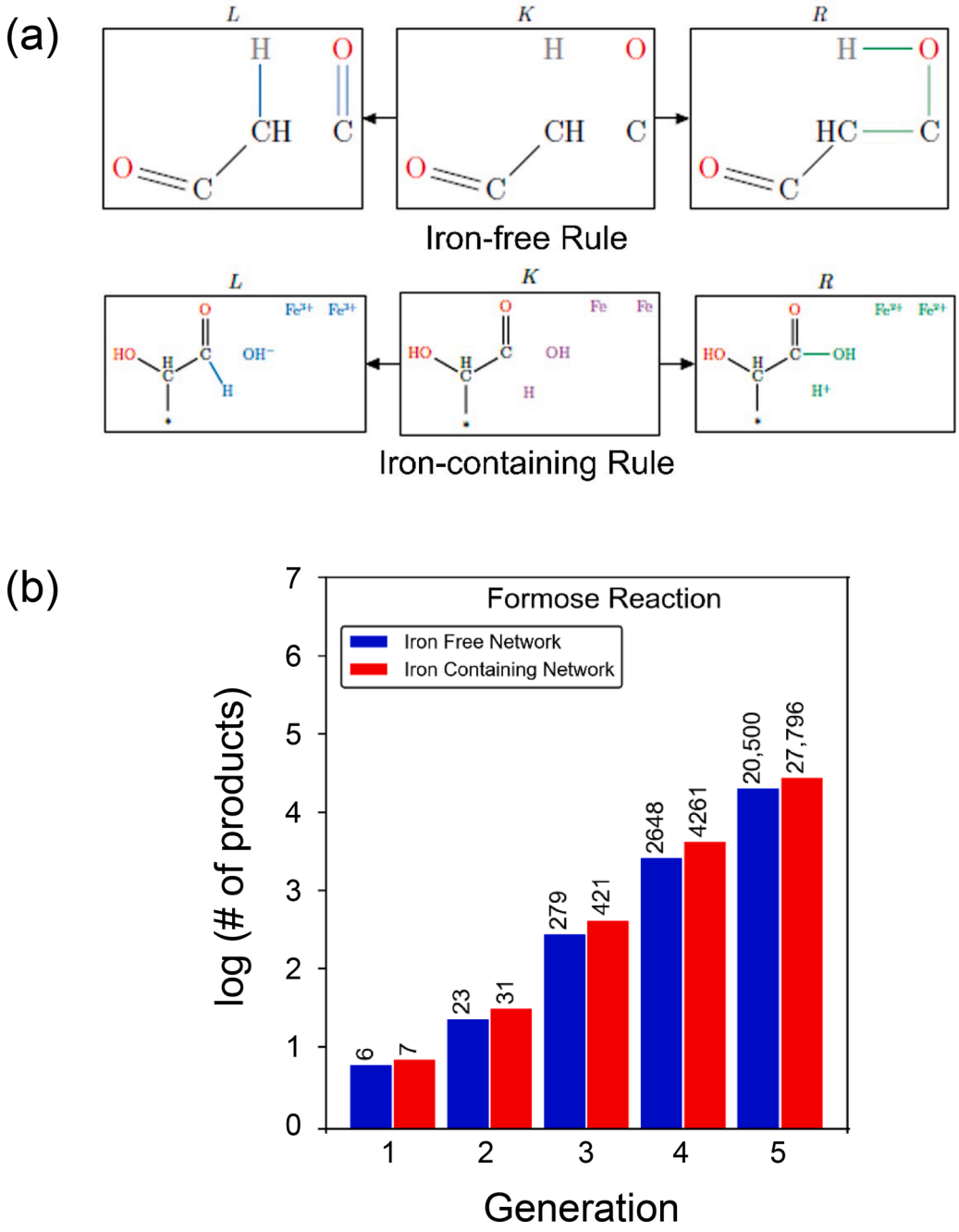

Fig. 30. (a) Examples of iron-independent aldol condensation reaction (upper) and iron-dependent two-electron oxidation of an aldehyde accompanied by the reduction of two iron(III) atoms to two iron(II) atoms (lower) as encoded in MØD. (b) The number of products in formose reaction in the absence (blue) or presence (red) of iron species as a function of reaction generation. Reproduced from ref. [86] under the terms and conditions of the Creative Commons Attribution (CC BY) license (http://creativecommons.org/licenses/by/4.0/).

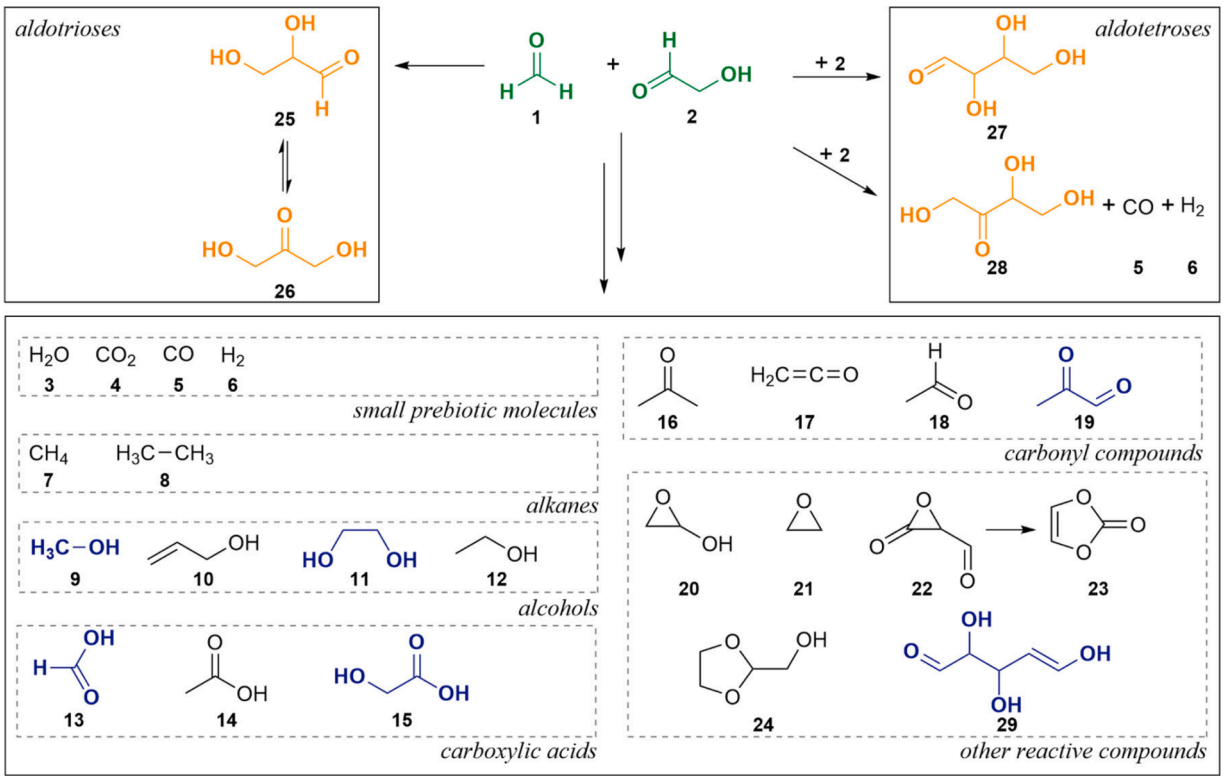

Fig. 31. Overview of relevant molecular species obtained from six formose reaction network simulations starting from formaldehyde and glycolaldehyde at a ratio of 4:1 and 5 % of added argon atoms. Feedstock compounds are highlighted in green, while obtained aldoses are colored in orange. The depicted reaction paths to the aldotrioses and aldotetroses were extracted as such from the generated networks. Side products of the formose reaction network are depicted in dark blue. Reproduced with permission from ref. [87]. Copyright 2022 American Chemical Society.

Since silicate minerals are the main components of rocky planets, Lambert et al. [97] investigated the formation and stabilization of monosaccharides using sodium silicate. When glycolaldehyde or glyceraldehyde was mixed with sodium silicate at room temperature, 2:1 complexes of tetrose or hexose with silicate were detected by MS (Fig. 36). Furthermore, it was also indicated that the complexation suppressed decomposition of the monosacchrides. Vazquez-Mayagoitia et al. [98] employed DFT calculations to investigate the relative stabilities of 2:1 complexes of aldopentoses (*i.e.*, arabinose, lyxose, ribose, and xylose) with silicate. Five stereoisomers were examined for each aldose complex. The least stable stereoisomer of the ribose/silicate complex was more stable than the most stable stereoisomers of complexes of the other pentoses. These observations imply that formose reaction in the presence of silicate minerals preferentially forms a silicate complex of ribose.

Usami and Okamoto [99] investigated formose reaction and its elementary reactions using hydroxyapatite as a catalyst, which is composed of PO_4^{3-} and Ca^{2+}. Hydroxylapatite powder was added to an aqueous solution of a 1:2 mixture of formaldehyde and glycolaldehyde. The reaction mixture was heated at 80 °C for 128 h to obtain ribose in a 0.28 % yield as one of the main products. Based on the results of the elementary reactions using hydroxylapatite, the reaction pathway was predicted as follows (Fig. 37). 1,3-Dihydroxyacetone is formed by carbonyl transfer of glyceraldehyde produced by the reaction of formaldehyde with glycolaldehyde. Glycolaldehyde and 1,3-dihydroxyacetone in the reaction mixture form ribulose, which is then converted to ribose via carbonyl shift. Camprubi et al. [100] performed formose reaction in the presence of acetyl phosphate, a simple phosphorylating agent, to investigate phosphorylation of the intermediate to form selectively ribose. The reaction was carried out by heating a mixture containing formaldehyde (0.5 M), $Ca(OH)_2$ (0.167 M), $CaCO_3$ (0.167 M), lithium potassium acetyl phosphate or K_2HPO_3 (400 mM), and water (2 mL) at 60 °C for 0.5, 1, 2, 3, and 5 h while adjusting the pH with 5 M NaOH. The product was derivatized with 3-amino-9-ethylcarbazole, and the monosaccharide samples obtained by desalting the water-soluble fraction were characterized by HPLC and LC-MS. The main products were pentoses, and hexoses, tetroses, and trioses were also detected. The phosphorylated monosaccharides were barely detectable. Mechanistic analysis by LC-MS suggested that the enhanced selectivity for pentoses was due to the termination of formose reaction by precipitation of Ca^{2+} ions as phosphate minerals, *e.g.*, apatite and hydroxyapatite.

Furukawa et al. [101,102] also focused on the effect of boric acid in the process of ribose formation under prebiotic conditions (Fig. 38a). Furukawa et al. [101] investigated the stability of aldopentoses in the presence of borate. A borax solution containing borate (40 or 80 mM B $(OH)^{4-}$) was heated to 45 °C, and an aldopentose (*i.e.*, ribose, arabinose, xylose, or lyxose) (1 mM) and $Ca(OH)_2$ (2.14 g L^{-1}) were then added. The solution pH was 12.0 – 12.2. Heating was continued at 45 °C. Portions of the reaction mixture were taken at 90 min intervals and the amounts of remaining aldopentoses were evaluated by LC-MS. The data indicated that the stability of ribose was significantly improved in the presence of $B(OH)^{4-}$ (80 mM), *i.e.*, an equimolar amount of the pentose (Fig. 38a). Furukawa et al. [102] also investigated the effect of silicate or phosphate on the stability of aldopentoses. An aldopentose (*i.e.*, ribose, arabinose, xylose, or lyxose) (1 mM) was added to saturated aqueous Ca $(OH)_2$ containing sodium silicate or sodium phosphate (40 or 80 equivalents relative to the aldopentose). The mixture was then heated at 45 °C, and the amount of remaining aldopentose was estimated by LC-MS. In both cases, the decomposition rates of ribose and lyxose were reduced compared to those of xylose and arabinose (Fig. 38b). However, no complexes of aldopentoses with sodium silicate or sodium phosphate were observed by NMR. When sodium silicate and sodium phosphate were added, precipitation as calcium salts was observed. From these results, it was concluded that the decrease in the decomposition rate of

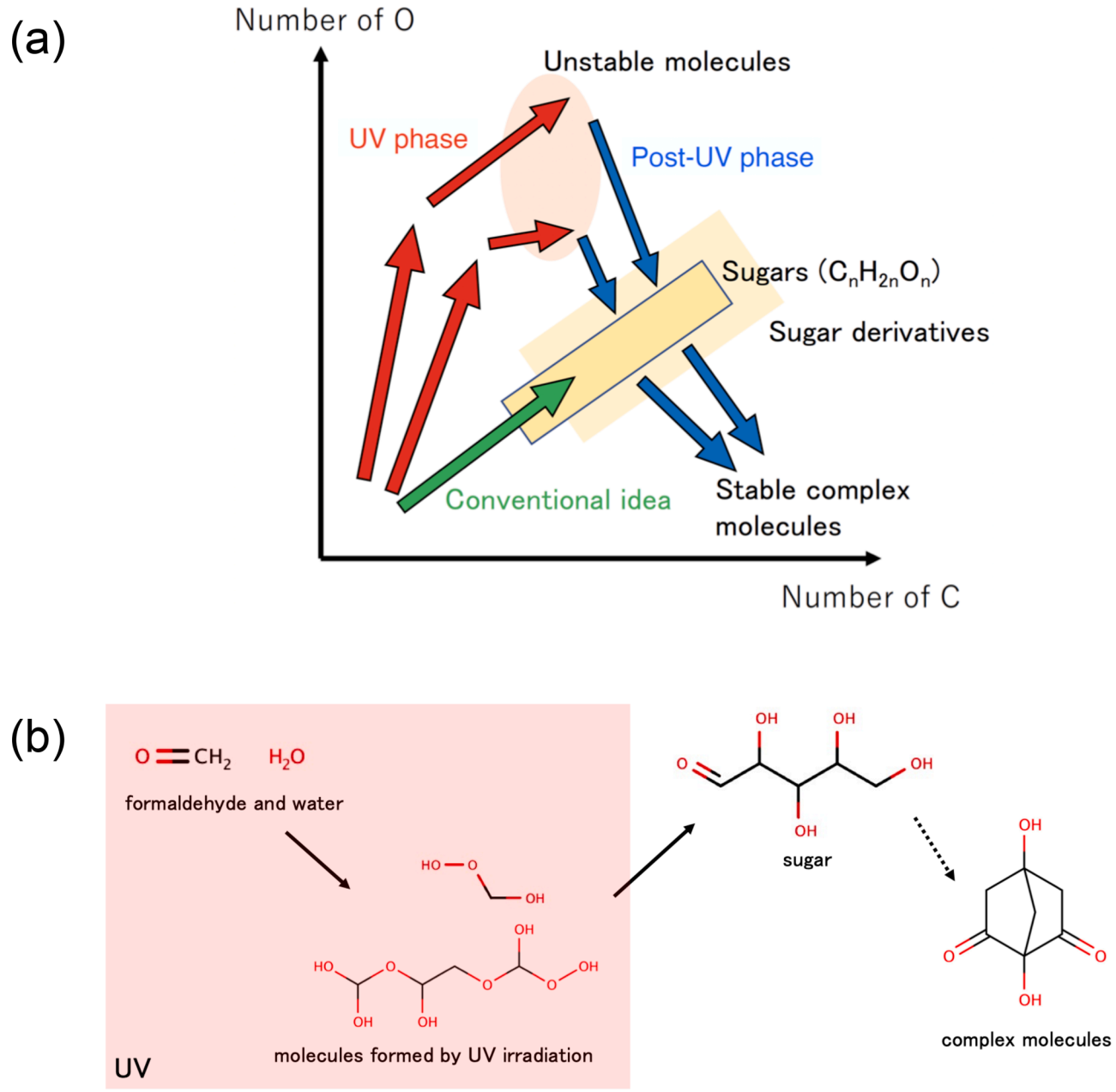

Fig. 32. (a) Monosaccharide synthesis pathways shown by the simulation using UV irradiation (the red and blue arrows) and by the conventional formose-type reactions (the green arrow). The horizontal and vertical axes are the numbers of carbon and oxygen atoms contained in molecules, respectively. (b) Example reaction paths of ribose synthesis. The red shaded region represents the evolution during the UV phase and the non-shaded region shows the evolution in the post-UV phase. Reproduced from ref. [88] under the terms and conditions of the Creative Commons Attribution (CC BY) license (http://creativecommons.org/licenses/by/4.0/).

aldopentoses in the presence of sodium silicate or sodium phosphate was due to a decrease in the Ca^{2+} concentration and not due to stabilization by sodium silicate or sodium phosphate.

Paschek et al. [103] investigated simplified formose reaction in which ribose is formed from one formaldehyde molecule and two glycolaldehyde molecules inside carbonaceous chondrite parent bodies. The amount of ribose calculated based on the simplified reaction equation under conditions inside a carbonaceous planetesimal was found to be strongly dependent on the initial abundances of glycolaldehyde and formaldehyde. The simulated ribose abundances were in good agreement with those measured in carbonaceous chondrites. To an aqueous solution containing formaldehyde (1.34 M) and glycolaldehyde (0.269 M, 20 mol%), 10 mol% of catalyst (*i.e.*, $Ca(OH)_2$, $CaCO_3$, K_2CO_3, or KOH) was added. The mixture was heated at 40 °C or 60 °C for 180 min. The products obtained were trimethylsilylated and characterized by GC-MS to evaluate the ribose fraction in the pentose. For all the catalysts, the ribose fraction was $(2.4 - 4.1) \times 10^{-2}$, which was consistent with the simulation results.

3.3.4. *Formation of ribonucleosides and ribonucleotides*

Powner et al. [104] showed that activated pyrimidine ribonucleotides were formed in a short sequence via arabinose aminooxazoline and anhydronucleoside intermediates using cyanamide, cyanoacetylene, glycolaldehyde, glyceraldehyde, and inorganic phosphate as starting materials (Fig. 39a). This route does not involve ribose and nucleobases. Inorganic phosphate is required from the beginning to act as an acid/base catalyst, a nucleophilic catalyst, a pH buffer, and a chemical buffer to control the three early reactions. Meanwhile, inorganic phosphate is

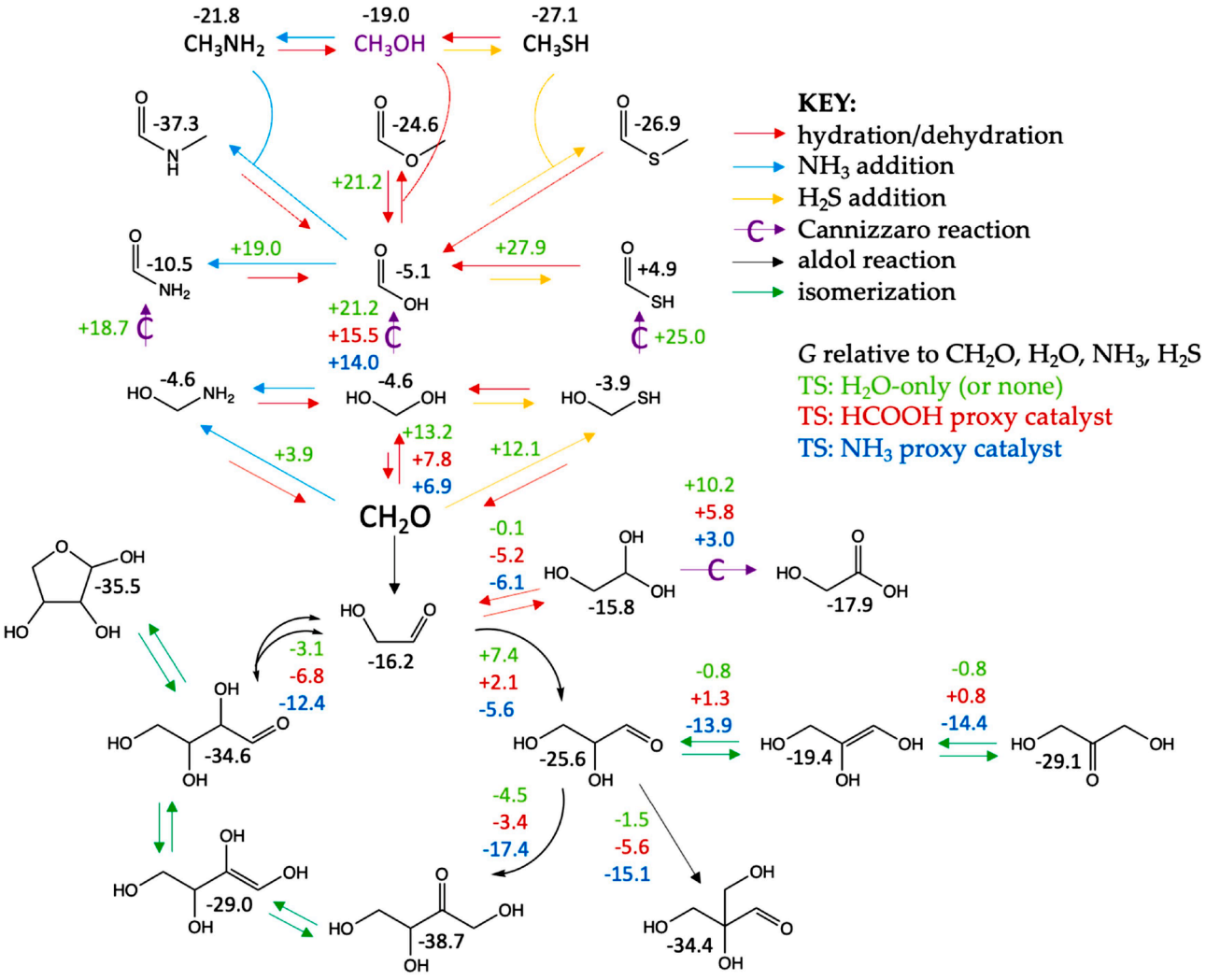

Fig. 33. Overall free energy map with *G* values in kcal relative to CH_2O, H_2O, NH_3, and H_2S. Reproduced from ref. [89] under the terms and conditions of the Creative Commons Attribution (CC BY) license (http://creativecommons.org/licenses/by/4.0/).

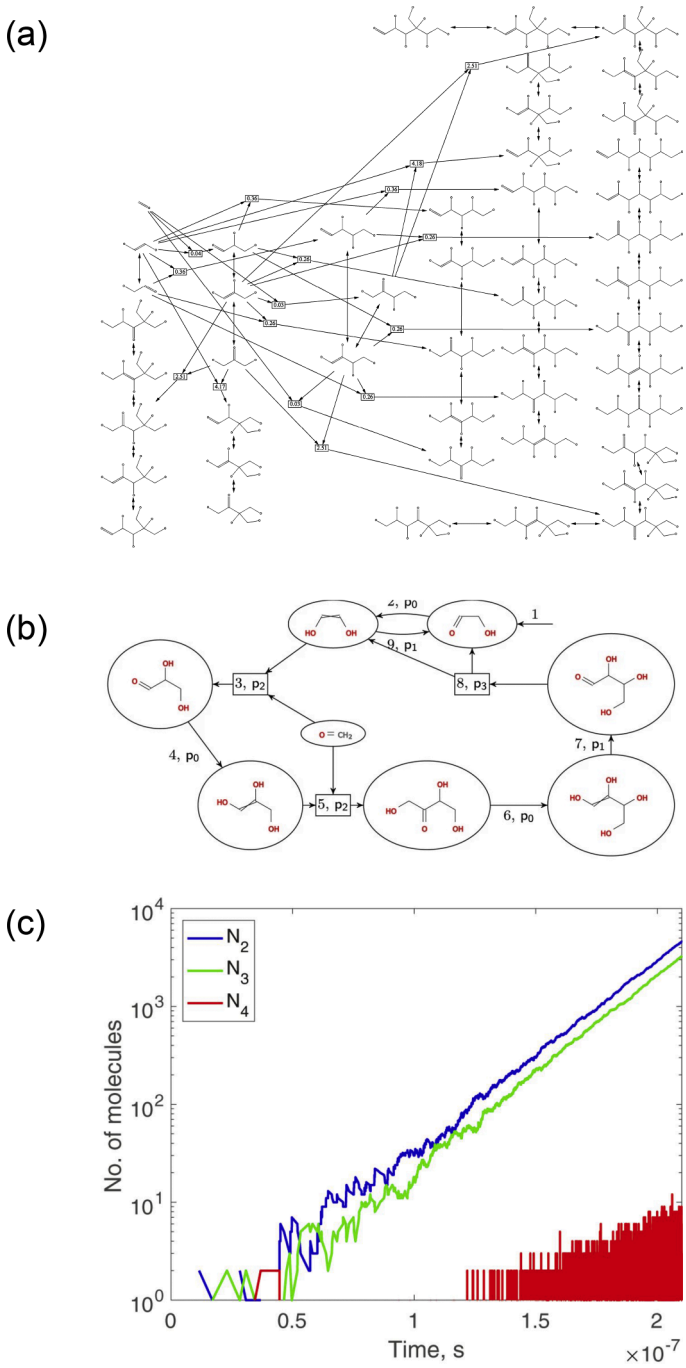

Fig. 34. (a) Formose reaction network. The initial mixture consists of formaldehyde and glycolaldehyde, and reacts via aldol condensations and dismutations. Reproduced with permission from ref. [90]. Copyright 2003 American Chemical Society. (b) Chemical reaction network for formose reaction. Reproduced from ref. [91] under the terms and conditions of the Creative Commons Attribution (CC BY) license (http://creativecommons.org/licenses/by/2.0/). (c) Time evolution of the numbers of glycolaldehyde (N_2), glyceraldehyde (N_3), and tetroses (N_4) produced. Reproduced from ref. [93] under the terms and conditions of the Creative Commons Attribution (CC BY) license (http://creativecommons.org/licenses/by/4.0/).

incorporated into nucleotides later in the reaction sequence. Zhao and Wang [105] used the selective binding of ribose over other monosaccharides by clay minerals doped with metal cations to select ribose from formose reaction products and form ribonucleotides. A suspension of kaolinite, montmorillonite, or silica doped with Cu^{2+}, Fe^{2+}, Ca^{2+}, or Mg^{2+} was added to a neutral aqueous solution of a mixture of aldopentoses (arabinose, lyxose, ribose, and xylose) and stirred at room temperature for 3 h at 1000 rpm. The supernatant was then separated from the clay minerals by centrifugation. Aqueous ammonia was added to the clay minerals to desorb the adsorbed aldopentoses. The samples derivatized with 1-phenyl-3-methyl-5-pyrazolone were characterized by HPLC. The HPLC data indicated that ribose was selectively adsorbed on all the clay minerals. When the formose reaction was conducted for a mixture of glycolaldehyde and glyceraldehyde using $Ca(OH)_2$ as a catalyst in the presence of clay minerals for 0.5 h at room temperature, ribose was preferentially adsorbed on the clay minerals from the reaction mixture. The adsorbed ribose was available for synthesis of nucleosides and nucleotides using 4,6-diamino-5-formamidopyrimidine (Fig. 39b). Based on DFT calculations, Jeilani and Nguyen [106] proposed a free radical pathway for the formation of RNA nucleosides, in

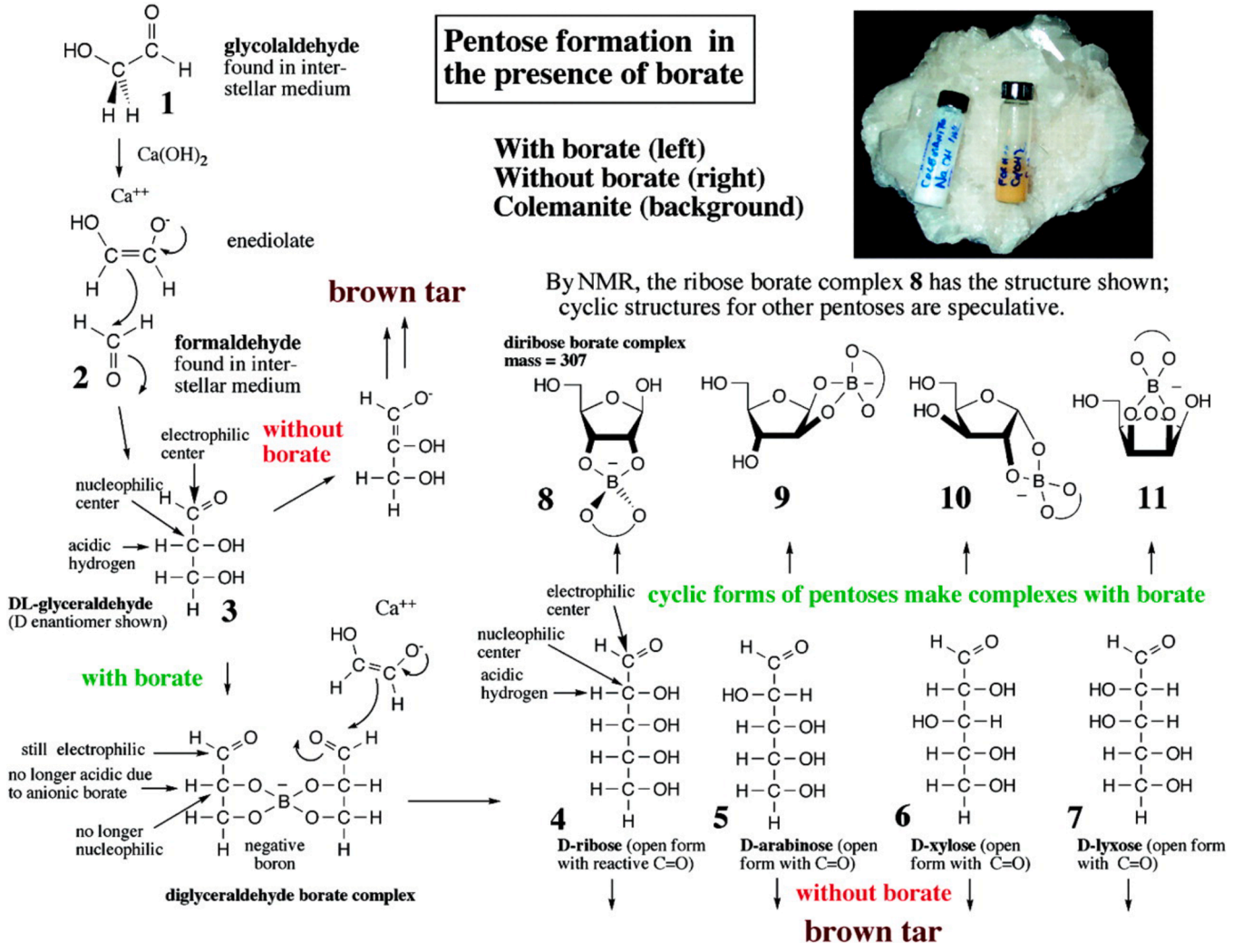

Fig. 35. Pentose formation in the presence of borate. Reproduced with permission from ref. [96]. Copyright 2004 American Association for the Advancement of Science.

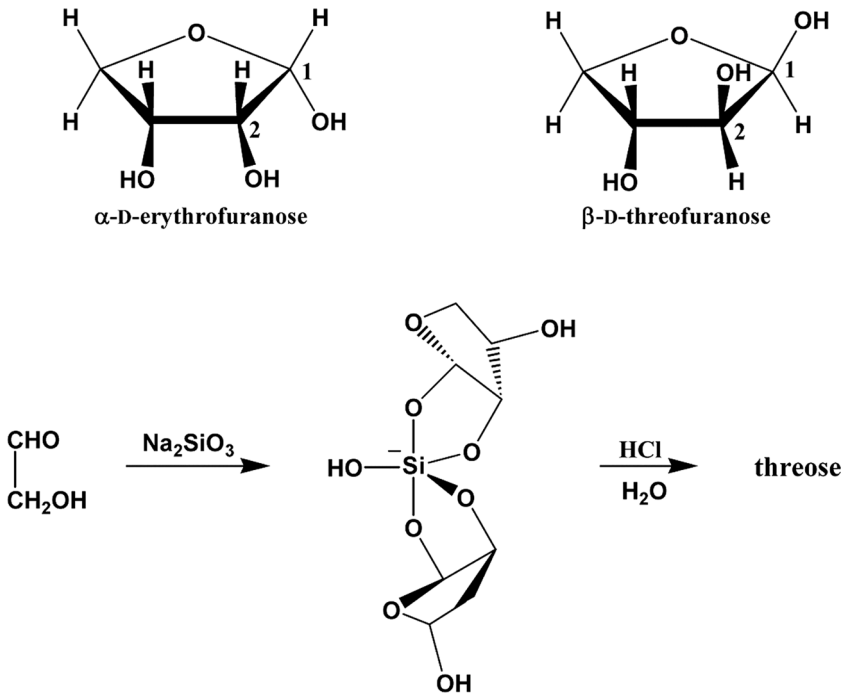

Fig. 36. The preferred structures of erythrose and threose for reaction with sodium silicate, in which the 1- and 2-hydroxy groups are *cis* (upper). The bottom-up synthesis of threose from glycolaldehyde (lower). In the presence of sodium silicate, the aldol dimer is sequestered as its 2:1 silicate complex. Reproduced with permission from ref. [97]. Copyright 2010 American Association for the Advancement of Science.

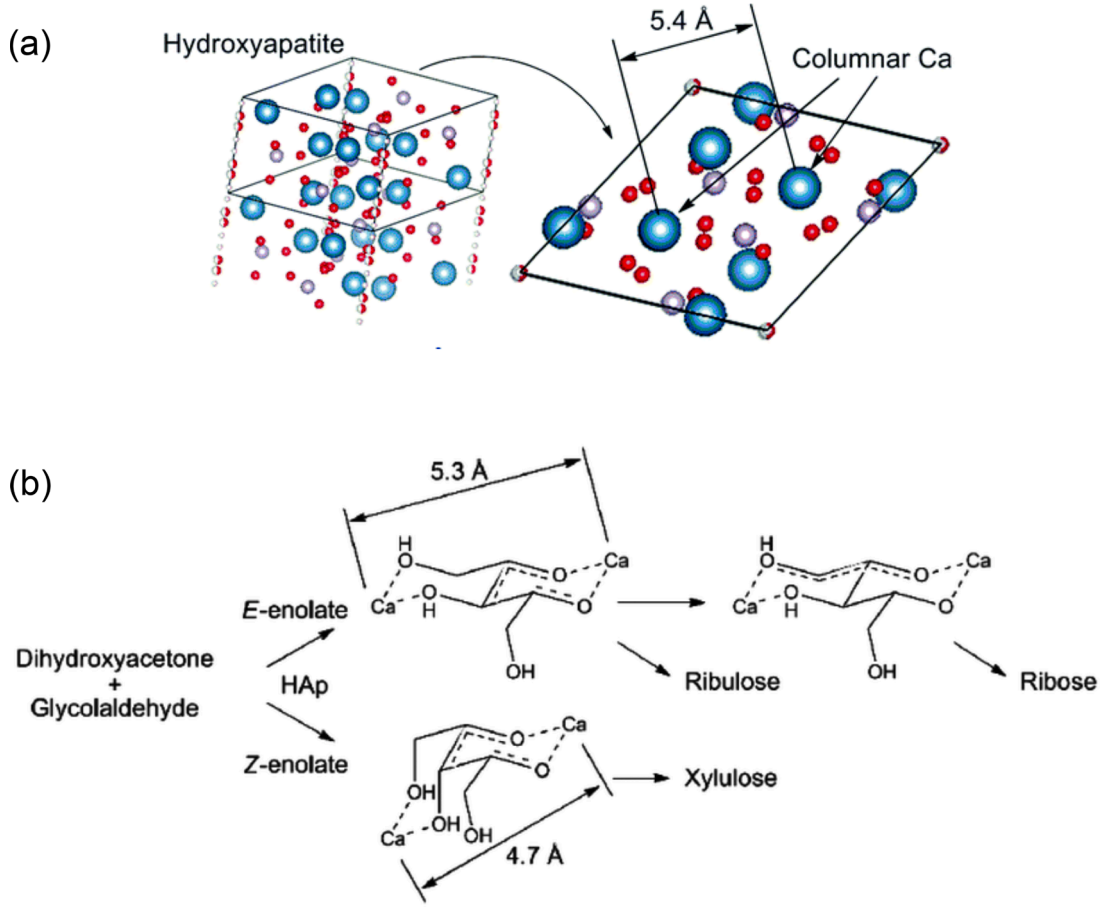

Fig. 37. (a) The crystal structure of hydroxyapatite. (b) Proposed chelating structures in the cross-aldol reaction and subsequent aldose–ketose isomerization in the presence of two chelated calcium ions. Reproduced with permission from ref. [99]. Copyright 2017 The Royal Society of Chemistry.

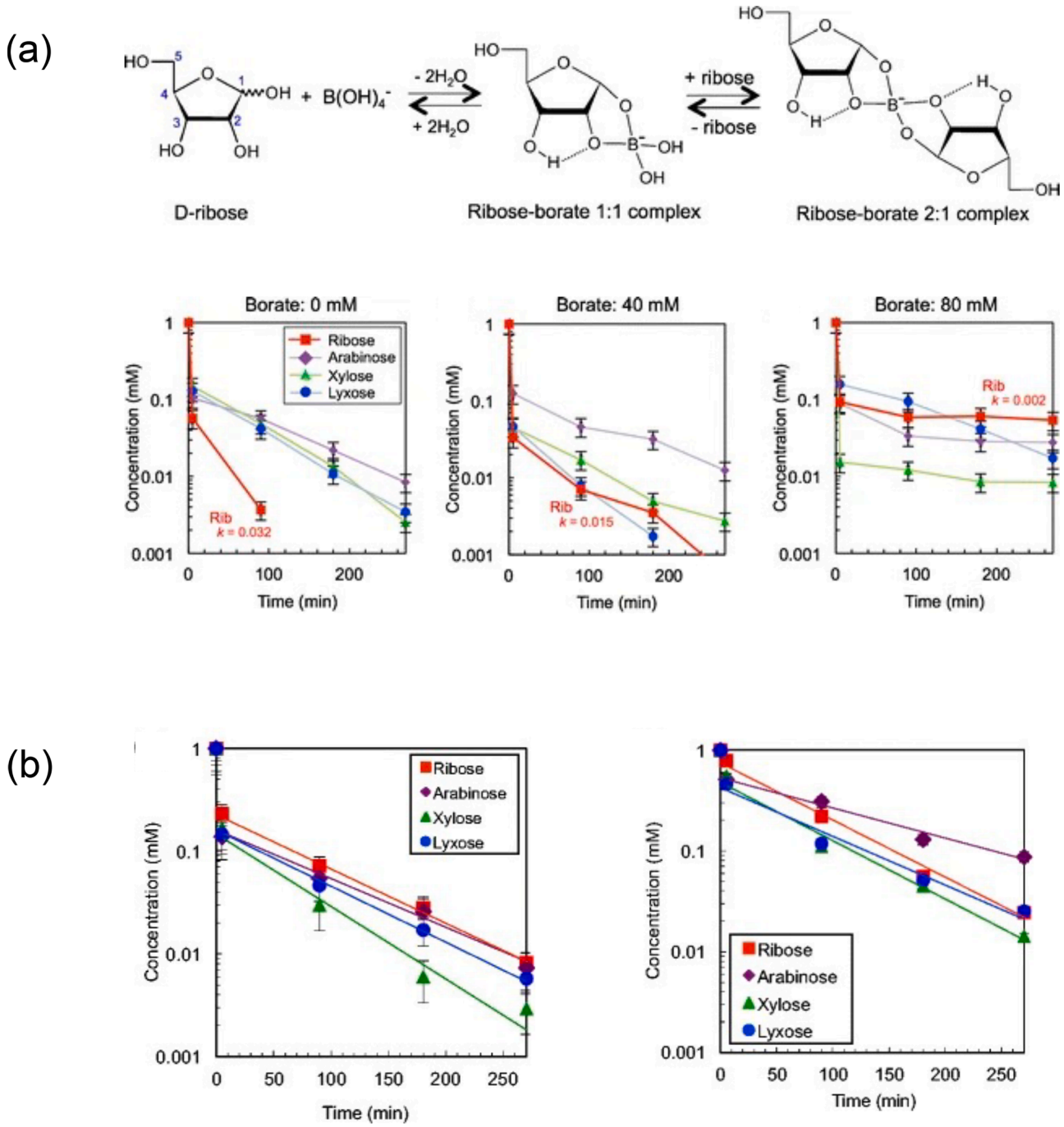

Fig. 38. (a) Formation of ribose–borate complexes (upper). Changes in the concentration of aldopentoses incubated in a borate-free solution and borate solutions (40 and 80 mM) at 45 °C (lower). Reproduced with permission from ref. [101]. Copyright 2013 Springer Nature. (b) Changes in the concentration of aldopentoses incubated in sodium silicate (80 mM, pH 12.5 – 12.9) and sodium phosphate (80 mM, pH 12.6 – 13.1) at 45 °C. Reproduced with permission from ref. [102]. Copyright 2016 Springer Nature.

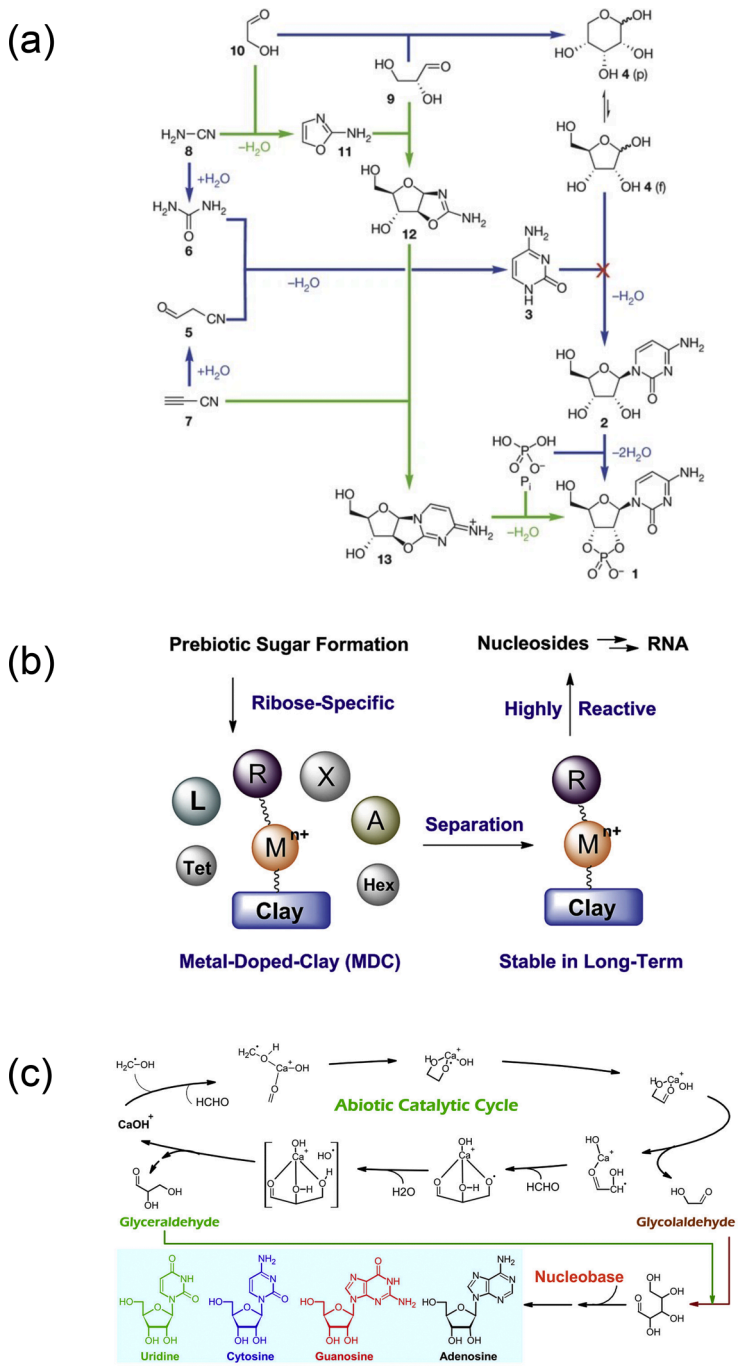

Fig. 39. (a) Previously assumed synthesis of β-ribocytidine-2′,3′-cyclic phosphate **1** (blue; note the failure of the step in which cytosine **3** and ribose **4** are proposed to condense together) and the successful new synthesis (green). Here p and f denote pyranose and furanose, respectively. Reproduced with permission from ref. [104]. Copyright 2009 Springer Nature. (b) A conceptual illustration of ribose selection (A, arabinose; L, lyxose; R, ribose; X, xylose; Tet, tetroses; Hex, hexoses) and synthesis of nucleosides. Reproduced with permission from ref. [105]. Copyright 2021 Elsevier. (c) A conceptual illustration of autocatalysis in formose reaction and formation of RNA nucleosides. Reproduced with permission from ref. [106]. Copyright 2020 American Chemical Society.

which the hydroxymethyl radical (•CH_2OH) generated under conditions, *e.g.*, heat, UV light, and discharge, was the main reactant (Fig. 39c). In the pathway, ribose and all RNA nucleosides were formed with a relatively low energy barrier. Formose reaction proceeded with or without Ca^{2+} and $CaOH^+$ ions. When $CaOH^+$ was involved in the reaction, an autocatalytic cycle for the formation of glycolaldehyde and glyceraldehyde was confirmed. This result suggests that Ca^{2+} cations are not involved in the production of ribose from glyceraldehyde. Furthermore, these pathways produced 1,3-dihydroxyacetone and erythrose. The DFT calculation data showed that the glycosidic bond was formed between ribose and nucleobases, and ribose formed a cyclic free radical that reacts with neutral nucleobases.

3.3.5. *The origin of chirality*

Cowan and Furnstahl [107] discussed the possibility that parity non-conservation effects might be involved in stereoselectivity in life using a model that explains chiral selectivity through the autocatalytic reaction of glyceraldehyde. They showed that a small energy difference in the formation of stereoisomers in the Ca^{2+} (or Sr^{2+}, Ba^{2+})-catalyzed coupling of formaldehyde and glycolaldehyde was large enough to give

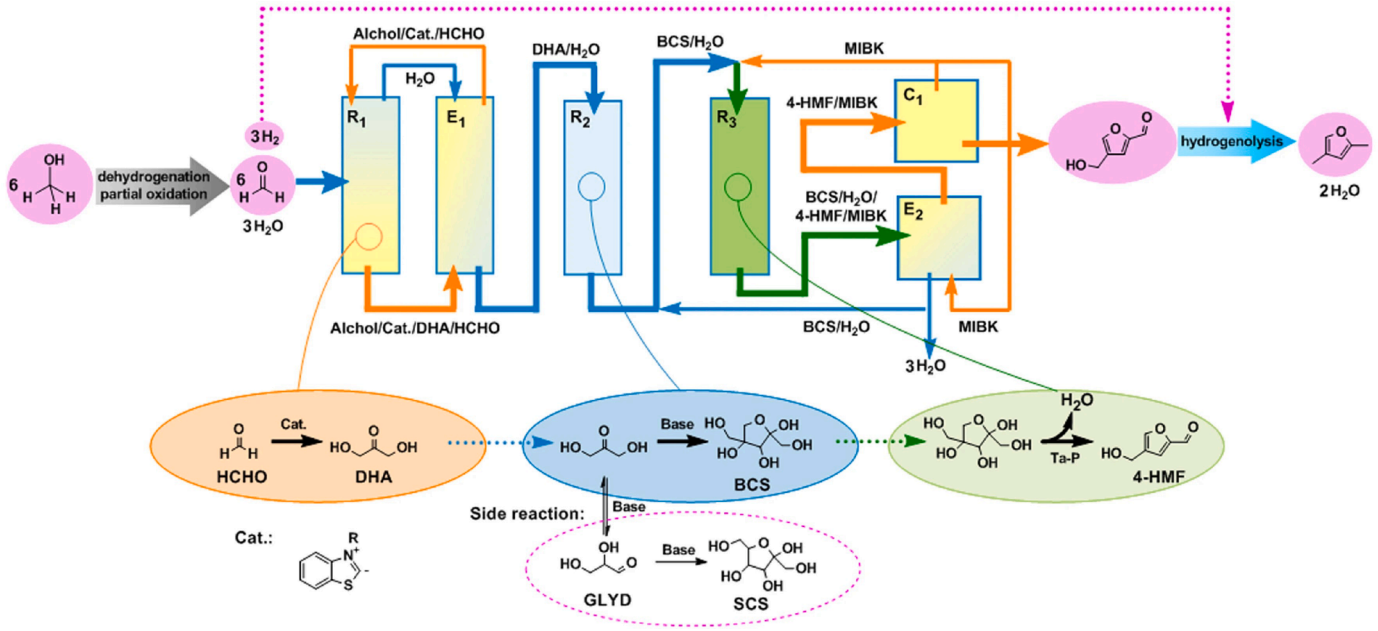

Fig. 40. Schematic diagram of the process for conversion of methanol to 2,4-dimethylfuran. Reproduced with permission from ref. [108]. Copyright 2013 Springer Nature.

an effective enantiomeric excess, defined by the ratio of rate constants replicated over evolutionary time (50 million years or more).

3.4. Applications of formose reactions

3.4.1. Production of chemicals based on formose reactions

Deng et al. [108] combined formose reaction with biomass gasification and aqueous phase processing to produce liquid transportation fuels (Fig. 40). 3-Hexylbenzothiazolium bromide and triethylamine were heated in 1,4-dioxane at 80 °C for 12 h, and the precipitated triethylammonium bromide was filtered off to prepare a catalyst solution. Formaldehyde obtained from biomass via methanol was mixed with the catalyst solution. The reaction mixture was heated at 80 °C for 1 h to produce 1,3-dihydroxyacetone (96 % purity, 30 % yield). Aldol condensation of the 1,3-dihydroxyacetone followed by dehydration gave 4-hydroxymethylfurfural (4-HMF). The resulting 4-HMF was then hydrogenated to produce 2,4-dimethylfuran (2,4-DMF) or C9 – C15 branched alkanes as liquid transportation fuels.

3.4.2. Chemical treatments using formose reaction

Glyphosate (*N*-(phosphonomethyl)glycine) is one of the widely used pesticide ingredients. Xing et al. [109] used formose reaction to treat glyphosate wastewater. Glyphosate wastewater containing organic phosphorus (40 – 600 mg L^{-1}) and formaldehyde (1 – 4 %) was subjected to catalytic wet oxidation (CWO) using activated carbon modified by H_2O_2 oxidation and thermal treatment with melamine as a catalyst, and >90 % of the organic phosphorus was removed. The CWO wastewater was further treated with lime at 80 °C to remove the remaining phosphorus compounds and formaldehyde, thereby improving the biodegradability.

3.4.3. Cultivation of microorganisms using formose

Cestellos-Blanco et al. [66] used the product obtained from formose reaction using the electrochemically produced glycolaldehyde as a cocatalyst to culture *E. coli* (see Section 3.1.7). The reaction solution was filtered to remove precipitate, and the product was recovered by removal of the solvent. An appropriate amount of the product, *i.e.*, formose (0 % – 0.1 % (w/v)) was added to the M9 minimal medium and sterilized with a syringe filter, and then XL1-blue *E. coli* cells were inoculated into the M9 minimal medium supplemented with glucose or formose. Growth curves of *E. coli* were generated by reading the optical density (OD) of a 48-well plate using a plate reader at 37 °C for 12 h The growth of *E. coli* using the formose was slower than that using glucose, indicating that the metabolic efficiency of formose is low. Tabata et al. [17] used the product obtained from formose reaction using Na_2WO_4 as a catalyst and glycolaldehyde as a cocatalyst, including 1,3,4-trihydroxy-3-(hydroxymethyl)butan-2-one, 1,3,4,5-tetrahydroxypentan-2-one, and 1,2,4,5,6-pentahydroxyhexan-3-one, to culture soil microorganisms collected from forest soil near the National Institute of Advanced Industrial Science and Technology in Hokkaido (see Section 3.1.2). After several days of cultivation, microbial growth was observed. After the start of cultivation, the supernatant of the microbial culture medium was characterized by HPLC, and it was confirmed that the peak intensity of the monosaccharides decreased over time (Fig. 41a). In particular, 1,3,4-trihydroxy-3-(hydroxymethyl)butan-2-one was almost consumed after 8 days. Tabata et al. [110] carried out formose reaction of formaldehyde (2 M) and 1,3-dihydroxyacetone (20 mM) using $Ca(OH)_2$ (100 mM) as a catalyst at 80 °C for 1.5 min to obtain a product containing hexoses and pentoses as the main components. They cultured *C. glutamicum* under oxygen-limiting conditions with the product as the sole carbon source, allowing *C. glutamicum* to produce lactate (Fig. 41b). Some of the monosaccharides produced by formose reaction inhibited cell proliferation, but the rate of cell proliferation increased using a product treated with 2 M NaOH overnight at room temperature.

4. Summary and outlook

This review provides an overview of key studies from the second wave of formose research, which began in the early 2000s and lasted nearly two decades. Since the number of publications has continued to increase, this wave is expected to continue for another 20 years or more. The second wave will further make significant progress, and future innovative breakthroughs are expected to enhance the ability to utilize formose reaction for a variety of fundamental studies and industrial applications.

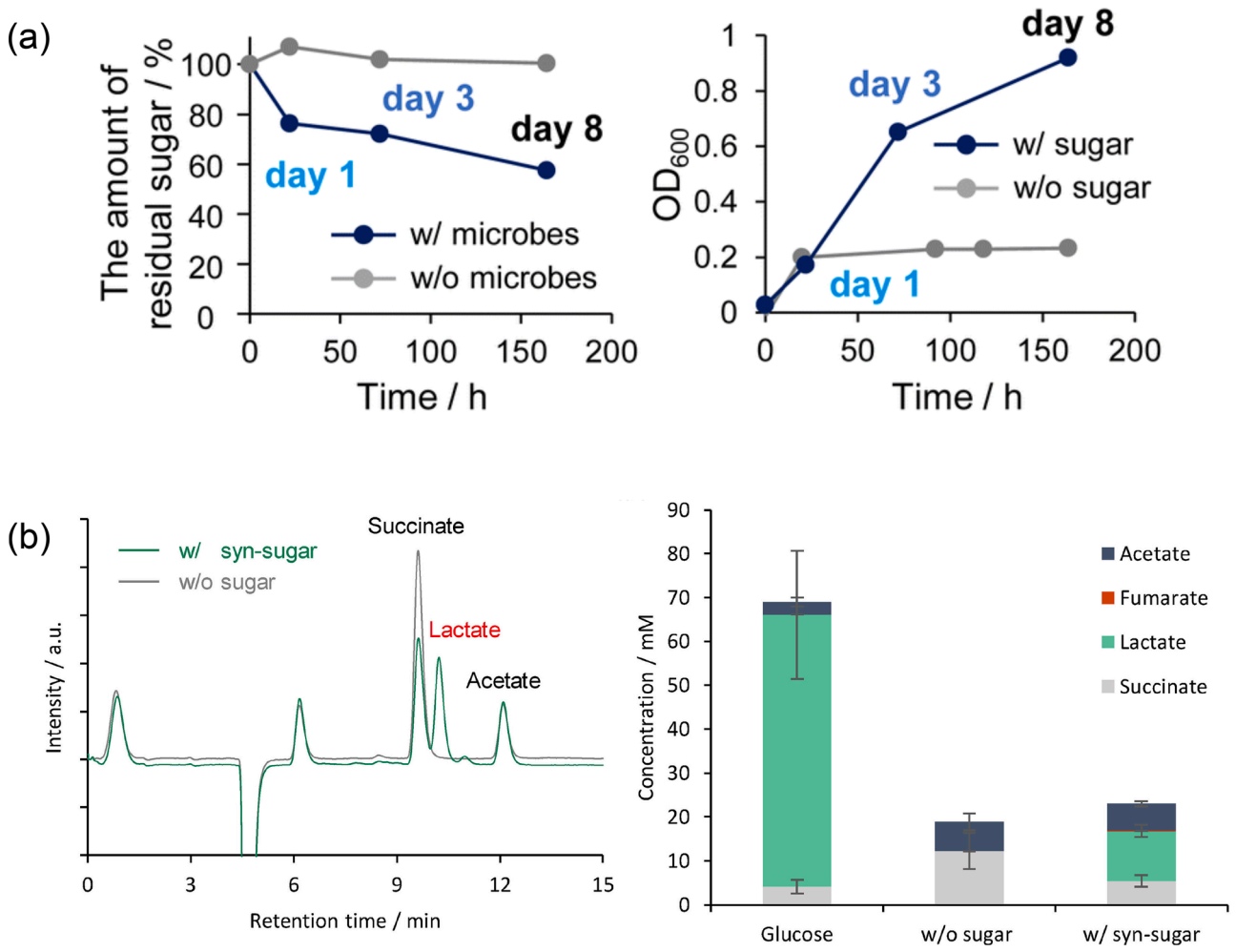

Fig. 41. (a) The time evolutions of total residual concentration of pentoses and hexoses (left) and OD_{600} (right) after cultivation. Results obtained without microbes and without sugar are also shown for comparison (gray lines). Reproduced with permission from ref. [17]. Copyright 2023 The Royal Society of Chemistry. (b) HPLC chromatograms of the supernatant collected 24 h after the reaction (left). The gray line shows the result when the sugar was not added, and the green line shows the results when the synthesized sugar solution was added at 1 % (w/v). Quantitative results of organic acids after the reaction based on the HPLC analysis (right). Reproduced with permission from ref. [110]. Copyright 2024 Wiley-VCH.

CRediT authorship contribution statement

Akihito Hashidzume: Writing – review & editing, Writing – original draft, Visualization, Conceptualization.

Declaration of competing interest

I declare that I have no known competing financial interests or personal relationships that could have appeared to influence the work reported in this review article. This work was conducted solely for the purpose of summarizing and providing an academic overview of the second wave of formose research and its future prospects. No funding sources or external interests influenced the content or conclusions of this review.

Data availability

No data was used for the research described in the article.

References

[1] A. Butlerow, Bildung einer zuckerartigen Substanz durch Synthese, Ann. Chem. 120 (1861) 295–298.
[2] O. Loew, Einige Bemerkungen über Formose, Ber. Dtsch. Chem. Ges. 20 (1887) 141–144.
[3] W. Gilbert, Origin of life: the RNA world, Nature 319 (1986), 618-618.
[4] G.F. Joyce, L.E. Orgel, Prospects for understanding the origin of the RNA world, in: R.F. Gesteland, T.R. Cech, J.F. Atkins (Eds.), The RNA World, Cold Spring Harbor Laboratory Press, Cold Spring Harbor, NY, 1999, pp. 49–77.
[5] T. Mizuno, A.H. Weiss, Synthesis and utilization of formose sugars, Adv. Carbohydr. Chem. Biochem. 29 (1974) 173–227.
[6] R. Shapiro, Prebiotic ribose synthesis: a critical analysis, Orig. Life Evol. Biosph. 18 (1988) 71–85.
[7] Y. Shigemasa, H. Saimoto, Formose, Synthesis of saccharides from formaldehyde, Trends Glycosci. Glycotechnol. 2 (1990) 119–123.
[8] Z. Iqbal, S. Novalin, The formose reaction: a tool to produce synthetic carbohydrates within a regenerative life support system, Curr. Org. Chem. 16 (2012) 769–788.
[9] I.V. Delidovich, A.N. Simonov, O.P. Taran, V.N. Parmon, Catalytic formation of monosaccharides: from the formose reaction towards selective synthesis, ChemSusChem 7 (2014) 1833–1846.
[10] Q.P. Tran, Z.R. Adam, A.C. Fahrenbach, Prebiotic reaction networks in water, Life 10 (2020) 352.
[11] T. Matsumoto, H. Yamamoto, S. Inoue, Selective formation of triose from formaldehyde catalyzed by thiazolium salt, J. Am. Chem. Soc. 106 (1984) 4829–4832.
[12] T. Matsumoto, M. Yamane, S. Inoue, Selective synthesis of DL-dendroketose from formaldehyde, Chem. Lett. (1984) 1819–1822.
[13] A.K. Eckhardt, M.M. Linden, R.C. Wende, B. Bernhardt, P.R. Schreiner, Gas-phase sugar formation using hydroxymethylene as the reactive formaldehyde isomer, Nat. Chem. 10 (2018) 1141–1147.
[14] A.K. Eckhardt, R.C. Wende, P.R. Schreiner, 1,3-Dioxolane-4-ol hemiacetal stores formaldehyde and glycolaldehyde in the gas-phase, J. Am. Chem. Soc. 140 (2018) 12333–12336.

[15] N.F. Kleimeier, A.K. Eckhardt, R.I. Kaiser, Identification of glycolaldehyde enol (HOHC=CHOH) in interstellar analogue ices, J. Am. Chem. Soc. 143 (2021) 14009–14018.
[16] A.N. Simonov, O.P. Pestunova, L.G. Matvienko, V.N. Parmon, The nature of autocatalysis in the butlerov reaction, Kinet. Catal. 48 (2007) 245–254.
[17] H. Tabata, G. Chikatani, H. Nishijima, T. Harada, R. Miyake, S. Kato, K. Igarashi, Y. Mukouyama, S. Shirai, M. Waki, Y. Hase, S. Nakanishi, Construction of an autocatalytic reaction cycle in neutral medium for synthesis of life-sustaining sugars, Chem. Sci. 14 (2023) 13475–13484.
[18] C. Ono, S. Sunami, Y. Ishii, H.-J. Kim, T. Kakegawa, S.A. Benner, Y. Furukawa, Abiotic ribose synthesis under aqueous environments with various chemical conditions, Astrobiology 24 (2024) 489–497.
[19] D. Kopetzki, M. Antonietti, Hydrothermal formose reaction, New J. Chem. 35 (2011) 1787–1794.
[20] A. Omran, C. Menor-Salvan, G. Springsteen, M. Pasek, The messy alkaline formose reaction and its link to metabolism, Life 10 (2020) 125.
[21] A. Omran, Plausibility of the formose reaction in alkaline hydrothermal vent environments, Orig. Life Evol. Biosph. 53 (2020) 113–125.
[22] M. Masaoka, T. Michitaka, A. Hashidzume, Formose reaction accelerated in aerosol-OT reverse micelles, Beilstein J. Org. Chem. 12 (2016) 2663–2667.
[23] P.M. Gardner, K. Winzer, B.G. Davis, Sugar synthesis in a protocellular model leads to a cell signalling response in bacteria, Nat. Chem. 1 (2009) 377–383.
[24] H. Lu, A. Blokhuis, R. Turk-MacLeod, J. Karuppusamy, A. Franconi, G. Woronoff, C. Jeancolas, A. Abrishamkar, E. Loire, F. Ferrage, P. Pelupessy, L. Jullien, E. Szathmary, P. Nghe, A.D. Griffiths, Small-molecule autocatalysis drives compartment growth, competition and reproduction, Nat. Chem. 16 (2024) 70–78.
[25] H.-J. Kim, A. Ricardo, H.I. Illangkoon, M.J. Kim, M.A. Carrigan, F. Frye, S. A. Benner, Synthesis of carbohydrates in mineral-guided prebiotic cycles, J. Am. Chem. Soc. 133 (2011) 9457–9468.
[26] T. Imai, T. Michitaka, A. Hashidzume, Formose reaction controlled by boronic acid compounds, Beilstein J. Org. Chem. 12 (2016) 2668–2672.
[27] T. Michitaka, T. Imai, A. Hashidzume, Formose reaction controlled by a copolymer of *N,N*-dimethylacrylamide and 4-vinylphenylboronic acid, Polymers (Basel) 9 (2017) 549.
[28] N. Ishihara, G. Chikatani, H. Nishijima, H. Tabata, Y. Hase, Y. Mukouyama, S. Nakanishi, S. Mukaida, Developing a design guideline of boronic acid derivatives to scavenge targeted sugars in the formose reaction products using DFT-based machine learning, Chem. Lett. 53 (2024) upae087.
[29] S. Chakraborty, N. Nemeria, A. Yep, M.J. McLeish, G.L. Kenyon, F. Jordan, Mechanism of benzaldehyde lyase studied via thiamin diphosphate-bound intermediates and kinetic isotope effects, Biochemistry 47 (2008) 3800–3809.
[30] S. Poust, J. Piety, A. Bar-Even, C. Louw, D. Baker, J.D. Keasling, J.B. Siegel, Mechanistic analysis of an engineered enzyme that catalyzes the formose reaction, ChemBioChem 16 (2015) 1950–1954.
[31] X. Lu, Y. Liu, Y. Yang, S. Wang, Q. Wang, X. Wang, Z. Yan, J. Cheng, C. Liu, X. Yang, H. Luo, S. Yang, J. Gou, L. Ye, L. Lu, Z. Zhang, Y. Guo, Y. Nie, J. Lin, S. Li, C. Tian, T. Cai, B. Zhuo, H. Ma, W. Wang, Y. Ma, Y. Liu, Y. Li, H. Jiang, Constructing a synthetic pathway for acetyl-coenzyme A from one-carbon through enzyme design, Nat. Commun. 10 (2019) 1378.
[32] T. Li, Z. Tang, H. Wei, Z. Tan, P. Liu, J. Li, Y. Zheng, J. Lin, W. Liu, H. Jiang, H. Liu, L. Zhu, Y. Ma, Totally atom-economical synthesis of lactic acid from formaldehyde: combined bio-carboligation and chemo-rearrangement without the isolation of intermediates, Green Chem. 22 (2020) 6809–6814.
[33] N. Massad, S. Banta, Development of a kinetic model and figures of merit for formaldehyde carboligations catalyzed by formolase enzymes, Biotechnol. Bioeng. 119 (2022) 3140–3148.
[34] J. Yang, S. Sun, Y. Men, Y. Zeng, Y. Zhu, Y. Sun, Y. Ma, Transformation of formaldehyde into functional sugars via multi-enzyme stepwise cascade catalysis, Catal. Sci. Technol. 7 (2017) 3459–3463.
[35] H. Tajima, T. Niitsu, H. Inoue, Polymerization of formaldehyde by an immobilized thiamine catalyst on cation-exchange resin, J. Chem. Eng. Jpn. 32 (1999) 776–782.
[36] H. Tajima, T. Niitsu, H. Inoue, Repeated use of thiazolium catalyst immobilized on cation-exchange resin, J. Chem. Eng. Jpn. 33 (2000) 793–796.
[37] H. Tajima, T. Niitsu, H. Inoue, M.M. Ito, Effects of thiazolium counter anion and reaction media on the activity of immobilized thiazolium catalyst, J. Chem. Eng. Jpn. 34 (2001) 553–557.
[38] H. Tajima, K. Tabata, T. Niitsu, H. Inoue, The formose reaction on a synthetic zeolite impregnated with thiazolium catalyst, J. Chem. Eng. Jpn. 35 (2002) 564–568.
[39] H. Tajima, H. Inoue, M.M. Ito, A computational study on the mechanism of the formose reaction catalyzed by the thiazolium salt, J. Comput. Chem., Jpn. 2 (2003) 127–134.
[40] J. Wang, H. Li, J. Chen, C. Wang, Synthesis of 1,3-dihydroxyacetone *via* heterogeneous base-free formaldehyde condensation, New J. Chem. 47 (2023) 20123–20127.
[41] A.N. Simonov, L.G. Matvienko, O.P. Pestunova, V.N. Parmon, N.A. Komandrova, V.A. Denisenko, V.E. Vas'kovskii, Selective synthesis of erythrulose and 3-pentulose from formaldehyde and dihydroxyacetone catalyzed by phosphates in a neutral aqueous medium, Kinet. Catal. 48 (2007) 550–555.
[42] A.N. Simonov, O.P. Pestunova, L.G. Matvienko, V.N. Snytnikov, O.A. Snytnikova, Y.P. Tsentalovich, V.N. Parmon, Possible prebiotic synthesis of monosaccharides from formaldehyde in presence of phosphates, Adv. Space Res. 40 (2007) 1634–1640.
[43] A. Hashidzume, T. Fujimoto, M. Masaoka, Y. Sanada, T. Sato, Preparation and catalytic activity of porous alumina by the sol-gel process in the presence of saccharides, Kobunshi Ronbunshu 67 (2010) 312–317.
[44] M. Gull, M.A. Mojica, F.M. Fernández, D.A. Gaul, T.M. Orlando, C.L. Liotta, M. A. Pasek, Nucleoside phosphorylation by the mineral schreibersite, Sci. Rep. 5 (2015) 17198.
[45] S. Pallmann, M. Šteflová, S. Haas, A. Lamour, O. Henß, Trapp, Schreibersite: an effective catalyst in the formose reaction network, New J. Phys. 20 (2018) 055003.
[46] S. Colón-Santos, G.J.T. Cooper, L. Cronin, Taming the combinatorial explosion of the formose reaction via recursion within mineral environments, ChemSystemsChem 1 (2019) e1900014.
[47] A. Omran, A. Gonzalez, C. Menor-Salvan, M. Gaylor, J. Wang, J. Leszczynski, T. Feng, Serpentinization-associated mineral catalysis of the protometabolic formose system, Life 13 (2023) 1297.
[48] V. Vinogradoff, V. Leyva, E. Mates-Torres, R. Pepino, G. Danger, A. Rimola, L. Cazals, C. Serra, R. Pascal, C. Meinert, Olivine-catalyzed glycolaldehyde and sugar synthesis under aqueous conditions: application to prebiotic chemistry, Earth Planet. Sci. Lett. 626 (2024) 118558.
[49] A. Vojood, M. Khodadadi-Moghaddam, G. Ebrahimzadeh-Rajaei, S. Mohajeri, A. Shamel, Increasing in the selectivity of formose reaction for glyceraldehyde production in the presence of fumed silica and montmorillonite catalysts, Chem. Methodol. 5 (2021) 422–432.
[50] A. Vojood, Comparison of mono-ethylene glycol prebiotic synthesis efficiency via formose reaction in methanol and water as solvents: a short communication, Am. J. Phys. Chem. 12 (2023) 17–21.
[51] A. Vojood, Synthesis of ethane-1,2-diol (ethylene glycol) through formose reaction in methanol solvent, Adv. J. Chem. A 7 (2024) 289–294.
[52] V. Balloi, M.A. Diaz-Perez, M.A. Lara-Angulo, D. Villalgordo-Hernández, J. Narciso, E.V. Ramos-Fernandez, J.C. Serrano-Ruiz, Metal–organic frameworks as formose reaction catalysts with enhanced selectivity, Molecules 28 (2023) 6095.
[53] M. Waki, S. Shirai, Y. Hase, Saccharide formation by sustainable formose reaction using heterogeneous zeolite catalysts, Dalton Trans. 53 (2024) 2678–2686.
[54] S. Lamour, S. Pallmann, M. Haas, O. Trapp, Prebiotic sugar formation under nonaqueous conditions and mechanochemical acceleration, Life 9 (2019) 52.
[55] M. Haas, S. Lamour, S.B. Christ, O. Trapp, Mineral-mediated carbohydrate synthesis by mechanical forces in a primordial geochemical setting, Commun. Chem. 3 (2020) 140.
[56] J. Yang, X. Fang, G. Ren, T. Yu, Mechano-catalysis boosts glycolaldehyde conversion to tetroses over a new Zn-COF catalyst, New J. Chem. 47 (2023) 558–562.
[57] O. Pestunova, A. Simonov, V. Snytnikov, V. Stoyanovsky, V. Parmon, Putative mechanism of the sugar formation on prebiotic Earth initiated by UV-radiation, Adv. Space Res. 36 (2005) 214–219.
[58] O.A. Snytnikova, A.N. Simonov, O.P. Pestunova, V.N. Parmon, Y.P. Tsentalovich, Study of the photo-induced formose reaction by flash and stationary photolysis, Mendeleev Commun. 16 (2006) 9–11.
[59] S.V. Stovbun, A.A. Skoblin, A.M. Zanin, V.A. Tverdislov, O.P. Taran, V. N. Parmon, Formation of chiral structures in photoinitiated formose reaction, High Energy Chem. 52 (2018) 108–116.
[60] S.V. Stovbun, A.A. Skoblin, A.M. Zanin, V.A. Tverdislov, O.P. Taran, V. N. Parmon, Formation of chiral structures in UV-initiated formose reaction, Dokl. Phys. Chem. 479 (2018) 57–60.
[61] S.V. Stovbun, A.M. Zanin, M.V. Shashkov, A.A. Skoblin, D.V. Zlenko, V. A. Tverdislov, M.G. Mikhaleva, O.P. Taran, V.N. Parmon, Spontaneous resolution and super-coiling in xerogels of the products of photo-induced formose reaction, Orig. Life Evol. Biosph. 49 (2019) 187–196.
[62] S.V. Stovbun, A.M. Zanin, A.A. Skoblin, M.A. Tregubova, V.A. Tverdislov, O. P. Taran, V.N. Parmon, Formation of chiral and supercoiled structures in photoinduced formose reaction in the de novo model, Russ. J. Phys. Chem. B 13 (2019) 486–501.
[63] S. Abe, I. Yoda, K. Kobayashi, Y. Kebukawa, Gamma-ray-induced synthesis of sugars in meteorite parent bodies, ACS Earth Space Chem. 8 (2024) 1737–1744.
[64] A. Hashidzume, T. Imai, N. Deguchi, T. Tanibayashi, T. Ikeda, T. Michitaka, S. Kuwahara, M. Nakahata, Y. Kamon, Y. Todokoro, Preferential formation of specific hexose and heptose in the formose reaction under microwave irradiation, RSC Adv. 13 (2023) 4089–4095.
[65] S. Homnan, Y. Chimupala, W. Jaikla, M. Jitevisate, P. Nimmanpipug, C. Suwannajak, P. Wongkummoon, S. Rimjaem, Spectroscopic FTIR study for pathway of ribose formation via formose reaction in astrochemistry, J. Phys.: Conf. Ser. 2653 (2023) 012073.
[66] S. Cestellos-Blanco, S. Louisia, M.B. Ross, Y. Li, N.E. Soland, T.C. Detomasi, J. N. Cestellos Spradlin, D.K. Nomura, P. Yang, Toward abiotic sugar synthesis from CO_2 electrolysis, Joule 6 (2022) 2304–2323.
[67] N.E. Soland, I. Roh, W.-S. Huynh, P. Yang, Synthesis of carbohydrates from methanol using electrochemical partial oxidation over palladium with the integrated formose reaction, ACS Sustain. Chem. Eng. 11 (2023) 12478–12483.
[68] I.V. Delidovich, A.N. Simonov, O.P. Pestunova, V.N. Parmon, Catalytic condensation of glycolaldehyde and glyceraldehyde with formaldehyde in neutral and weakly alkaline aqueous media: kinetics and mechanism, Kinet. Catal. 50 (2009) 297–303.
[69] A. Ricardo, F. Frye, M.A. Carrigan, J.D. Tipton, D.H. Powell, S.A. Benner, 2-Hydroxymethylboronate as a reagent to detect carbohydrates: application to the analysis of the formose reaction, J. Org. Chem. 71 (2006) 9503–9505.

[70] C. Appayee, R. Breslow, Deuterium studies reveal a new mechanism for the formose reaction involving hydride shifts, J. Am. Chem. Soc. 136 (2014) 3720–3723.
[71] R. Breslow, Mechanism of the formose reaction, Tetrahedron Lett. 1 (1959) 22–26.
[72] L. Cheng, C. Doubleday, R. Breslow, Evidence for tunneling in base-catalyzed isomerization of glyceraldehyde to dihydroxyacetone by hydride shift under formose conditions, Proc. Natl. Acad. Sci. 112 (2015) 4218–4220.
[73] A. Briš, M.G. Baltussen, G.L. Tripodi, W.T.S. Huck, P. Franceschi, J. Roithová, Direct analysis of complex reaction mixtures: formose reaction, Angew. Chem. Int. Ed. 63 (2024) e202316621.
[74] W.E. Robinson, E. Daines, P. van Duppen, T. de Jong, W.T.S. Huck, Environmental conditions drive self-organization of reaction pathways in a prebiotic reaction network, Nat. Chem. 14 (2022) 623–631.
[75] P. van Duppen, E. Daines, W.E. Robinson, W.T.S. Huck, Dynamic environmental conditions affect the composition of a model prebiotic reaction network, J. Am. Chem. Soc. 145 (2023) 7559–7568.
[76] M.G. Baltussen, T.J. de Jong, Q. Duez, W.E. Robinson, W.T.S. Huck, Chemical reservoir computation in a self-organizing reaction network, Nature 631 (2024) 549–555.
[77] A.F. Jalbout, L. Abrell, L. Adamowicz, R. Polt, A.J. Apponi, L.M. Ziurys, Sugar synthesis from a gas-phase formose reaction, Astrobiology 7 (2007) 433–442.
[78] A.F. Jalbout, Prebiotic synthesis of simple sugars by an interstellar formose reaction, Orig. Life Evol. Biosph. 38 (2008) 489–497.
[79] J. Proppe, T. Husch, G.N. Simm, M. Reiher, Uncertainty quantification for quantum chemical models of complex reaction networks, Faraday Discuss. 195 (2016) 497–520.
[80] S. Thripati, R.O. Ramabhadran, Metal-ion- and hydrogen-bond-mediated interstellar prebiotic chemistry: the first step in the formose reaction, J. Phys. Chem. A 121 (2017) 8659–8674.
[81] A. Kong, A. Guljas, I.G. Csizmadia, R. Fournier, B. Fiser, A. Rágyanszki, Sugars in space: a quantum chemical study on the barrierless formation of dihydroxyacetone in the interstellar medium, Can. J. Chem. 99 (2020) 326–329.
[82] A. Venturini, J. González, Prebiotic synthesis of glycolaldehyde and glyceraldehyde from formaldehyde: a computational study on the initial steps of the formose reaction, ChemPlusChem 89 (2024) e202300388.
[83] D. Cantillo, M. Ávalos, R. Babiano, P. Cintas, J.L. Jiménez, J.C. Palacios, On the prebiotic synthesis of D-sugars catalyzed by L-peptides: assessments from first-principles calculations, Chem. Eur. J. 18 (2012) 8795–8799.
[84] D. Rappoport, C.J. Galvin, D.Y. Zubarev, A. Aspuru-Guzik, Complex chemical reaction networks from heuristics-aided quantum chemistry, J. Chem. Theory Comput. 10 (2014) 897–907.
[85] G.N. Simm, M. Reiher, Context-driven exploration of complex chemical reaction networks, J. Chem. Theory Comput. 13 (2017) 6108–6119.
[86] S.R. Shahi, H.J. Cleaves, II, The effects of iron on in silico simulated abiotic reaction networks, Molecules 27 (2022) 8870.
[87] A. Stan, B.v.d. Esch, C. Ochsenfeld, Fully automated generation of prebiotically relevant reaction networks from optimized nanoreactor simulations, J. Chem. Theory Comput. 18 (2022) 6700–6712.
[88] H. Takehara, D. Shoji, S. Ida, Monte Carlo simulation of sugar synthesis on icy dust particles intermittently irradiated by UV in a protoplanetary disk, A&A 662 (2022) A76.
[89] J. Kua, L.P. Tripoli, Exploring the core formose cycle: catalysis and competition, Life 14 (2024) 933.
[90] G. Benkö, C. Flamm, P.F. Stadler, A graph-based toy model of chemistry, J. Chem. Inf. Comput. Sci. 43 (2003) 1085–1093.
[91] J. Andersen, C. Flamm, D. Merkle, P. Stadler, Inferring chemical reaction patterns using rule composition in graph grammars, J. Syst. Chem. 4 (2013) 4.
[92] J.L. Andersen, C. Flamm, D. Merkle, P.F. Stadler, Chemical transformation motifs—Modelling pathways as integer hyperflows, IEEE/ACM Trans. Comput. Biol. Bioinform. 16 (2019) 510–523.
[93] Y. Liu, D.J.T. Sumpter, Mathematical modeling reveals spontaneous emergence of self-replication in chemical reaction systems, J. Biol. Chem. 293 (2018) 18854–18863.
[94] D.T. Halfen, A.J. Apponi, N. Woolf, R. Polt, L.M. Ziurys, A systematic study of glycolaldehyde in Sagittarius B2(N) at 2 and 3 mm: criteria for detecting large interstellar molecules, Astrophys. J. 639 (2006) 237–245.
[95] Y. Furukawa, Y. Chikaraishi, N. Ohkouchi, N.O. Ogawa, D.P. Glavin, J. P. Dworkin, C. Abe, T. Nakamura, Extraterrestrial ribose and other sugars in primitive meteorites, Proc. Natl. Acad. Sci 116 (2019) 24440–24445.
[96] A. Ricardo, M.A. Carrigan, A.N. Olcott, S.A. Benner, Borate minerals stabilize ribose, Science 303 (2004) 196.
[97] J.B. Lambert, S.A. Gurusamy-Thangavelu, K. Ma, The silicate-mediated formose reaction: bottom-up synthesis of sugar silicates, Science 327 (2010) 984–986.
[98] A. Vazquez-Mayagoitia, S.R. Horton, B.G. Sumpter, J. Sponer, J.E. Sponer, M. Fuentes-Cabrera, On the stabilization of ribose by silicate minerals, Astrobiology 11 (2011) 115–121.
[99] K. Usami, A. Okamoto, Hydroxyapatite: catalyst for a one-pot pentose formation, Org. Biomol. Chem. 15 (2017) 8888–8893.
[100] E. Camprubi, S.A. Harrison, S.F. Jordan, J. Bonnel, S. Pinna, N. Lane, Do soluble phosphates direct the formose reaction towards pentose sugars? Astrobiology 22 (2022) 981–991.
[101] Y. Furukawa, M. Horiuchi, T. Kakegawa, Selective stabilization of ribose by borate, Orig. Life Evol. Biosph. 43 (2013) 353–361.
[102] S. Nitta, Y. Furukawa, T. Kakegawa, Effects of silicate, phosphate, and calcium on the stability of aldopentoses, Orig. Life Evol. Biosph. 46 (2016) 189–202.
[103] K. Paschek, K. Kohler, B.K.D. Pearce, K. Lange, T.K. Henning, O. Trapp, R. E. Pudritz, D.A. Semenov, Possible ribose synthesis in carbonaceous planetesimals, Life 12 (2022) 404.
[104] M.W. Powner, B. Gerland, J.D. Sutherland, Synthesis of activated pyrimidine ribonucleotides in prebiotically plausible conditions, Nature 459 (2009) 239–242.
[105] Z.-R. Zhao, X. Wang, A plausible prebiotic selection of ribose for RNA - formation, dynamic isolation, and nucleotide synthesis based on metal-doped-clays, Chem 7 (2021) 3292–3308.
[106] Y.A. Jeilani, M.T. Nguyen, Autocatalysis in formose reaction and formation of RNA nucleosides, J. Phys. Chem. B 124 (2020) 11324–11336.
[107] J.A. Cowan, R.J. Furnstahl, Origin of chirality in the molecules of life, ACS Earth Space Chem. 6 (2022) 2575–2581.
[108] J. Deng, T. Pan, Q. Xu, M.-Y. Chen, Y. Zhang, Q.-X. Guo, Y. Fu, Linked strategy for the production of fuels via formose reaction, Sci. Rep. 3 (2013) 1244.
[109] B. Xing, H. Chen, X. Zhang, Removal of organic phosphorus and formaldehyde in glyphosate wastewater by CWO and the lime-catalyzed formose reaction, Water Sci. Technol. 75 (2017) 1390–1398.
[110] H. Tabata, H. Nishijima, Y. Yamada, R. Miyake, K. Yamamoto, S. Kato, S. Nakanishi, Microbial biomanufacturing using chemically synthesized non-natural sugars as the substrate, ChemBioChem 25 (2024) e202300760.